EFFECTS OF MILL ROTATIONAL SPEED ON THE BATCH GRINDING KINETICS OF A UG2 PLATINUM ORE

By

DINEO MOKGANYETJI MAKGOALE

Submitted in accordance with the requirements for

the degree of

MAGISTER TECHNOLOGIAE

in the subject

ENGINEERING: CHEMICAL

at the

UNIVERSITY OF SOUTH AFRICA

SUPERVISOR: Prof. FRANCOIS MULENGA

November 2019

Declaration

Name: Dineo Mokganyetji Makgoale

Student number: 60889012

Degree: Magister Technologiae

Title: Effects of mill rotational speed on the batch grinding kinetics of a UG2 platinum ore

I declare that the above dissertation is my own work and that all the sources that I have used or quoted have been indicated and acknowledged by means of complete references.

I further declare that I submitted the dissertation to originality checking software and that it falls within the accepted requirements for originality.

I further declare that I have not previously submitted this work, or part of it, for examination at UNISA for another qualification or at any other higher education institution.

_____ _____

SIGNATURE DATE

Abstract

In this study, the effect of speed was investigated on the breakage rate of UG2 platinum ore in a batch mill of 5 dm^3 and 175 mm internal diameter. One size fraction method was carried out to perform the experiment. Five mono-sized fractions in the range of 1.180 mm to 0.212 mm separated by $\sqrt{2}$ series interval were prepared. The fractions were milled at different grinding times (0.5, 2, 4, 15 and 30 min) and three fractions of mill critical speed were considered (20%, 30%, and 40%). The target of critical speed below 50% was due to the need of lower energy consumption in milling processes. The selection and breakage function parameters were determined and compared for fractions of critical speed.

First the grinding kinetics of the ore was determined and it was found that the material breaks in non-first order manner. Thereafter, effective mean rate of breakage was determined. It was found that the rate of breakage increased with increase of mill speed and optimum speed was not reached in the range of chosen mill speed fractions. Again the rate of breakage was plotted as a function of particle size, the optimum size was 0.8 mm when milling at 30% critical speed. As for 20% and 30% optimum size was not reached. The selection function parameters estimated at 30% critical speed were a_0 = 0.04 min^{-1}, α = 1.36, μ = 0.9 mm, and Λ = 3. Breakage function parameters were determined and was noticed that the material UG2 platinum ore is non-normalised, i.e. Φ value was changing from 0.25 to 0.90 depending on feed size and mill speed. The parameters β and γ were constant at 7.3 and 1.17 respectively.

Key terms: Population balance Model, ball milling, communition, Size specific energy, Selection function, breakage function, mill critical speed, Platinum ore, milling kinetics, breakage rate.

Dedication

This work is dedicated to my sweet family:

My Husband, Theophilus Machuene Moloto.

My Mother-in-law, Kgadi Dorreis Moloto.

My brothers, Mmakgati Potsiso Johnson Makgoale, Abel Lengana Makgoale, Puleng Chumudi Makgoale, Thankiso Segosele Makgoale and Shima kyvas Makgoale.

My sisters-in-law, Kwena Violet Moloto, Mosima Makolobe Moloto, and Khomotso Maphuti Moloto.

And my beautiful parents who brought me into this world. I am really grateful to you.

Acknowledgements

I would like to thank the following people for making this research to be successful:

My supervisor Prof Francois Mulenga for his support, guidance, motivation and above all for his patience

The University of South Africa for giving me the opportunity to study at their institution

The University of Johannesburg for allowing me to use their ore sample

The University of the Witwatersrand for allowing me to use their laboratory and equipment

Bruce Mothibedi, Jeanet Smith and Dr Murray Bwalya Mulenga for their support while doing my experimental work

My family for their love and having trust in me especially my husband for his support, patience and understanding

My church pastors for praying with me

My friend Olayemi Fakayode for his guidance, support and sharing of research knowledge with me.

My colleagues Kutullo Mapotsane, Talent Mbelembe, Maggie Bohlolo and Amugelani Baloyi for their suggestions on research write-up

Thank you to all individuals who contributed to the success of this study in anyhow.

Thank you Almighty God for giving me the strength to make this work possible. Thank you Lord for answering my prayers!

Table of Contents

List of Figures

List of Tables

List of Symbols

Symbols	Units	Descriptions
a_0	min^{-1}	The specific rate of breakage at the standard size X_0 = 1 mm
α	-	Selection function parameter which is material-dependent in Equation 2.12
Λ	min^{-1}	Selection function parameter which is a material-dependent in Equation 2.13
μ	mm	Selection function parameter which is primarily a function of milling conditions in Equation 2.13
$b_{i,j}$	-	Primary breakage distribution function of a particle of size *j* breaking into size *i*
$B_{i,j}$	-	Cumulative breakage distribution function of a particle of size *j* breaking into size *i*
β	-	Breakage function parameter characteristic of the material
D	m	Mill diameter
$C_1\ C_2\ C_3\ C_4\ and\ C_5$	-	Correction factors applied during scale-up in Equation 2.14
c	-	The parameter that is usually taken to be equal to 1.2 for dry milling and 1.32 for wet milling in Equation 2.18
d	m	Ball diameter
F_c	%	fraction of the mill filled by the powder bed
e	J/kg	Specific energy
E	J	Net energy consumed after grinding
E_i	$J\ kg^{-1}$	Size specific energy

f_c	%	The fraction of the mill filled by the powder bed
g	m/s^2	Gravitational acceleration
i	%	Broken size class fraction
j	%	Feed size class fraction
J	%	Ball filling or fraction of mill volume occupied by grinding balls at rest including interstices
K	-	Acceleration-deceleration parameter *(k*) in Equation 2.9
L	m	Length of the mill
M	kg	Mass of load in the mill
$M_j(t)$	kg	Mass fraction of size *j* particles in the mill feed at grinding time *t*
N_c	rpm	The theoretical speed at which a single ball loaded into the mill starts to stick against the mill wall (critical speed)
N_0	-	Reflect the change in ball size and from batch to full-scale milling; default value is 1
N_1	-	Reflect the change in mill diameter and from batch to full-scale milling; default value is 0.5
N_2	-	Reflect the change in mill diameter and from batch to full-scale milling; default value is 0.3
N_3	-	Reflect the change in ball size and from batch to full-scale milling; default value is 2
N_4	-	Represents the adjustment needed to account for larger mills; its default value is 0.2
N_r	rpm	angular speed of grinding mill
p	Kg/m^3	Bulk density of the charge

$P_i(t)$	%	Fraction by weight in the mill charge less than size X_j at the short grinding time t
$P_{imodel}(t)$	%	Predicted mass fraction retained on size screen *x* after grinding of single-sized material of initial size *x* for a total grinding time *t*
P_{net}	Watts	Net power draw by the mill
Q_i	-	The correction factor which is 1 for small particles and less than 1 for the particles too large to be fractured by grinding media in Equation 2.13
ϕ_c	%	Mill speed expressed as a fraction of theoretical critical speed
Φ_j	%	Fraction of fines produced in a single fracture event. It is dependent on the material being crushed
γ	-	Breakage function parameter which is material-dependent in Equation 2.27
δ	-	Breakage function parameter which is material-dependent in Equation 2.28
R^2	-	Coefficient of determination
r_i	m	The inner radius of the ball charge
r_m	m	The internal radius of the mill
θ_T	m	the toe of the ball media charge
θ_s	m	the shoulder of the ball media charge
S_i	min^{-1}	Rate of breakage of size *i*
S_j	min^{-1}	Rate of breakage of size *j*
$S_{j,slow}$	min^{-1}	Slow breakage rate of size *j*
$S_{j,fast}$	min^{-1}	Fast breakage rate of size *j*

T	-	Denotation of batch grinding parameters in Equations 2.14 to 2.19
t	min	Grinding time used in batch mill
U	%	Volumetric fraction of space between grinding balls at rest filled by powder
X_0	mm	Standard size equals to 1 mm
X_i	mm	Lower screen size of the particle size interval *i*
X_{i+1}	mm	Upper screen size of the particle size interval *i*
X_j	mm	Lower screen size of the particle size interval *j*
X_{j+1}	mm	Upper screen size of the particle size interval *j*

Chapter 1 Introduction

1.1 Background

Milling is generally the second stage of comminution or particle size reduction used in mineral processing after crushing. The process finds wide use in industries such as mining, fine chemicals, food manufacturing, aerospace, automobile, nanotechnology, cement, pigments, and pharmaceuticals (Charkhi et al., 2010; Frances et al., 1996; Han et al., 2016; Kwon et al., 2014; Zhao et al., 2017). Milling can be dry or wet depending on the nature of the feed material (Frances et al., 1996; Kotake et al., 2011; Ozkan et al., 2009) or end-product target requirements.

In mineral processing, the principal objective of comminution in general and ball milling in particular is to liberate the mineral of interest from the unwanted minerals (Wills and Napier-Munn., 2005; Zhao et al., 2017). The level of size reduction depends on the demand for a particular product size range and subsequent separation processes. In the case of ball milling, a cylindrical vessel loaded with loose spherical grinding balls is used. The rotating motion imparted on the mill shell allows the grinding media to tumble and break ore particles by a combination of impact, compression, and attrition. Impact breakage occurs when grinding media come into forcible contact with each other. Breakage by compression and attrition arises primarily due to the frictional force caused by grinding balls rubbing against one another.

The three breakage mechanisms experienced inside a ball mill as a result of the tumbling motion of grinding media are illustrated in Figure 1.1. Breakage by attrition and compression generally leads to the production of fine material while impact breakage generates a coarser product (King, 2001).

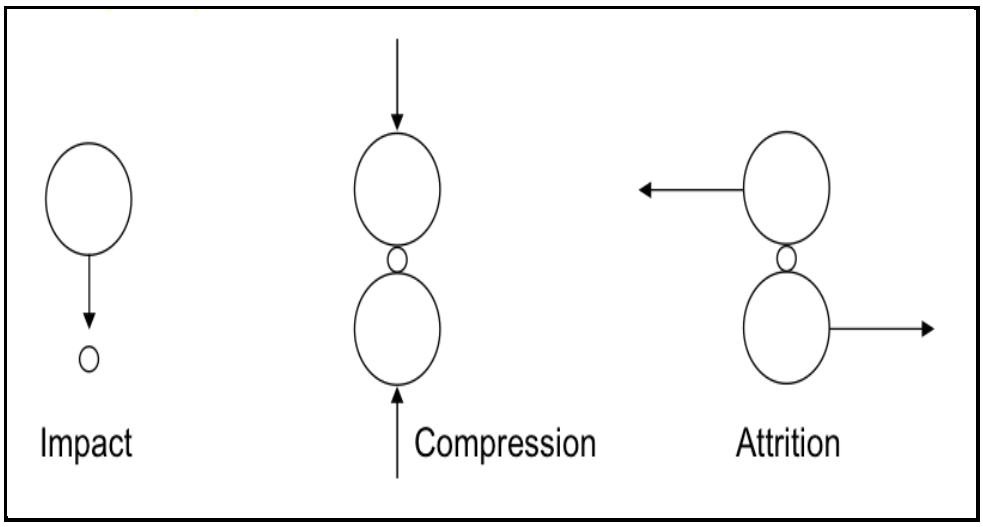

Figure 1.1 Breakage mechanisms occurring in ball mills: bigger circles represent grinding balls and small circles represent ore particles (Chierigati, 2001)

The relative contribution of the three mechanisms to breakage is to a large extent dependent upon the rotational speed of the ball mill (Gupta and Yan, 2006). Indeed, low mill speed results in a rolling motion of the media charge known as cascading motion. This motion engenders high levels of friction between grinding balls and ore particles. An environment is then created where breakage by attrition and by compression is more prevalent with less-to-no impact breakage. Here, attrition is due to the rubbing of ore particles between grinding balls as shown in Figure 1.1. Compression, on the other hand, is generated by the weight of the media charge applied against the mill shell with particles caught between balls and shell. As mill speed is increased, a fraction of the media charge is thrown in the air in free-fly motion before landing around the lower region of the cascading load or toe (See Figure 1.2). This is known as the cataracting motion of the media charge responsible for impact breakage. Note that the abrasion zone indicated in Figure 1.2 represents the zone of the cascading media charge experiencing breakage by abrasion. The reason for this is that the terms abrasion and attrition have been used loosely and interchangeably in several textbooks and references (Kelly and Spottiswood, 1982; King, 2001; Wills and Napier-Munn, 2005).

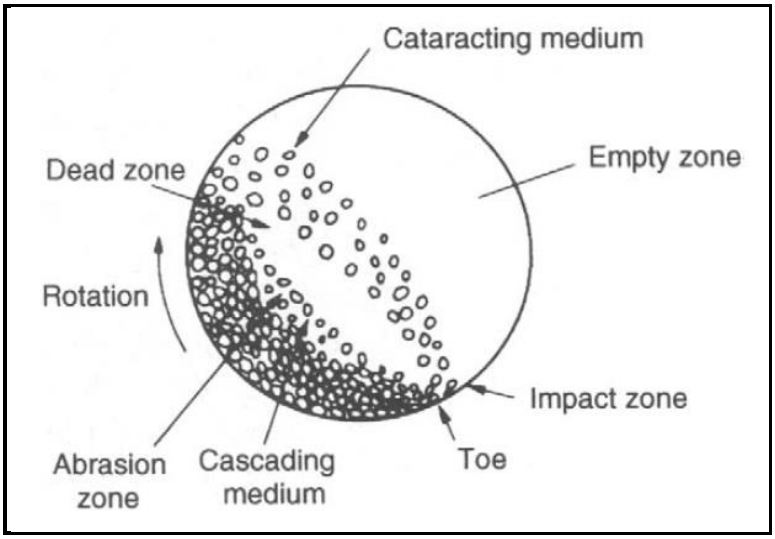

Figure 1.2 Motion of the media charge of a ball mill with the abrasion zone referring to the cascading zone of attrition breakage (Wills and Napier-Munn, 2005)

A further gradual increase in rotational speed incurs increasing cataracting and decreasing cascading. Eventually, the charge tends to cling on the mill wall in what is referred to as a centrifuging motion of the charge. The theoretical speed at which one grinding ball gets stuck against the mill shell is known as the critical speed. The rotational speed of a ball mill is generally quoted as a fraction of the critical speed.

It is evident from the above that mill speed plays a big role in the internal motion of the charge and hence towards breakage. At low speeds or speeds below 50% of the critical speed, attrition and compression are prevalent with high production of fine particles. For high speeds or speeds above 90% of critical, no breakage occurs due to the centrifuging charge. Note that ball mills in the minerals industry are commonly operated between 65% and 90% of critical where impact breakage is considered to be the highest. This research intends to ascertain whether low speeds can yield any benefit in terms of energy consumption as a result of attrition and compression breakage.

1.2 Statement of the research problem

Ball milling is notoriously known to be an energy-inefficient process with high levels of energy consumption for limited output (Bouchard et al., 2017). As a result, many efforts have been made to optimize various parameters that influence efficiency. Factors affecting ball milling performance include rotational speed, slurry density, ball size, ball shape, liner profile, and mill operational design to name a few. The rotational speed has been identified among these factors as a key parameter that can substantially influence the efficiency of a ball mill (Charkhi et al., 2010; Frances et al., 1996).

The effects of mill speed on breakage have been extensively studied and modelled between 50% and 90% of critical (Austin et al., 1984; Deniz, 2013; Petrakis et al., 2017). Yet, it is in this speed range commonly used in mineral processing that mills have been reported to be inefficient. While near-centrifuging speeds above 90 % of critical produce no grinding, mills run at low speeds can still achieve breakage by attrition and compression. The latter conditions may require prolonged milling time before sufficient fine particles are produced. However, it is to be established whether meaningful breakage can be incurred without limited use of energy. It becomes therefore crucial to understand the relationship between breakage and energy consumption at a low rotational speed. In this dissertation, the breakage rate of UG2 a platinum-bearing ore in a batch mill was investigated. The endeavour is expected to provide answers to how energy is expended during breakage by attrition and compression.

1.3 Aim and objectives of the research

The aim of this dissertation is primarily to evaluate the effects of mill speeds below 50% of the critical speed on the grinding kinetics of a platinum-bearing ore known as

UG2. The need for the research stems from the limited availability of literature on milling at low rotational speeds. And since power drawn by a ball mill increases with the rotational speed before dropping at near-centrifuging speeds (Gupta et al., 2006), there may be economic and energy incentives to operate ball mills at low speeds. However, the effort required to achieve the target grind should be established.

The three key research objectives pursued in line with the abovementioned aim of the study are as follows:

- Monitor the milling kinetics of the UG2 ore under batch conditions at selected speeds below 50% of critical using the one-size-fraction method.
- Determine the breakage and selection function parameters of the UG2 ore from the batch grinding data collected.
- Estimate the performance of the batch mill at the selected speeds in terms of energy expenditure and quality of the final grind.

It is important to point that the UG2 ore was selected for use in experimental batch test work. This platinum-bearing ore is found in South Africa in the Upper Group 2 reef or UG2 for short. The UG2 is one of the platinum-rich layers of the South African Bushveld Complex; it accounts for 60% of platinum reserves (Cawthorn, 1999). However, a lot of energy is required to liberate the ore from the rock matrix and reach a fineness of about 80% passing 75 µm (Wills and Napier-Munn, 2005). This is the main reason that motivated the use of the UG2 ore for experimental testing. As such, it is hoped that the benefits of low-speed-operated mills may further be explored for the efficient recovery of platinum group metals (PGMs). Note that the phrase “low speed” has been used in this dissertation to refer to fractional speeds below 50% of the critical speed.

1.4 Research questions

A lot of work has been reported on batch milling under industrially accepted conditions (Austin et al., 1984; Petrakis et al., 2017; Tangsathitkulchai, 2003). However, little has been reported on unusual operating conditions such as low rotational speeds. Yet, low speeds may have the advantage of fine milling with associated low energy consumption (Metzger et al., 2011). It is in line with this that the following research questions were formulated:

- How does the low rotational speed of a ball mill affect the breakage kinetics of the ore?
- Can the linear time population balance model be used and extended to applications involving ball mills operated at low speeds?

A secondary aspect resulting from the research questions above has been that of looking at how efficient milling is at low speed. The widely accepted size-specific energy (SSE) was used as an indicator of energy efficiency in tumbling mills (Ballantyne et al., 2014). A cut-off grind size set at 75 µm was considered in line with the product size specifications of UG2 ore in the South African industry. In doing so, it was possible to investigate energy consumption while accounting for the final grind size. In the end, a comparison was done to determine whether energy is better utilised when breakage is done by attrition and compression than when impact breakage is predominant.

1.5 Layout of the dissertation

The present research is organised in six chapters starting with chapter one being the introduction. It comprises background, research problem, research questions, aim and objectives of the study.

The literature review is given in chapter two. Factors affecting ball mill performance, milling kinetics modelling, the power draw of ball mills and ball mill benchmarking are

covered in this chapter. It was noted from the literature review that limited work has been done on the effects of mill speed on the breakage behaviour of UG2 ore specifically at low speeds.

Chapter three describes in details the materials, equipment and method used to conduct the experiments. A great deal is devoted to presenting the batch grinding tests carried out following standard experimental protocols. Difficulties encountered during laboratory work are finally stated.

Chapter four features the full description of the results and logical explanation of the obtained results. Population balance model is used as an approach to the analysis of batch grinding data. The UG2 ore is characterised in terms of breakage rate and breakage function parameters.

Chapter five covers the discussion of the results and the significance of the findings. Milling performance is reported in terms of the so-called “size-specific energy” and grind.

Chapter six is a wrap-up of the research providing concluding remarks and recommendations for future work.

Chapter 2 Literature review

2.1 Introduction

Comminution is a term used in mineral processing for ore size reduction. The main purpose of comminution is to liberate valuable minerals from the gangue minerals. In nature, minerals are usually found locked inside the rocks hence the need to be liberated. Comminution is generally done in two stages: crushing and milling. Wills and Napier-Munn (2005) defined crushing as "the first stage in the process of comminution and milling as the last stage".

A milling system is classified based on the grinding media employed in its operation or according to the motion of its charge. In terms of grinding media used, a mill can be classified as ball mill, rod mill and autogenous mill based on the use of the ball, rod and coarse rocks as grinding tools (grinding media). In terms of charge motion, a mill can be classified as tumbling or stirred mill. In a tumbling mill, the mill shell is rotated whereas, in a stirred mill, the mill shell is stationary while a motion is imparted to the charge by the movement of an internal stirrer. The other types of mills include vibratory, centrifugal, table and roller mills. For the purpose of this study, the ball mill is employed.

A ball mill is an example of a tumbling mill system; it exists in different sizes from laboratory scale to industrial scale. Its function may be regarded as the most important in the comminution process since it is usually required at the final stage of ore grinding. Several factors affect ball mill efficiency. These are discussed in the next section. The performance of a mill can be determined by the energy that it is using and the efficiency of breakage. In mineral processing, this is known as a high energy-consuming vessel. Population balance model (PBM) is recently used as a technique to evaluate the performance of mills. It uses the concept of breakage function and

selection function. This chapter covers factors affecting mill performance, modelling breakage mechanisms of the particles, the power draw of ball mills and benchmarking ball mill performance.

2.2 Factors affecting milling performance

Several factors influence the efficiency of a ball milling. These include ball filling (Deniz, 2012 & 2016) and powder filling (Deniz and Onur, 2002; Tangsathitkulchai, 2003), critical speed (Mulenga and Moys, 2014; Deniz, 2004), slurry concentration (Tangsathitkulchai, 2003; Mulenga et al., 2016) and ball size (Cho et al., 2013; Erdem et al., 2009). In this section, we are going to discuss ball filling, powder filling, ball size, mill rotational speed, feed size distribution and slurry density.

2.2.1. Ball filling

Ball filling is one of the most influential factors that affect the performance of a mill. It refers to the volume occupied by the bulk ball charge at rest in a mill including about 40% of this volume taken by the void space between balls (Frances et al., 1996; Austin et al., 1984). Ball filling, *J*, is defined as the fraction of the volume of the bulk media charge to the volume of the mill (Austin et al., 1984; Zhao et al., 2017). The following formal definition applies to ball filling:

$$J = \frac{Volume\ of\ balls}{Internal\ volume\ of\ mill}\ \frac{1}{1-0.4} \qquad \textbf{(2.1)}$$

The tumbling action and the rate of breakage depend on how much the mill volume is filled by the balls. For efficient milling, ball volume is usually 40 – 45% of the internal mill volume (Wills and Finch, 2015)

2.2.2. Powder filling

The fraction of the mill filled by the powder bed, f_c, is given by (Austin et al., 1984):

$$f_c = \frac{Volume\ of\ powder}{Internal\ volume\ of\ mill} \quad \textbf{(2.2)}$$

On the other hand, the ratio of the volume of powder to the volume of the grinding media at rest is known as powder filling, U. To relate powder loading to ball loading, the bulk volume of powder is compared to the formal porosity of the ball bed as follows (Deniz and Onur, 2002):

$$U = \frac{f_c}{0.4\ J} \quad \textbf{(2.3)}$$

Thus, powder filling, U, is the volumetric fraction of space between grinding balls at rest (assumed to be 0.4) that is filled or occupied by powder (Austin et al., 1984). Powder filling should not be under-filled or overfilled. When under-filled, leads to steel to steel conduct resulting in high energy consumption and the wearing of mill shell and grinding media, and when overfilled leads to powder cushioning which decrease the efficiency of breakage. Austin et al. (1984) recommended powder filling between 0.6 and 1.0 to be the most efficient in ball milling.

2.2.3. Ball size

The diameter and shape of grinding balls have been reported to have a profound influence on milling efficiency (Cho et al., 2013; Simba and Moys, 2014). The efficiency of grinding depends on the surface area of the grinding medium. Ball size commercially available for charging in grinding mills range from 10 mm to 150 mm. Determining the size of balls to be charged depends on the required size of the product, large balls for the coarse size and small balls for fine size (Cho et al., 2013). Usually, a range of sizes is added, which has been found to produce better grinding efficiency than single-sized balls (Cho et al., 2013). By so doing, the space between

the larger balls is filled with smaller sized balls which promote grinding efficiency. The charge should be graded such that the largest balls are just heavy enough to grind the largest and hardest particles in the feed.

2.2.4. Rotational speed

It is common practice in the mining industry to rate the rotational speed of a mill as a fraction of its critical speed. The critical speed is the theoretical speed at which a single ball loaded into the mill starts to stick against the mill wall. It is calculated in revolutions per minute (rpm) as follows (Austin et al., 1984):

$$N_c = \frac{42.3}{\sqrt{D-d}} \qquad \textbf{(2.4)}$$

Where D is the diameter of the mill in meters and d is the diameter of the largest ball loaded to the mill in meters.

The speed at which a mill runs is important since it governs the nature of the product and the wear rate experienced by the shell liners as well as the grinding balls. The tumbling action inside the mill also depends on mill speed. Gupta and Yan (2006) were able to argue that in practice mills should be driven at 50 – 90% of the critical speed with the choice being influenced by economic considerations.

2.2.5. Feed size distribution

The effect of particle size has been investigated as one of the factors affecting the breakage characteristics of the material (Tavares and king, 1998). It has been observed that bigger particles break more easily than small particles. The low strength in large particles is due to the flaws, pores and grain boundaries that are found. The number of flaws decreases with decreasing particle size. The larger the flaw, the

smaller the force or energy required to crack the particle. The findings were confirmed by Tavares and King (1998) as seen in Figure 2.1.

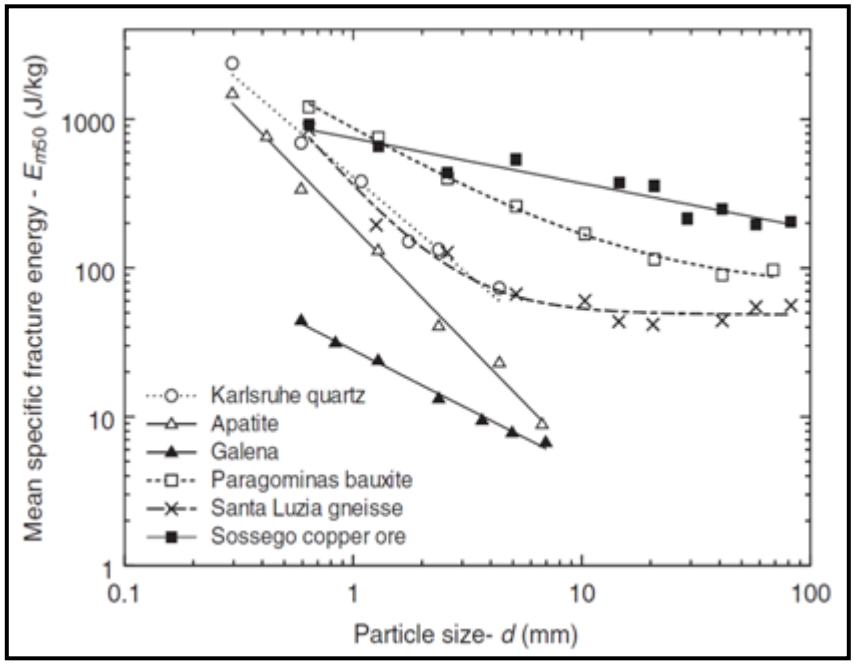

Figure 2.1 Variation of median particle fracture energy with particle size for various materials (Tavares and King, 1998)

It is clear that the energy needed to break particles decreases with increasing particle size. This suggests that energy has to be increased in order to break finer particles.

2.2.6. Slurry density

The slurry density or slurry concentration of the feed should be such that it exhibits features that show the consistency of ease of flow through the mill. Highly dense slurry causes decrease in size reduction efficiency (Frances et al., 1996) while too dilute slurry may cause the metal to metal contact, resulting in high steel ball consumption and reduction in efficiency. To mitigate all the above, ball mills should operate between 65% and 85% solids by weight depending on the ore to achieve good grinding efficiency (Tangsathitkulchai, 2003).

2.3 Modelling framework of ball milling

The discrete-size continuous-time "Population Balance Model" (PBM) is rate-mass balance model which has found extensive use in simulation, control and optimisation of various particulate processes. It has been proven to be an excellent tool in comminution process for prediction and simulation of the evolution behaviour of the particle size distribution (Austin et al., 1984; Chimwani et al., 2014; Petrakis et al., 2017; Zhao et al., 2017). The PBM can also elucidate the breakage mechanisms such as massive fracture, cleavage and attrition (Bilgili et al., 2004). PBM is employed in the creation of batch grinding equations. The selection function and breakage distribution function are the two common grinding kinetics functions used for the construction of the batch grinding equation. The parameters for the breakage rate define the rate at which a material is broken out of a given quantized size class, while the parameters for the breakage distribution characterize the fraction of the primary breakage output in the feed size class j which appears in the interval i of the smaller size class. Several size intervals described by a $\sqrt{2}$ screen sequence define the range of particle size class of interest from the top size interval 1 to the sink which refers to the n^{th} interval.

2.3.1 Batch milling equation

In preparation of a batch grinding, a mono-sized feed particle is prepared to evaluate the breakage kinetics. The procedure is known as the one-size-fraction method (Austin et al., 1984). In this method, the top size of the starting feed charge is kept constant and milled at a time t_1, then particle size distribution analysis performed by sieving and weighing. The same sample is then returned for milling at time t_2 and re-analysed and so on. In so doing, the disappearance rate of the feed size particles j is monitored and the appearance of product size distribution i is determined which is said to be performing rate-mass balance.

It is widely accepted that milling follows a first-order kinetics similar to chemical reactor design for size class j defined between two successive screens x_{j+1} (upper screen) and x_j (lower screen) (Ipek et al., 2005; Matija et al., 2010; Acar et al., 2013; Petrakis et al., 2017). In other words, the rate of breakage of particles of size j is proportional to the mass M_j in the size class j (Austin et al., 1984):

$$\frac{dM_j(t)}{dt} = -S_j M_j(t) \quad \textbf{(2.5)}$$

Where $M_j(t)$ is the mass fraction of size j particles in the mill feed at grinding time t and S_j is the specific rate of breakage of size j. If S_j is constant during the course of grinding, the breakage is said to be ''first order'' (Austin, 1972). The integrated equation is given as:

$$M_j(t) = M_j(0)e^{[-S_j t]} \quad \textbf{(2.6)}$$

Therefore, a plot of log $M_j(t)$ versus t should give a straight line, if grinding proceeds in a first-order manner and the rate of breakage S_j, can be determined from the slope of the plot (Austin et al., 1972). The relationship is illustrated in Figure 2.2.

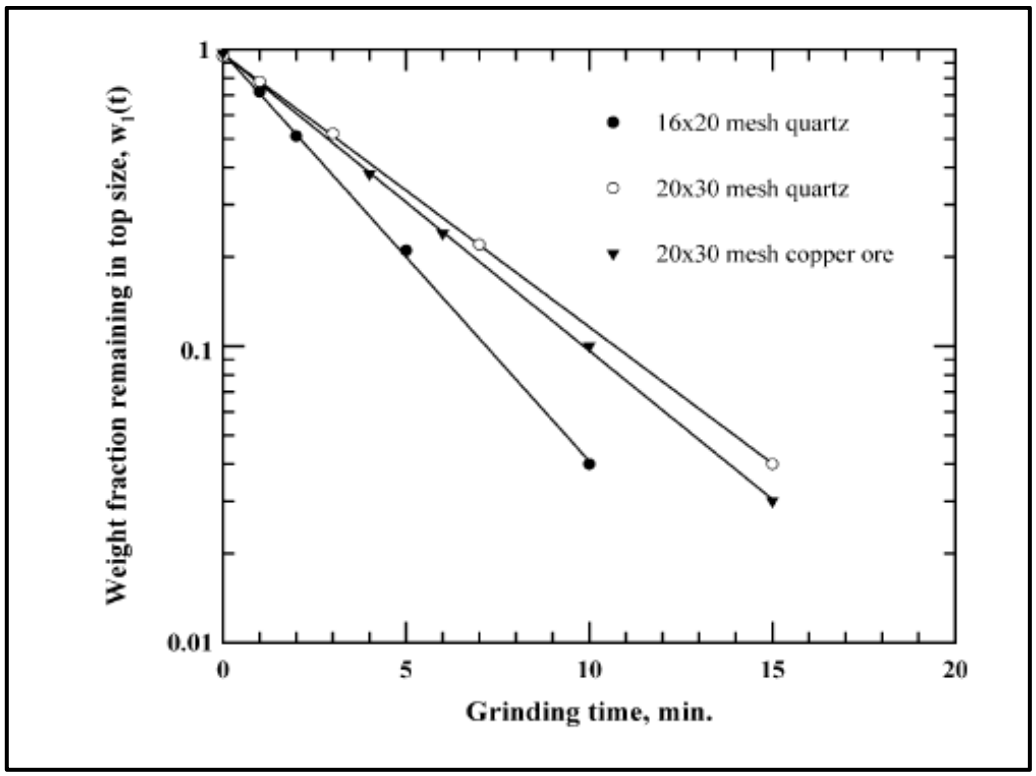

Figure 2.2 Illustrations of first-order plots for batch dry grinding of single-sized fractions copper and quartz ore. Experimental conditions: J = 0.3; U = 1.0; d = 25.4 mm; ϕ_c = 0.70 of critical speed (Tangsathitkulchai, 2002)

Figure 2.2 shows the breakage kinetics of dry grinding quartz and copper ore with their respective mono-sized feed breaking in a first-order manner. It can be seen that the straight line is produced and the rate of breakage can be determined by the slope of the line considered to be constant.

Another important breakage parameter is known as "the primary breakage distribution", $b_{i,j}$, which is the set of daughter fragments produced by the first breakage of size *j*. The breakage function has to be analysed at a short grinding time before re-breakage of these products (Austin et al., 1984). Thus,

$$\sum_{i=n}^{j+1} b_{i,j} = 1, \ i > j \qquad \textbf{(2.7)}$$

By performing a rate-mass balance or population balance on material in size interval *j* present at time *t* in a mill,

$$\frac{dM_i(t)}{dt} = -S_i M_i(t) + \sum_{j=1}^{i-1} b_{i,j} S_j M_j(t), \quad n \geq i \geq j. \qquad \textbf{(2.8)}$$

Equation (2.8) is the typical batch grinding equation usually refers to as the "basic rate-mass balance" for a first-order grinding system. The net rate of the production of size i material equals to the sum rate of the appearance of all larger sizes minus the rate of its disappearance by breakage. The solution to this set of differential equations provides a prediction of the product size distribution at various grinding times, provided the starting feed size mass $M_j(0)$, for given values of S_j and $b_{i,j}$ (determined experimentally) is known.

2.3.2 Non-linear breakage kinetics

The deviation of first-order breakage is observed in some cases (Herbst et al., 1973; Austin et al., 1984; Gupta, 1987; Tangsathitkulchai and Austin, 1985; Fuerstenau et al., 1990; Rajamani and Verma, 1991), therefore, non-linear equation of the population balance was determined to describe the breakage (Tangsathitkulchai, 2002; Austin and Bagga, 1981; Bilgili and Scarlet, 2005). Bilgili and Scarlet (2005) introduced the acceleration-deceleration parameter *(k*) in the disappearance rate Equation (2.6) to explain the deviations. The non-first-order model was expressed as:

$$M_j(t) = -M_j(0) e^{[-S_j t(1+kt/2]} \qquad \textbf{(2.9)}$$

The factor $k = 0$ for normal first-order grinding; $k > 0$ for grinding with acceleration effect; and $k < 0$ for grinding with deceleration effect.

The first-order kinetics is not a fixed law, like in chemical reaction engineering. One can use the nth-order kinetics as opposed to first-order kinetics (Fogler, 1992). In the

case where material consists of fast and slow breakage, is considered as second- order law and can be formulated as follows (Austin et al., 1977):

$$M_j(t) = M_j(0)e^{[-S_{j,slow}(t)]} + [1 - M_j(0)]e^{[-S_{j,fast}(t)]} \quad \textbf{(2.10)}$$

Where $M_j(t)$ is the mass fraction retained at top sieve class after breakage at time t, $M_j(0)$ is mass before breakage, $S_{j,slow}$ and $S_{j,fast}$ is the rate of breaking material at slow and fast breakage region respectively.

Austin et al. (1984) suggested that if the degree of first-order deviation is not large, the effective mean rate of breakage can be defined. It is determined by finding the time required to break 95% of the feed material and substitute it in Equation (2.6) to calculate the value of the selection function.

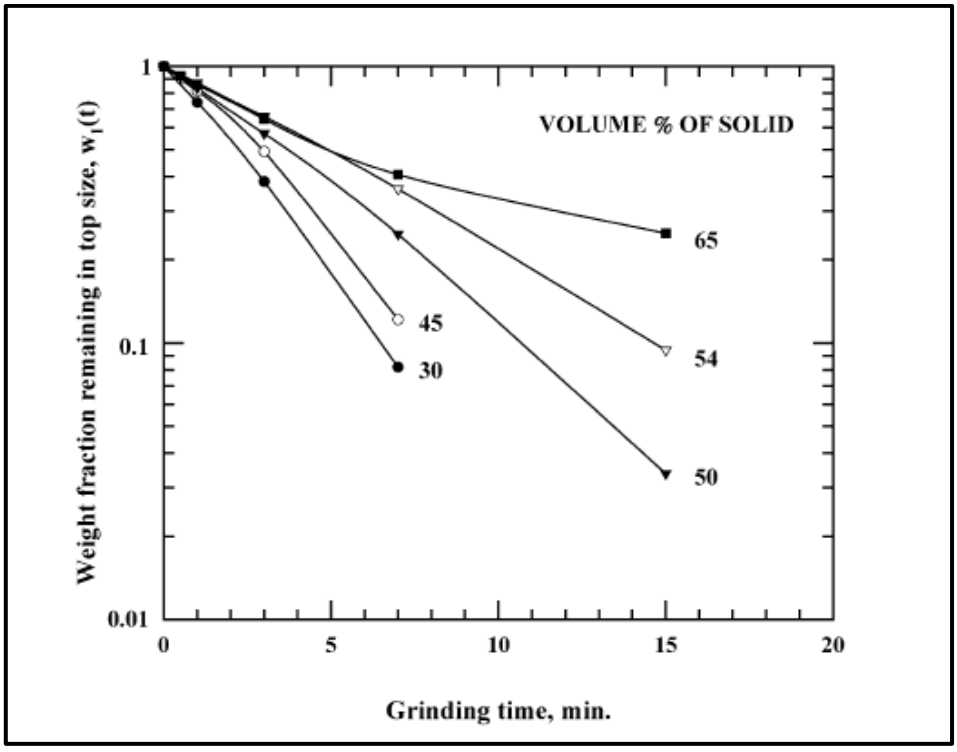

Figure 2.3 Illustrations of deviation of first-order law for batch grinding at various slurry concentrations. Experimental conditions: J = 0.3; U = 1.0; d = 25.4 mm balls; and ϕ_c = 70% of critical (Tangsathitkulchai, 2002)

Figure 2.3 illustrates the deviation of first-order breakage. Acceleration or deceleration of the breakage rate occurs depending on the grinding conditions such as operating parameters and material properties. The plots of the first-order for wet grinding quartz over varying slurry concentrations are shown. According to Figure 2.3, it can be seen that the breakage of the top size fraction strays from the typical first-order postulation, the specific breakage rate being accelerated as the size becomes smaller. However, at higher concentrations of the solid, the extent of the rate of acceleration seems to reduce. This explains the deceleration in the specific breakage rate when the concentration of the slurry becomes very high.

2.3.3 Selection function

When a ball mill is operated in a batch mode, it is compared to a closed reactor in which none of the material is going in or out during the grinding process, resulting in all material contained in the mill being exposed to equal grinding time. The fractions of the material that will be broken per unit time represent the rate of breakage or the selection function (S_j).

The selection function has also been shown to be dependent on the particle size. Figure 2.4 shows the variation of rate of breakage with particle size x_{j+1} (the upper size of the j class interval) consisting of single size feed.

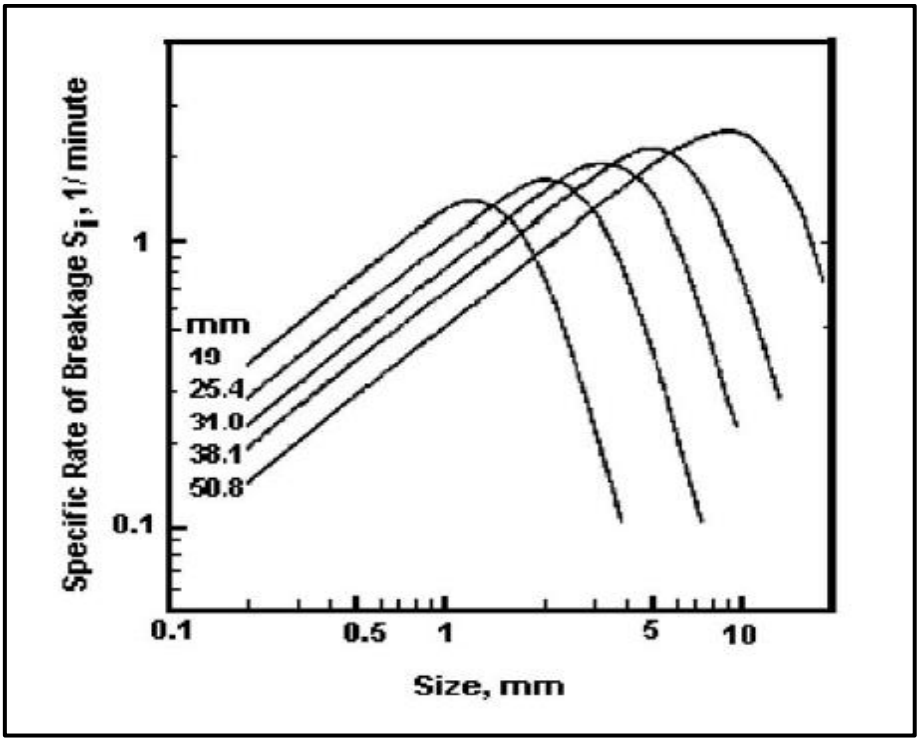

Figure 2.4 Variation of the rate of breakage with feed size for various ball diameters (Austin et al., 1984)

Equation (2.12) below is used to describe the observation in Figure 2.4 (Ipek et al., 2005; Petrakis et al., 2017):

$$S_j(t) = a_0 \left(\frac{X_{j+1}}{X_0}\right)^{\alpha} Q_i \qquad \textbf{(2.12)}$$

Where a_0 is the specific rate of breakage at the standard size X_0 = 1 mm; X_{j+1} is the upper limit of size class *j*; α is a parameter characteristic of the material milled. Q_i is the correction factor which is 1 for small particles (i.e. normal breakage) and less than 1 for the particles too large to be fractured by grinding media (i.e. abnormal breakage). It can be estimated as follows:

$$Q_i = \frac{1}{1+\left(\frac{X_{j+1}}{\mu}\right)^{\Lambda}} \qquad \textbf{(2.13)}$$

With μ being a parameter dependent on milling conditions while Λ is a material-dependent parameter showing how rapidly the breakage rate decreases with particle size.

The value of α is a positive value, normally in the range 0.5 to 1.5 providing the test condition are in the normal operating range but the value of a_0 varies with milling conditions (Austin et al., 1984).

It is shown in Figure 2.4 that the breakage rate (S_j) increases with size and starts to decrease for larger sizes. The maximum occurs in the rate of breakage because as the particles get larger, they are difficult to be nipped by the balls. For large sizes, it was found that the disappearance of material from given top size interval j is often not first order, but appears to have faster initial rate and slower following rate. It might be argued, however, that the increased breakage rate of the top size particles might be associated with the change in breakage mechanism probably due to the top size fraction becoming weaker as grinding proceeds. We refer to the first-order breakage of fine material as normal breakage and non-first-order breakage of large particles as abnormal breakage.

It has also been shown by many researchers that the breakage rate of a given size fraction changes with mill design and operating conditions (Oliveira and Tavares, 2018; Mulenga et al., 2016; Chimwani et al., 2014). In that case, Equation (2.12) and can be generalised as (Herbst and Fuerstenau., 1980):

$$S_j = a_{0T}\left(X_{j+1}\right)^{\alpha} \frac{1}{1+\left(\frac{X_{j+1}}{C_1\,\mu_T}\right)^{\Lambda}} C_2\, C_3\, C_4\, C_5 \qquad \textbf{(2.14)}$$

Where: $C_1 = \left(\frac{D}{D_T}\right)^{N_2} \left(\frac{d}{d_T}\right)^{N_3}$ **(2.15)**

$$C_2 = \left(\frac{d_T}{d}\right)^{N_0} \qquad \textbf{(2.16)}$$

$$C_3 = \left(\frac{D}{D_T}\right)^{N_1}, D \leq 3.81\ m \text{ or } C_3 = \left(\frac{3.81}{D_T}\right)^{N_1}\left(\frac{D}{3.81}\right)^{N_1-N_4}, D > 3.81\ m \quad \textbf{(2.17)}$$

$$C_4 = \frac{1+6.6(J_T)^{2.3}}{1+6.6(J)^{2.3}}\exp[-c(U-U_T)] \quad \textbf{(2.18)}$$

$$C_5 = \left(\frac{\phi_c-0.1}{\phi_{cT}-0.1}\right)\left(\frac{1+\exp\,[15.7*(\phi_{cT}-0.94)]}{1+\exp\,[15.7*(\phi_c-0.94)]}\right) \quad \textbf{(2.19)}$$

Equation (2.14) allows prediction of scale up selection function parameters of feed particle size class j based on batch laboratory data. Terms C_1 to C_5 in Equations (2.15) to (2.19), are correction factors applied during scale-up. In the full-scale mill, D is the mill diameter, d is the ball diameter, J the fractional mill filling, U is the powder filling, and ϕ_c is the fractional speed. Correspondingly, parameters D_T, d_T, J_T, U_T, and ϕ_{cT} represent the batch grinding conditions used in Equation (2.14). The parameter c contained in the expression for C_4 is usually taken to be equal to 1.2 for dry milling and 1.32 for wet milling (King, 2001), it is accounting for the changes from laboratory dry milling to industrial wet milling and Austin et al. (1984) proposed the value of c = 1.32 to be adequate when scaling up batch grinding data to wet full-scale milling.

Exponent factors N_0, N_1, and N_2 reflect the change in mill diameter and ball size from batch to full-scale milling; their default values are 1, 0.5, and 0.2 respectively. Parameter N_3 serves for the effects of ball diameter and has a default value of 2. Its value has been argued to depend on the material used (Kelsall et al., 1968; Yildirim et al., 1999; Austin et al., 2007; Napier-Munn et al., 1999; Katubilwa and Moys, 2009). Parameter N_4 represents the adjustment needed to account for larger mills; its default value is 0.2 (Austin and Klimpel, 1984).

2.3.4 Breakage function

Breakage function is defined as the weight fraction of broken products from size interval j which appears in size range i on primary fracture, i.e., before re-breakage of these products (Austin et al., 1984). In this approach, it is assumed that particle size

reduction is a sum of a recurring breakage. The breakage or appearance function is used to describe the distribution of sizes produced after a single step of breakage of a particle. Consequently, the comparative distribution of each size fraction after the breakage is recognized as a full depiction of the product. The primary breakage distribution functions of a particle of size j to size i are defined as follows (Austin et al., 1984):

$$b_{i,j} = \frac{Mass\ of\ particles\ from\ class\ j\ broken\ to\ size\ i}{Mass\ of\ particles\ of\ class\ j\ broken} \quad \textbf{(2.23)}$$

The fragments produced after a breakage event are mixed into a bulk of the powder and then return for breakage, in turn have a probability of being re-fractured. It is convenient to represent the set of primary daughter fragments, from breakage of size j as cumulative form (Austin et al., 1984):

$$B_{i,j} = \sum_{k=n}^{i} b_{k,j} \quad \textbf{(2.24)}$$

So that $b_{i,j} = B_{i,j} - B_{i+1,j}$ **(2.25)**

$B_{i,j}$ is the sum fraction of material less than the upper size interval i resulting from the primary breakage of the material of size j. Austin et al. (1984) have shown that the value of $B_{i,j}$ can be estimated from a size analysis of the product from a short grinding time of a starting mill charge predominantly in size j. This is summarised in what is known as the BII-method as follows:

$$B_{i,j} = \frac{\log\left[(1-P_i(0))\right]/\log\left[\left(1-P_i(t)\right)\right]}{\log\left[(1-P_{j+1}(0))\right]/\log\left[\left(1-P_{j+1}(t)\right)\right]}, \qquad n \geq i \geq j+1 \quad \textbf{(2.26)}$$

Where $P_i(t)$ is the fraction by weight in the mill charge less than size X_j at the short grinding time t. The breakage function $B_{i,j}$ is commonly described using the following empirical function (Austin, 1972):

$$B_{i,j} = \Phi_j \left(\frac{X_{i-1}}{X_j}\right)^{\gamma} + (1 - \Phi_j)\left(\frac{X_{i-1}}{X_j}\right)^{\beta} \quad \textbf{(2.27)}$$

Where $\Phi_j = \Phi_1 \left(\frac{X_i}{X_1}\right)^{-\delta}$ **(2.28)**

and δ, Φ_j, γ, and β are curve-fitting parameters dependent on the ore type (Teke et al., 2002; Ipek et al., 2005; Petrakis et al., 2017). There are also collectively known as the breakage function parameters.

Parameter Φ_j is the intercept at $\left(\frac{X_{i-1}}{X_j}\right)^{\gamma} = 1$ (see Figure 2.5 for reference); it represents the fraction of fines that are produced in a single fracture event. Parameter γ is the slope of the lower section of the $B_{i,j}$ curve and β is the slope of the steeper section of the $B_{i,j}$ curve as shown in Figure 2.5 (Austin et al., 1984).

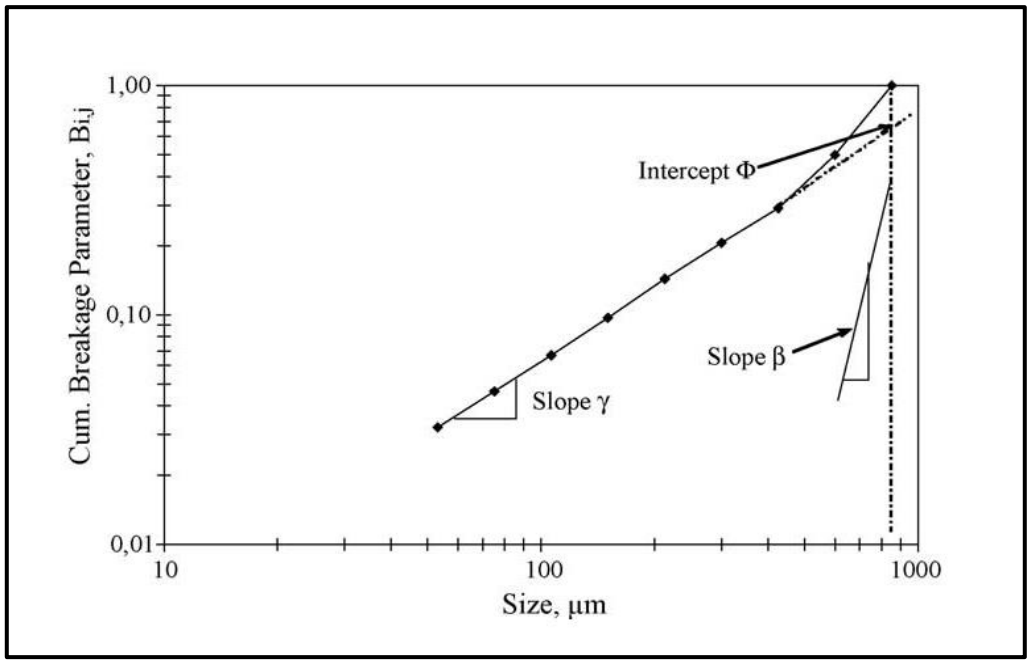

Figure 2.5 Primary breakage distribution function parameters for mono-sized feed fraction ground in the mill (Ipek et al., 2005).

The breakage function parameters do not need any scale-up if the material is considered normalisable, that is, if the parameter $\Phi_j = \Phi$ is constant for all breaking sizes (Austin et al., 1984).

2.3.5 Effects of rotational speed on ball milling

Many researchers have investigated the effects of speed on breakage behaviour of ores in ball mills (Gupta and Sharma, 2014; Austin et al., 1984; Deniz., 2013; Deniz, 2004; Ozkan et al., 2009; Fuerstenau., 1978). Breakage parameters are compared with a fraction of critical speed to evaluate the effect of speed on breakage rate. Milling conditions such as mill speed are usually compared with selection function parameters since for normalised material the breakage function parameters are not affected by changing mill operating conditions (Austin et al., 1984). Figure 2.6 shows the variation of the rate of breaking dolomite sample with a fraction of mill critical speed obtained by Fuerstenau (1978).

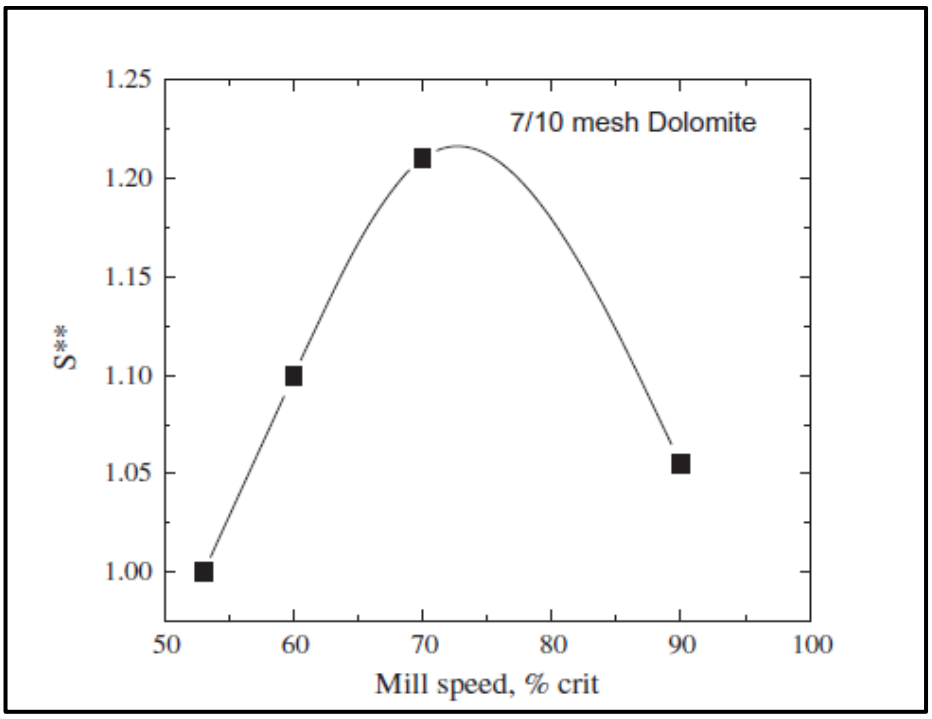

Figure 2.6 Variation of breakage rate with mill speed. Experimental conditions: D = 0.255 m, d = 25.4 mm, J = 0.5, and U = 1.0 (Fuerstenau, 1978)

It can be seen that selection function increases with mill speed and peaks around 75% of critical; this is followed by a drop. Ball mills have been experimentally found to be efficient at 75% of critical (Austin et al., 1984; Gupta and Sharma, 2014; Herbst and Fuerstenau, 1972).

Deniz (2004) also investigated the effects of speed on milling rate using limestone and clinker ore. Six mono-sized fractions were prepared and dry-ground in batch mode in a laboratory-scale mill. The speed of the mill varied between 55% and 95% of critical and milling was done for the various times between 1 and 18 min. The following testing conditions were maintained: ball size d = 25 mm; ball filling J = 20%; and powder filling U = 52.5%. His reported findings are summarised in Figures 2.7 and 2.8 where breakage rate is plotted as a function of mill speed and particle size respectively.

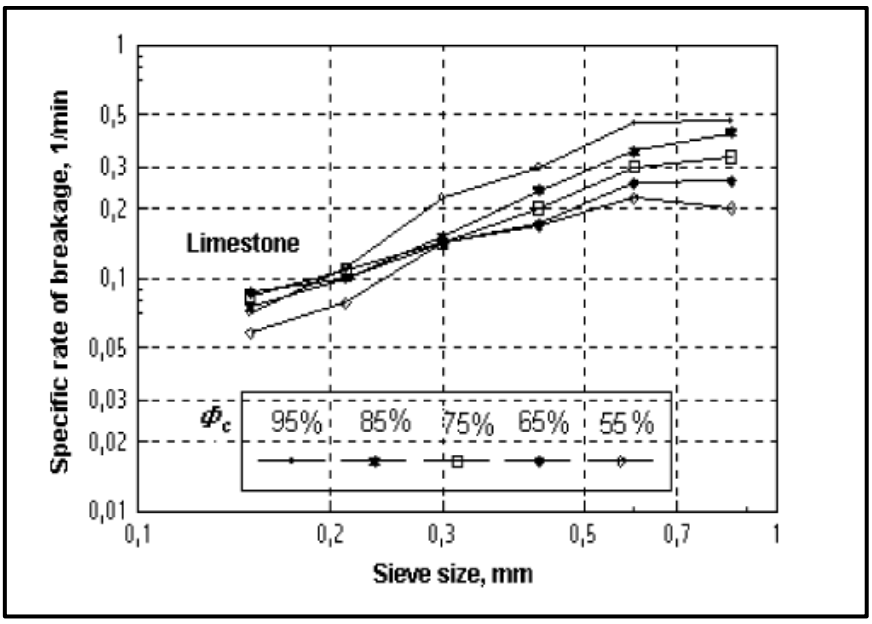

Figure 2.7 Specifics rate of breakage of limestone ore as a function of feed size for various speeds. Experimental conditions: D = 200 mm, d = 25 mm, J = 20%, U = 0.525 (Deniz, 2004)

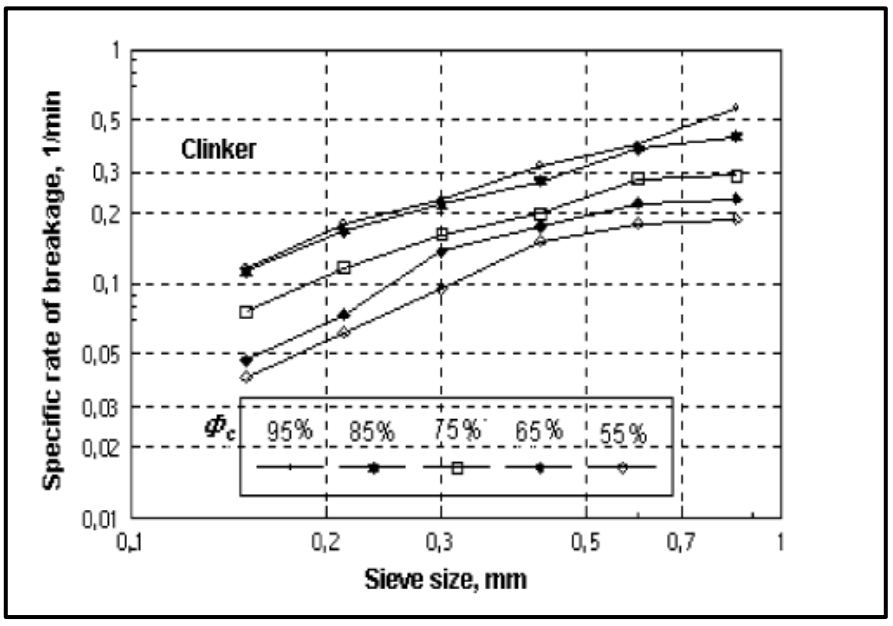

Figure 2.8 Specifics rate of breakage of clinker ore as a function of feed size for various fraction of critical speed. Experimental conditions: D = 200 mm, d = 25 mm, J = 20%, U = 0.525 (Deniz, 2004)

It can be seen from Figures 2.7 and 2.8 that the rate of breakage increases with speed for every size fraction considered and at all speeds. Unlike the consensus, Deniz (2004) found that optimum grinding occurs at 85% of the critical speed.

2.4 Theoretical power draw of a ball mill

Austin et al. (1984) defined power draw as "the energy expended per unit time to cause motion of charge in a mill". In comminution progressions, the power draw of a mill is one of the essential parameters to consider for its efficient operation (Datta et al., 1999). Power required depends on the hardness of the material, the feed size and final product size target. Ball mills are one of the greatest energy consumption equipment in mineral processing (Bouchard et al., 2017), which leads to high research on the effect of operating variables on mill performance. Mill load and rotating speed are the most parameters that affect energy consumption in ball mills (Morrell, 2016). Figures 2.7 and 2.8 illustrate the effects of mill speed and mill load respectively. The highlighted range indicates the usual range used in the industry. It can be seen that power drawn increased with speed. However, when the speed gets closer to the critical the power consumption starts to drop and material starts to centrifuge resulting in no grind.

It can also be seen from Figure 2.8 that more energy is required as the mass in the mill increases. For greater mill performance in terms of energy consumption, mill fillings should be kept low in the range of 20% to 45%.

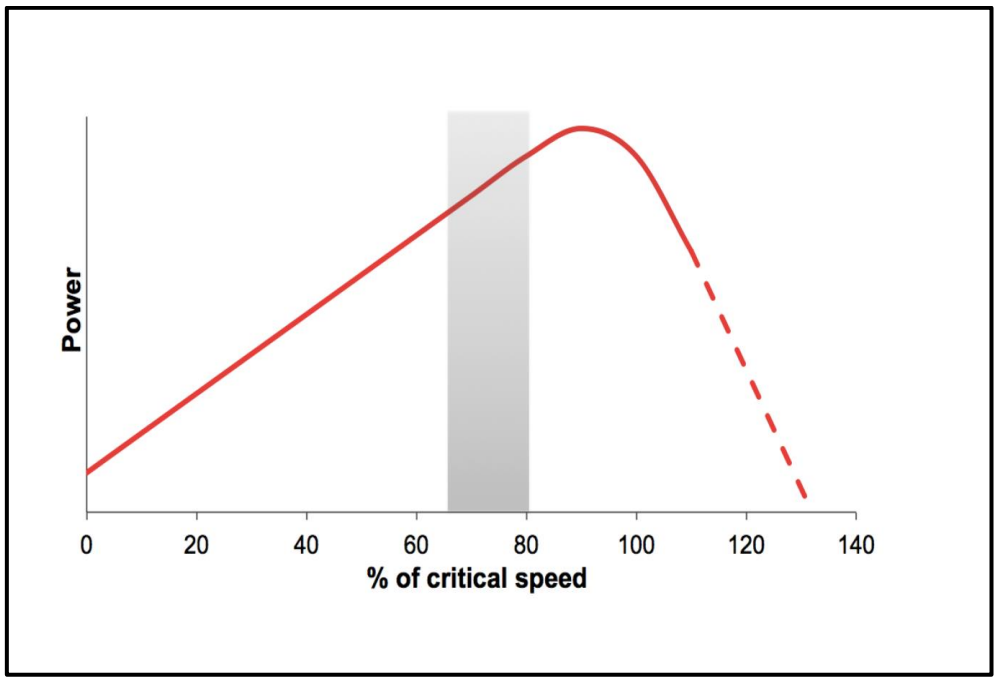

Figure 2.9 Variation of the power draw of a ball mill with its rotational speed (after Kelly and Spottiswood, 1982)

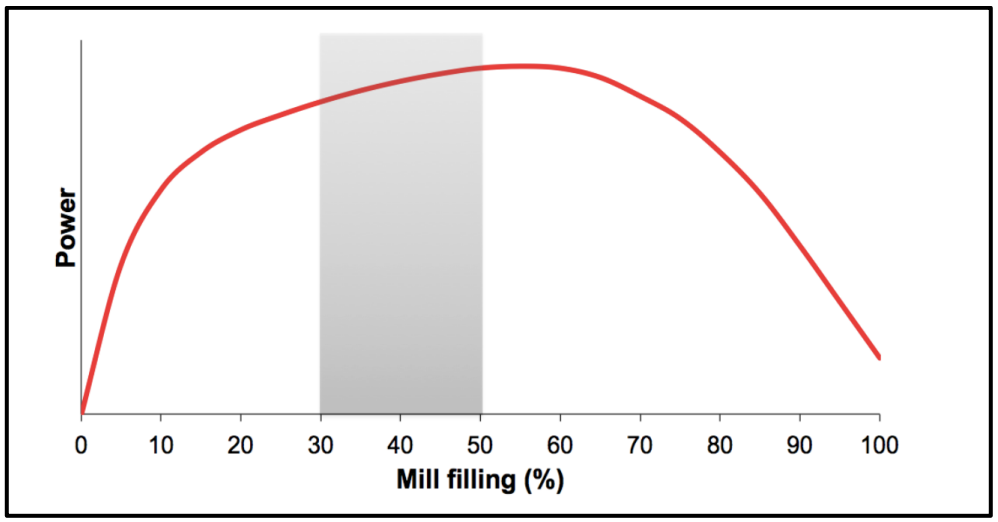

Figure 2.10 Effects of mill filling on the power draw of a ball mill (after Kelly and Spottiswood, 1982)

The mill power can be calculated by the following formula (Stamboliadis et al., 2011)

$$P_{net} = 9.9.M.N.D \qquad \textbf{(2.29)}$$

Where M is the total mass (kg) of feed material and balls, N is the rotational speed (rps), and D is the internal mill diameter of the mill (m).

The energy consumed by the mill is proportional to the time t and is given by:

$$E = P.t \quad \textbf{(2.30)}$$

Where P_{net} is the net power of the mill (W) estimated using Equation (2.29), t is the grinding time (s) and E is the net energy (J) consumed after grinding time t.

In past years, several researchers have developed models for the prediction of the power draw of a ball mill system. These include Hogg and Fuerstenau (1972); Arbiter and Harris (1982); and Morrell (1996). In the present dissertation, only Morrell's model of mill power draw is briefly presented owing to its accuracy.

The development of Morrell's power draw is based on empirical data from several industries mills. The theoretical model is regarded as the reference in comminution research despite its complexity (Napier-Munn et al., 1999).

In Morrell's power model, an angular ring was used to represent the region of the mill charge which drew power (Figure 2.11). The latter represented the rising bulk charge of the mill, neglecting cascading and cataracting material. The active zone of charge is assumed that it occupies the space between an inner radius and the mill radius. The extent of this zone is limited by the toe and shoulder of the charge. The power draw of a mill is given by (Morrell, 1996):

$$P = 2\pi gLp \int_{r_i}^{r_m} \int_{\theta_T}^{\theta_s} N_r r^2 cos\theta \; d\theta \, dr \quad \textbf{(2.31)}$$

Where g is gravitational acceleration; L is the mill length; p is the bulk density of the charge; N_r is the angular speed of a mill; r_i is the inner radius of the ball charge; r_m is the internal radius of the mill, θ_T and θ_s are the toe and shoulder of the ball media charge respectively.

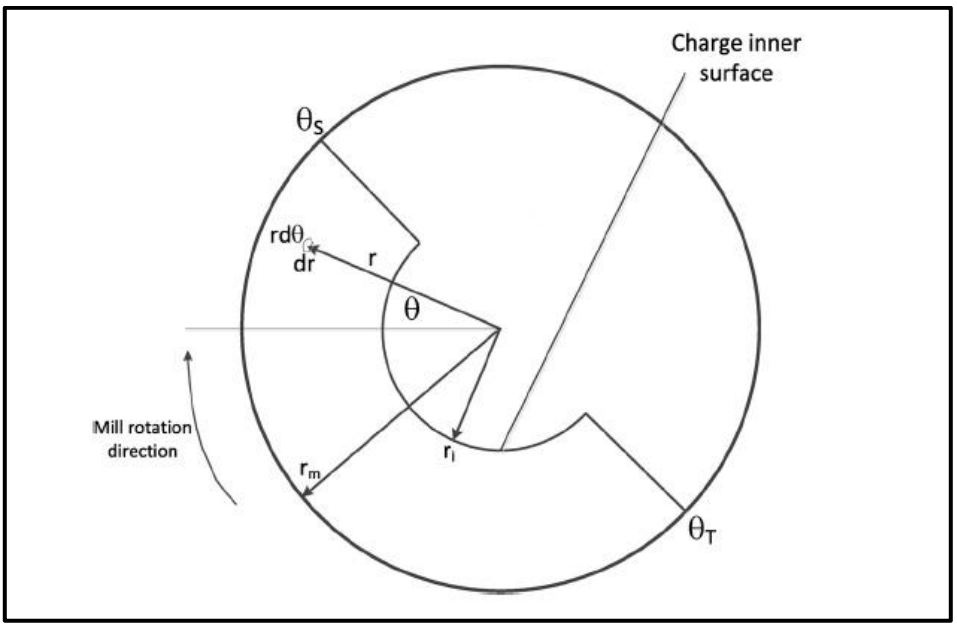

Figure 2.11 Load behaviour of a ball mill used in the derivation of Morrell's theoretical power model (Morrell, 1996)

Equation (2.29) works well at speeds below 60% of critical whereas Morrell's will be required for cataracting speeds (above 60% of critical).

2.5 Benchmarking the performance of ball mills

Benchmarking is the process of comparing one organization's processes and performance metrics to best practices from other organizations. The parameters usually measured are the quality, time, energy and cost. To achieve an effective benchmark, a clear understanding of what to be measured and how to measure it must be well-defined.

In ball mill comminution, cost due to energy expenditure is one of the major criteria used for benchmarking performance (Fuerstenau, 2002; Rosa et al., 2014). This is because comminution by ball mill systems involves high energy expenditure. Single-particle size breakage, drop weight test, bond work index, and grind curves are the

techniques characterising material breakage properties and these are briefly reviewed below.

2.5.1 Single-particle breakage

Breakage of particles in ball mills is a complicated task. There are complex interactions inside a mill in operation. This makes it difficult to analyse the breakage characteristic of particles, as a result, single particle test methods were implemented (Tavares, 2007). The mechanism of the particle breakage process is understood from single-particle fracture analyses.

The drop weight test is an example of a single impact and is one of the common methods used for investigating breakage characteristics of materials (Tavares, 2007). In this test method, a particle is placed and mounted on a steel plate and subjected to a tensile force by dropping a stopper from a height to impact it. From the balance of the detachment force and adhesive force for a critical particles size, the interfacial specific energy is calculated (Zafar et al., 2014). A schematic diagram of the drop weight tester is shown in Figure 2.12.

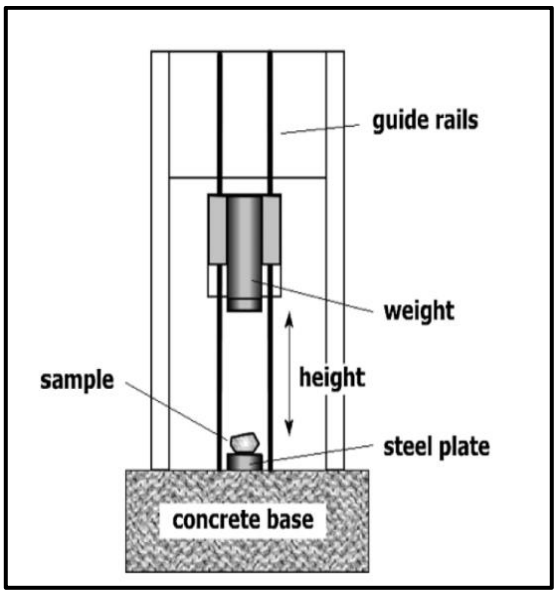

Figure 2.12 Drop weight tester (Tavares, 2007)

The input energy E_i transferred to the particle by dropping a weight from a certain height is given by:

$$E_i = M_b g h_o \qquad \textbf{(2.32)}$$

Where M_b is the mass of the drop weight and h_o is the drop height, that is, the distance between the bottom of the drop weight and the top of the particle.

Assuming the kinetic energy of a weight before impact is equal to the available potential energy before the weight is released. This kinetic energy is transferred to a particle and breaks it to produce the progeny particles. The latter are collected for the determination of product size distribution. The drop weight tester can be used to determine the breakage and energy utilisation parameters for comminution modelling. This, however, is beyond the scope of this research work.

Slow compression is another particle breakage test method. In this case, a particle is pressed between two objects. The tests are conducted using single-axis compression presses or using the rigidly mounted roll mill (Tavares, 2007).

A significant advantage of compression testing over traditional drop weight and pendulum (instrumented or not) devices is that the applied forces, and often the deformations, can be recorded during the test to determine load–deformation profile, and thus several strength-related aspect can be measured. In this regard, measures of particular interest are the energy at primary fracture, called particle fracture energy, and the total energy absorbed by the particle during the test (called comminution energy, E_c). Both can be calculated from direct numerical integration of the load-deformation profile.

$$E_c = \int_0^{\Delta_c} F\ \delta\Delta_c \qquad \textbf{(2.33)}$$

Where F is the load applied to the material and $\delta\Delta_c$ is an infinitely small element of the critical deformation Δ_c.

2.5.2 Bond work index

The commonest method used for the evaluation of the performance and determination of the power and mill size required for a given material is known as Bond's method. However, over the years, many mathematical models and simulation techniques have been developed to improve this technique (Reid, 1965; Austin et al., 1984).

Between 1960-1961, Bond described a parameter W_i as work index in his 'Third Theory of Comminution'. The W_i exhibits the resistance of a material to size reduction. Numerically, the Work index is the kWh per ton required to reduce the material from theoretically infinite size to 80% passing 100 µm. The typical Bond's Third Theory is expressed as follows:

$$\mathrm{E} = \frac{10Wi}{\sqrt{x_p}} - \frac{10Wi}{\sqrt{x_f}} \qquad \textbf{(2.34)}$$

Where E is the specific energy input (expressed in kWh/t); x_p is the size in mm at which 80% of the product passes; and x_f is the size in mm at which 80% of the feed passes.

2.5.3 Grind curves

The product of a mill responds according to the change in one of the prime operating variables, for example, ball filling, slurry concentration and mill speed. The effects of the change in the operating conditions on the mill performance have been investigated to a great extent for comparative documentation purpose (Mulenga et al., 2016; Simba and Moys, 2014; Tangsathitkulchai, 2003). The grind curves may be employed for the selection of the correct conditions for significant comparative tests (Mwansa et al., 2005).

The milling curves comprise a throughput curve, power curve, and grind curve as a function of mill filling. It is believed that these types of curves

- can be used to determine the optimum filling for the operations grind and throughput requirements.
- can be used by the mill operator or control system to determine stable regions and how to move between fillings.
- can be done for different ore types to guide operation.

Figure 2.13 shows one example of excellent grind curves produced from P9N AMIRA test work conducted at the AngloGold Ashanti Kopanang site (Mwansa et al., 2005). These curves relate the throughput, circuit product and power with mill filling and identify their variabilities.

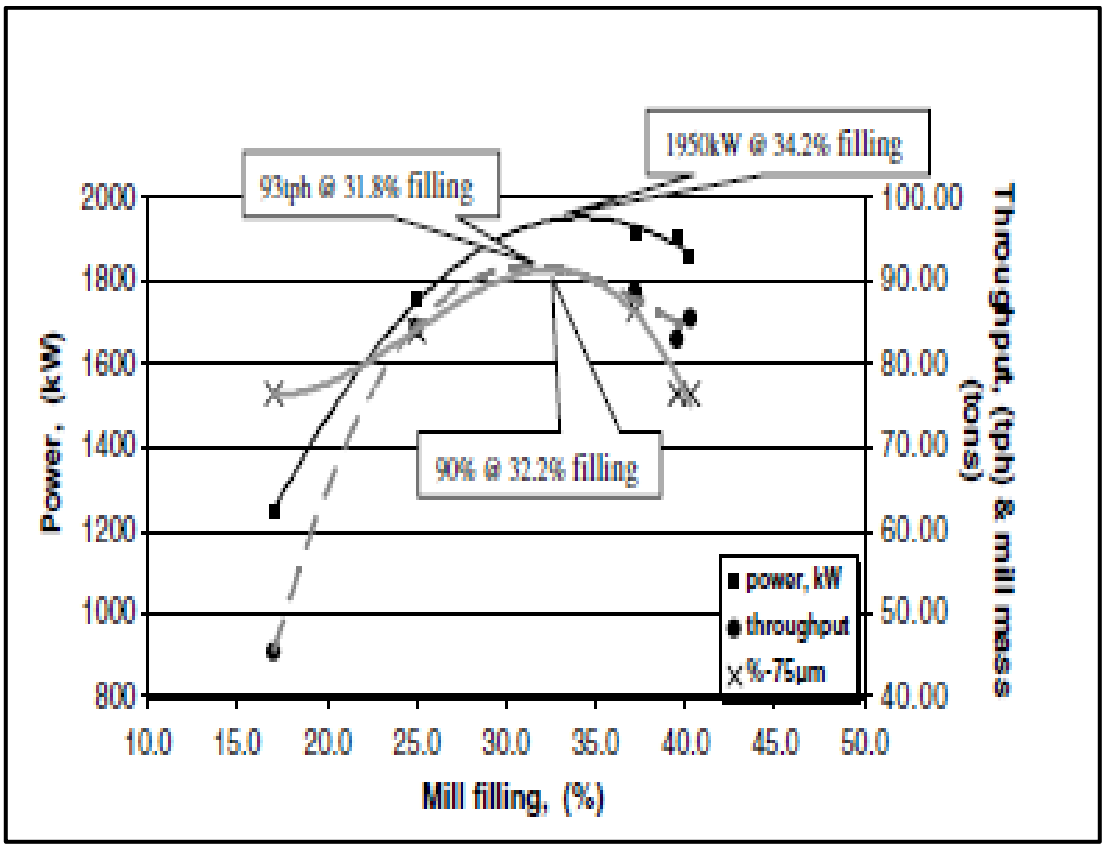

Figure 2.13 Example of grind curves (Mwansa et al., 2005)

In this instance, it is expedient that the mill should be run at a point just close to the power peak to provide optimal grind, with a small or negligible sacrifice of the throughput. According to Mwansa et al. (2005), remaining below the power peak makes the operational activities more stable.

The combination of the desired mill load and power-seeking may be used to control the mill. However, this type of analysis is preferentially performed on a continuous mill and not batch milling.

2.5.4 Size-specific energy

The size-specific energy (E_i) can be defined as "the energy required to produce new particles of a certain size" (Ballantyne et al., 2015). In 2014, Ballantyne and co-workers

proposed the size of -75 µm particles as a basis for the estimation of the E_i. In past years, several reports have shown linear relationships between the cumulative comminution energy consumption and material generated below 75 µm (Hukki, 1979; Levin, 1992; Musa et al., 2009; Hilden et al., 2010). The Ballantyne group also examined the energy required to break two different types of ores below -75 µm. Their findings are shown in Figure 2.14 below (Ballantyne et al., 2015).

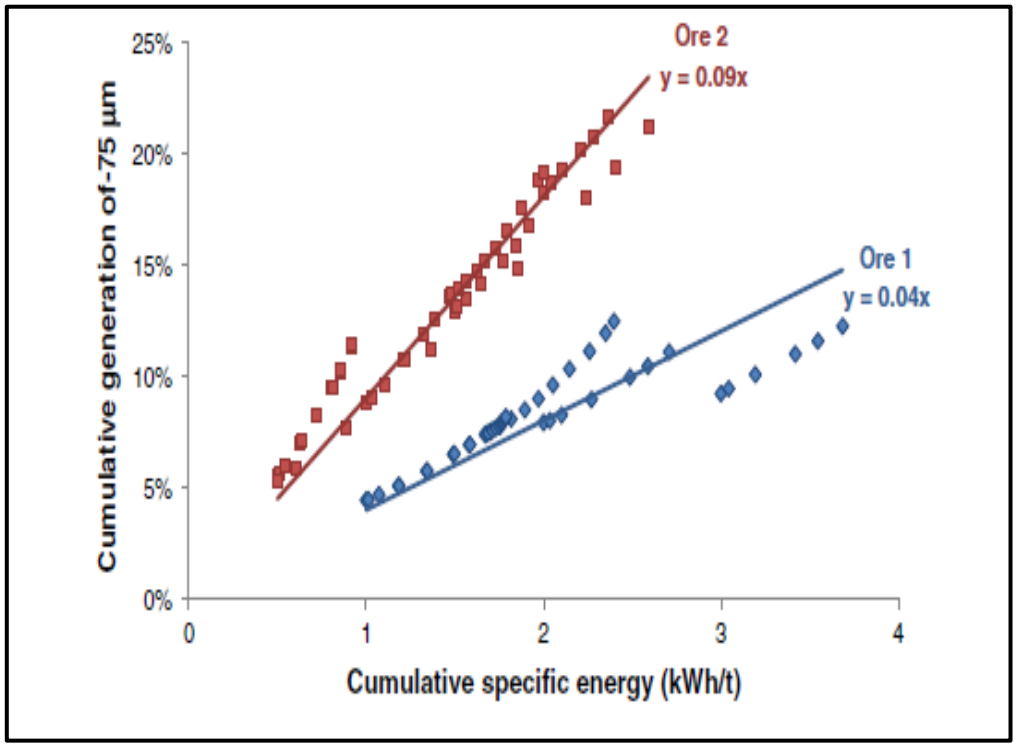

Figure 2.14 Illustration of energy required to break particle size to -75 µm (Ballantyne et al., 2015)

According to Figure 2.14, Ballantyne and co-workers were able to prove that the percentage grind increases as the cumulative specific energy increases. Also, they confirmed the postulation made by Levin in 1992 that the E_i was more appropriate for the measurement of fineness (Levin, 1992).

2.6 Concluding summary

Milling is considered a high energy-consuming comminution process in mineral processing. As a result of this, many researchers have investigated factors that affect milling performance to optimise its operation (Deniz, 2012 & 2016; Deniz and Onur, 2002; Tangsathitkulchai, 2003; Mulenga et al., 2016; Cho et al., 2013; Erdem et al., 2009). Mill rotational speed was identified as one of the most crucial factors (Mulenga and Moys, 2014; Deniz, 2004).

The rotating motion of the mill tumbles the charge (a mixture of balls and ore) and results in breakage of the particles as the balls rub and impact on each other. Three breakage mechanisms occur inside the mill as the results of tumbling motion which are impact, compression and attrition (King, 2001). Impact breakage occurs when grinding media come into forcible contact with each other. Breakage by compression and attrition arises primarily due to the frictional force caused by grinding balls rubbing against one another. The relative contribution of the three mechanisms to breakage is to a large extent dependent upon the rotational speed of the ball mill (Gupta and Yan, 2006). Depending on how fast the mill rotates the motion of the charge can be said to be cascading, cataracting or centrifuging. The cascading motion occurs when the mill rotates at a low speed below 50% of critical and more of attrition and compression involved which results in more production of fines. As the mill speed increases the charge starts to lift and falls as cataracting motion where more of impact takes place which results in coarse breakage. Again, when the mill speed increases further above 50% of critical the charge clings on the wall of the mill shell (centrifuging) where no breakage occurs, and the speed is known to be critical (Kelly and Spottiswood, 1982; King, 2001; Wills and Napier-Munn, 2005). Indeed, mill speed plays a big role in the internal motion of the charge and hence towards breakage.

The literature revealed that the effects of mill speed on breakage have been extensively studied and modelled between 50% and 90% of critical (Austin et al.,

1984; Deniz, 2013; Petrakis et al., 2017). Yet, it is in this speed range commonly used in mineral processing that mills have been reported to be inefficient.

Chapter 3 Experimental Section

Batch milling tests were performed at the University of the Witwatersrand using roll ball mill. The effects of rotational speed on grinding kinetics of UG2 ore were evaluated at three different mill fractional speeds, i.e. 20%, 30% and 40% respectively. The size intervals of feed samples considered as part of the test work were as follows: -1.180 +0.850 mm, -0.850 +0.600 mm, -0.600 +0.425 mm, -0.425 +0.300 mm, and -0.300 +0.212 mm. This section explains in details the methodology adopted for the laboratory test work. This includes the preparation of the mono-sized feed samples, the batch tests performed following what is known as the one-size-fraction method, and the systematic analysis of the particle sizes done on the various products generated by the batch mill. The equipment and material used for experimentation are also described. Briefly, the roll ball mill speed was set at 20% of the critical speed, followed by addition of feed of the first fraction to the mill and subsequently milling for different times: 0.5 min, 1.0 min, 2.0 min, 4.0 min, 15.0 min and 30.0 min. At the end of each milling time, particle size analysis was performed. The above was further repeated for 30% and 40% of critical speed.

3.1 Description of ore sample

The upper group two (UG2) chromitite ore sample was collected from the Department of Extraction Metallurgy, University of Johannesburg. The ore is a run-of-mine from Anglo American Platinum Waterval mine in Rustenburg. The UG2 is one of the three Bushveld complex ores; namely, Platreef and Merensky reefs. Each ore has distinctive properties and mineralogy (McLaren et al., 1982). They are mined for the recovery of platinum-group minerals (PGMs); namely, Platinum, Palladium, Osmium, Rhodium, Ruthenium and Iridium. Gold, Nickel and Copper are by-products of the ores. South

Africa is known as the largest producer of PGMs and has about 75% of the world Bushveld Complex reserves of PGMs ores (Cramer et al., 2004). UG2 ore has more reserves than any other Bushveld complex reefs (Cawthorn., 1999; Jones., 2005). In this study, UG2 ore was used and is discussed further.

UG2 reef contains between 4.4 and 10.6 g/t of PGMs (Leroy et al., 2011) and is known as the richest source of rhodium, which is an important constituent of the catalysts used in motor car exhaust systems (Jones., 2005). It is well known by a high content of chromite as the principal gangue mineral, but recently chromite gained value and no longer discarded as a waste mineral. Chromite constitute up to 80% of the mass of UG2 ore (Leroy et al., 2011) and is recovered as ferrochromium (FeCr) which is used to manufacture stainless steels (Barnes et al., 1987; Murthy et al., 2011) , at which the application and demand are increasing at high rate (Danha et al., 2017).

The major problem with chromite is in the smelting process; Pyrometallurgical process for further recovery of PGMs. It is forming high melting spinel restricting the recovery of PGMs, entrained during flotation due to over-grinding of the ore. The average grain size of PGMs in UG2 is about 15 µm with a maximum size of 25 µm (McLaren and De Villiers, 1982; Penberthy et al., 2000). To liberate the mineral, the ore has to be ground much finer at about 80% -75 µm (Jones, 2005*)*. This is a challenge since it conflicts with the coarseness requirement of chromite to limit entrainment. Indeed, grinding UG2 ore requires the knowledge of its breakage characteristics. This ore was identified to be fragile (Murthy et al., 2011) making the comminution easier and cost-effective. The mining costs of UG2 ore are lower mainly because of the high relative density of 4.3 g/cm^3 (Gruenenwaldt, 1977). The use of UG2 ore makes this study more significant because of its high demand and availability.

3.2 Experimental equipment

All the equipment used in this study was found at WITs mineral processing lab. The test work comprises weighing using top pan balance and analytical balance. Sieving was for feed preparation and after milling for particle size distribution analysis. Splitting of samples was done using vibratory spinning riffler and roll ball mill was used for batch grinding. All the aforementioned pieces of equipment were used repeatedly throughout the laboratory test work; they are explained below in details how they were used.

Top pan balance refers to weighing scale that has the pan that is not covered by any structure. It was used in this study to weigh masses from 100 g upwards because it could not read the small masses below 100 g. It was always ensured that the balance was cleaned before use and well calibrated. An empty pan was placed on top of the balance; then, the scale was reset to zero. The sample was poured in a pan as shown in Figure 3.1 and the mass recorded on a spread sheet.

Figure 3.1 Top pan balance

An analytical balance was also available for weighing samples. This type of balance is very sensitive; it was therefore used in this study to weigh small samples believed to

have a mass below 100g. A weighing bowl was placed inside the balance, after which all doors were closed, followed by tarring the weight to zero. Afterwards, the empty bowl was brought out, filled with the sample, placed back inside the balance and the sample mass read as the output mass reading on the balance.

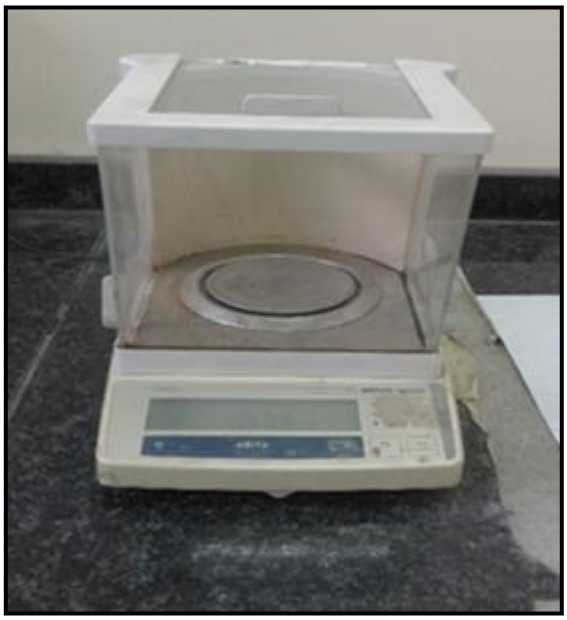

Figure 3.2 Analytical balance

A vibratory spinning riffler was used to homogenise and split samples into sub-samples of equal mass for later use as feeds to the batch mill. In terms of procedure of sample preparation, the material was first scooped from the bulk container and weighed to 2 kg. It was then poured from the top of the riffler in a cone-shaped hobber; the stream of material went down through the vibrating feeder. The spinning riffler which consists of 10 pots as shown in Figure 3.3 then split the material into 10 equal portions each weighing approximately 200 g. Five opposite pots were taken as representative samples, mixed and fed on a stack of sieves for the preparation of mono-size feeds.

Figure 3.3 Vibratory spinning riffler

Figure 3.4 Sieve shaker with a stack of sieves

Sieving was extensively done for feed preparation and particle size distribution analysis. Sieving for feed preparation was done as follows: Seven sieves were arranged in descending order from 1.180 mm to 0.150 mm following the $\sqrt{2}$ sequence as standard laboratory procedure and closed with a pan at the bottom to collect the fine fraction. Arranged sieves were placed on a sieve shaker and a mass of 1 kg was poured onto the top sieve. Sieves were balanced with a plate on top and tightened with two nuts as shown in Figure 3.4. The sample was then shaken for 20 min to expose the particles to the apertures. Mass retained on each sieve was emptied in a pan using a brush and weighed. Each mass fraction was stored in a plastic bag and labelled with permanent marker according to sieve size. This was done repeatedly until a sample of mass 700g accumulated for mono-sized feed fractions: -1.180+0.850 mm, -0.850+0.600 mm, -0.600+0.425 mm, -0.425+0.300 mm and -0.300+0.212 mm. The accumulation of 700g was done three times for feed sizes -1.180+0.850 mm, -0.850+0.600 mm and -0.600+0.425 mm to compare the effects of three mill speed fractions on grinding kinetics as their masses accumulated faster.

After each grinding test sieving was also performed for particle size distribution analysis, mill pot was emptied and sample separated from steel balls. The sample was then taken for sieving. A set of seven sieves were arranged the same way as for feed preparation. The first sieve was the upper sieve size directly above the feed size i.e. if feed size was -0.850+0.600 mm the arrangement of sieves started from 0.850 mm to 0.106 mm. The sample was then loaded on a top sieve and sieved for 20 min. The size that passed the finest sieve was collected in a pan. Fractions retained on each sieve were weighed and mass recorded on a sheet. The above procedure was done repeatedly after each grinding test. As known that sieving is an inefficient task due to near size particles blinding the aperture sizes, mass retained on the first sieve was added to the upper size fraction. It was also shown that after each sieving step there was no more than 0.01g fraction of mass sample lost as part of material handling. This mass was added to the last finer fraction to account for the discrepancies.

After each sieving test, the sieves were cleaned using the ultrasonic bath shown in Figure 3.5. The bath uses ultrasound to agitate water which makes it easy to remove stuck particles stuck within the aperture of the sieves. The cleaning process took 30 min after every use of the sieves. High-pressure air was used to dry the sieves while being careful not to bend the sieve wires or widen the aperture sizes. The same sieves were used throughout for consistency.

Figure 3.5 Ultrasonic bath

The batch ball mill used in this study was manufactured at Changsha Tencan Power Technology Company model QM-5. The mill volume was 5 dm^3 and 0.2 m long without lifters. The settings of the mill operation were done on the mill key operation screen (see Figure 3.7)

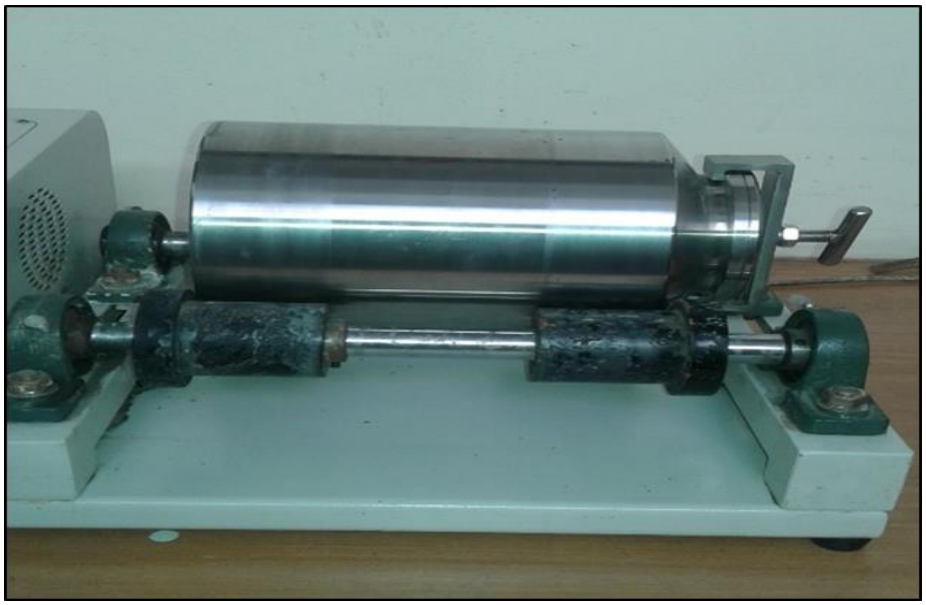

Figure 3.6 Laboratory roll ball mill

Legend	
MODE	Switch display mode
ENTER	Reads and stores the setting parameters
POTENTIOMETER	Regulates the rotating frequency
UP ARROW	Function code selection
DOWN ARROW	Function code selection
RIGHT DOUBLE ARROW	Monitoring mode, display data in a scroll
JOG	Multifunction key
RUN	Starts operation
STOP	stops operation

Figure 3.7 Control screen for the operation of the ball mill with the digital panel displaying the value and the code of a particular setting

The mill was set to rotate at three different speeds. The settings were done as follows: the mill pot was first filled with 4.3kg of 20 mm steel balls, closed and placed on mill stand as shown in Figure 3.6. A mark was pinpointed on mill pot using a marking pen as a reference to count a number of revolutions as the mill rotates. The stopwatch was used to time the revolutions as the mill was rotating. The potentiometer on the key operation display screen (Figure 3.7) was used to adjust the rotation frequency of the mill, clockwise to increase the rotation speed and anticlockwise to decrease. Mill started rotating by pressing the run button and the number of revolutions per minute was counted. Using the potentiometer, the speed was regulated to a point where 21.4 rpm or 20% of the critical speed was reached. Once done with 20% critical speed grinding tests, the mill rotation speed was adjusted again to 30% and 40% critical speed respectively.

3.3 Feed preparation

The UG2 ore sample was already crushed to less than 2 mm when collected from the University of Johannesburg. Five mono-sized feed samples were then prepared in the following size classes: -1.180 +0.850 mm, -0.850 +0.600 mm, -0.600 +0.425 mm, -0.425 +0.300 mm and -0.300+0.212 mm. The decision on the preparation of these fractions was based on the availability and the easy of how to prepare them. It was difficult to prepare very fine fractions below 0.106 mm. The mill diameter and ball size were also considered for the coarsest fraction.

Table 3.1 Experimental design

Feed size (mm)		Mill speed (% of critical)		
Upper	Lower	20%	30%	40%

1.180	0.850	X	X	X
0.850	0.600	X	X	X
0.600	0.425	X	X	X
0.425	0.300		X	
0.300	0.212		X	

Table 3.1 shows the experimental design and gives a summary of feed sizes considered to perform the test work at each critical speed.

It can be seen from Table 3.1 that fractions (-0.425+0.300 mm) and (-0.300+0.212 mm) were only tested at 30% of the critical speed. This is because the bulk sample contained less of this fraction and was not easily accumulated.

3.4 Batch grinding tests

The batch grinding tests were done using a roll ball mill shown in Figure 3.6. The mill characteristics are given in Table 3.2 together with the test conditions. A plastic measuring cylinder of 1000 ml was filled with 20 mm steel balls to make 20% of 5 dm^3 mill, i.e. J = 20%. Based on Equation (2.1), it was possible to back-calculate the mass of grinding media required for the set ball filling. The mass of steel balls was prepared using the top pan balance in Figure 3.1 and their mass recorded. A total mass of 700g sample was determined to be needed as the feed for each batch milling experiment. The mass of feed sample was determined using Equations (2.2) and (2.3) while powder filling was set at U = 0.4.

For each grinding test, the mill was therefore loaded with 4.3kg of steel balls and 700g of the UG2 feed sample. Dry grinding was performed next for milling times 0.5 min, 1.0 min, 2.0 min, 4.0 min, 15.0 min and 30.0 min. After each grinding time, the mill content was emptied into a container and weighed to determine the weight losses

due to material handling. This weight loss was noted to be negligible compared to the initial mass (700g) that there was no need for correction during mass reconciliation. After that, the size distribution of the product was obtained using standard sieve sets (see Figure 3.4) following the $\sqrt{2}$ sieving procedure. The various fractions retained on each sieve and the pan was measured using the analytical scale in Figure 3.2 and their masses recorded on a sheet. After the first grinding time t = 0.5 min, the fractions were recombined and loaded into the mill for grinding for 1.0 min, 2.0 min, 4.0 min, 15.0 min and 30.0 min respectively.

Table 3.2 gives an overview of the testing conditions that the batch mill was operated under.

Table 3.2 Mill characteristics and test conditions

Mill diameter, D (mm)	175
Mill length, L (mm)	208
Mill volume (dm^3)	5
Critical speed, N_c (rpm)	107
Mill speed, ϕ_c (% of critical)	20; 30; and 40
Steel ball size, d (mm)	20
Ball filling, J (%)	20
Ball charge weight (kg)	4.3
Powder filling, U (%)	40

It was decided to mill the UG2 ore under dry conditions as this is less challenging to handle than wet milling. Furthermore, dry milling tends to produce more consistent and reproducible results. This was deemed the preferred mode of operation also because not enough material was available to conduct replicate tests. Finally, the

limitation in terms of available single-sized feed samples also forced us to settle for a lower powder filling U = 40% and a ball filling J = 20%. The low powder filling reduced the work required for feed preparation sample and enabled us to accommodate more tests (see Table 3.1). The ball filling J = 20% was used with the understanding that many researchers have reported good kinetics results (e.g. Austin et al., 2007; Chimwani et al., 2013; Deniz, 2004; Gupta, 2016; Katubilwa and Moys, 2009).

And perhaps the most important point to make is that mill speeds ϕ_c below 50% of the critical speeds were chosen because very little to no research on this parameter is available in the literature. The selected speeds were set as described in Section 3.3 with Figure 3.6 as the supporting reference. The critical speed Φ, on the other hand, calculated using Equation (2.4) and use in setting up the speeds.

3.5 Difficulties encountered

There was not much challenge encountered in this experiment. Two major difficulties that influenced the course of action in the testing of the experimental design programme are discussed below.

The first critical challenge resided in the preparation of single-sized feed samples. The bulk sample contained more of the coarser size fractions than the finer material, i.e., material less than 0.425 mm. Accumulating fine fractions, therefore, required more stages of sieving and took longer. Eventually, only a limited mass of fine material was constituted for a single batch test per particle size interval at the lower end (see Table 3.1).

The second challenge was in the measurement of the rotating speed of the mill. A tachometer was not available for the purpose that it was decided to proceed to manual counting of the number of revolutions of the mill for selected periods and

parameter settings as per Figure 3.7. This enabled us to produce a calibration curve that was then to set the desired speed for a particular batch test.

Despite the above limitations, the experimental test work was conducted smoothly. Indeed, batch milling tests were performed using a laboratory roll ball mill to investigate the effect of speed on milling kinetics. The UG2 ore sample was used to perform the experiment. The ore is a run-of-mine from Anglo American Platinum Waterval mine in Rustenburg, South Africa. Five mono-sized lots of feed samples were prepared: -1.180 +0.850 mm, -0.850 +0.600 mm, -0.600 +0.425 mm, -0.425 +0.300 mm and -0.300 +0.212 mm). A mass of 4.3kg of steel balls of diameter 20 mm was used to fill the mill volume of 5 dm^3, i.e. J = 20%. A total mass of 700g sample representing a powder filling of U = 0.4 was used as the starting feed for all milling experiments.

For each test, the mill was loaded with balls and powder. The feed was then milled for selected time intervals. After each grinding time, the particle size distribution of the mill product was measured. A stack of seven sieves was arranged in descending order following the $\sqrt{2}$ sequence as standard laboratory procedure and closed with a pan at the bottom. Each sieving test was performed for 20 min while mass fractions retained on each sieve were weighed and recorded.

The above procedure was done repeatedly after each grinding test until the whole batch dataset was constituted. The next chapter describes the analysis techniques used to extract meaningful information from the dataset.

Chapter 4 Determination of the breakage function and selection function parameters of the UG2 ore

4.1 Introduction

This section covers the results obtained for the determination of breakage and selection function parameters. Indeed, "Knowledge of selection and breakage function parameters leads to improved equipment design criteria and consistent operating correlations" (Klimpel and Austin, 1977).

The breakage properties of the UG2 platinum ore were determined using the single-sized fraction method. This method consists of preparing one size fraction of material between two successive screens for batch milling. In this work, the upper and lower screens were symbolically represented by X_{j+1} (Upper screen) and X_j (lower screen) separated by $\sqrt{2}$ order used as feed. Breakage function parameters (β, γ and Φ) and selection function parameters (a, α, μ, Λ) were determined and compared for three mill speeds, i.e., 20%, 30%, and 40% of critical. All other operating parameters were kept constant except the speed and feed size distribution, the two variables required for the study.

4.2 Particle size distribution analysis

After grinding each feed size fraction, the size distributions analyses of mill product were constructed. Starting by presenting these results in this section was found to be more appropriate as all the upcoming analysis evolved from here. Tables 4.1 – 4.3 show the cumulative mass fractions passing each sieve after grinding. The distribution of the fragments produced from the feed, that is, material retained in top sieve size going down is used to define breakage function.

Table 4.1 Cumulative mass fractions passing sieve size for various batch milling times and mill speed ϕ_c = 20% of critical. Experimental conditions: feed size -1.180+0.850 mm, powder filling U = 40%, ball filling J = 20%, and ball size d = 20 mm

	Grinding time (min)				
Sieve size X_j (mm)	**0.5 min**	**2 min**	**4 min**	**15 min**	**30 min**
1.180	100	100	100	100	100
0.850	8.43	16.43	22.86	40.43	51.14
0.600	3.57	8.22	12.37	24.44	32.91
0.425	2.47	5.75	8.47	17.24	24.53
0.300	1.76	3.90	5.95	12.26	18.07
0.212	1.19	2.70	4.11	8.56	13.15
0.150	0.57	1.30	2.14	4.57	7.55
0.106	0.31	0.58	1.02	2.27	4.12

The latter is defined by Austin et al. (1984) as a fraction of feed material that appears in the lower fraction intervals at the short grinding time, explicitly, before re-breakage. It can be seen that the feed size fraction decreases as time increases; this is used for the first-order plots and to evaluate the breakage rate of the material.

Table 4.1 shows the cumulative mass distributions at various times. It can be seen that the distributed mass from feed size increases with grinding time. The increase of the distributed mass is due to the re-breakage of the material; hence calculations of the cumulative distribution function are done at short grinding times before re-breakage. Again it can be seen that the mass fraction of the feed disappears as grinding takes longer. The plot of the mass retained at top feed size versus grinding time gives the grinding kinetics.

Table 4.2 Cumulative mass fractions passing sieve size for various batch milling times and mill speed ϕ_c = 30% of critical. Experimental conditions: feed size -0.850+0.600 mm, powder filling U = 40%, ball filling J = 20%, and ball size d = 20 mm

	Grinding time (min)				
Sieve size X_j (mm)	**0.5 min**	**2 min**	**4 min**	**15 min**	**30 min**
0.850	100	100	100	100	100
0.600	7.71	16.43	24.71	43.43	55.29
0.425	2.85	7.71	11.82	24.92	33.99
0.300	1.75	4.27	7.05	15.69	22.84
0.212	1.17	2.69	4.42	10.16	15.39
0.150	0.82	1.68	2.81	6.23	9.67
0.106	0.60	0.97	1.61	3.26	5.38
0.075	0.59	0.78	1.58	2.46	4.31

Tables 4.1 to 4.3 present the same results at different grinding conditions. This will later be used for the determination of breakage and selection function parameters.

It can be seen from Tables 4.1 to 4.3 that mass passing from feed size class after first breakage time does not change with size or speed, that is to say, fraction of mass passing at the feed size is not significantly different at the time 0.5 min interval which are 8.43%, 7.71% and 8.29% for 20%, 30% and 40% of the critical speed respectively. But as the time interval increases, the mass starts to differ, increasing with speed.

Table 4.3 Cumulative mass fractions passing sieve size for various batch milling times and mill speed ϕ_c = 40% of critical. Experimental conditions: feed size -

0.600+0.425 mm, powder filling U = 40%, ball filling J = 20%, and ball size d = 20 mm

	Grinding time (min)				
Sieve size X_j (mm)	**0.5 min**	**2 min**	**4 min**	**15 min**	**30 min**
0.600	100	100	100	100	100
0.425	8.29	18.14	27.86	49.86	67.57
0.300	2.40	6.80	11.60	25.70	41.74
0.212	1.40	3.74	6.74	15.49	27.48
0.150	0.83	1.95	3.85	8.61	17.01
0.106	0.45	0.77	2.01	3.55	10.12
0.075	0.33	0.49	1.43	1.90	4.55
0.053	0.28	0.35	1.13	1.30	3.33

Figure 4.1 shows the cumulative particle size distribution curves of the results rendered in Table 4.1. The narrower particles distribution is observed at the shortest grinding time. However, the distribution gets wider as the milling time increases. It is clear that finer particles are produced at a longer grinding time. The same pattern is observed in all feed sizes tested at all speeds in this study and more data can be found in Appendix A.

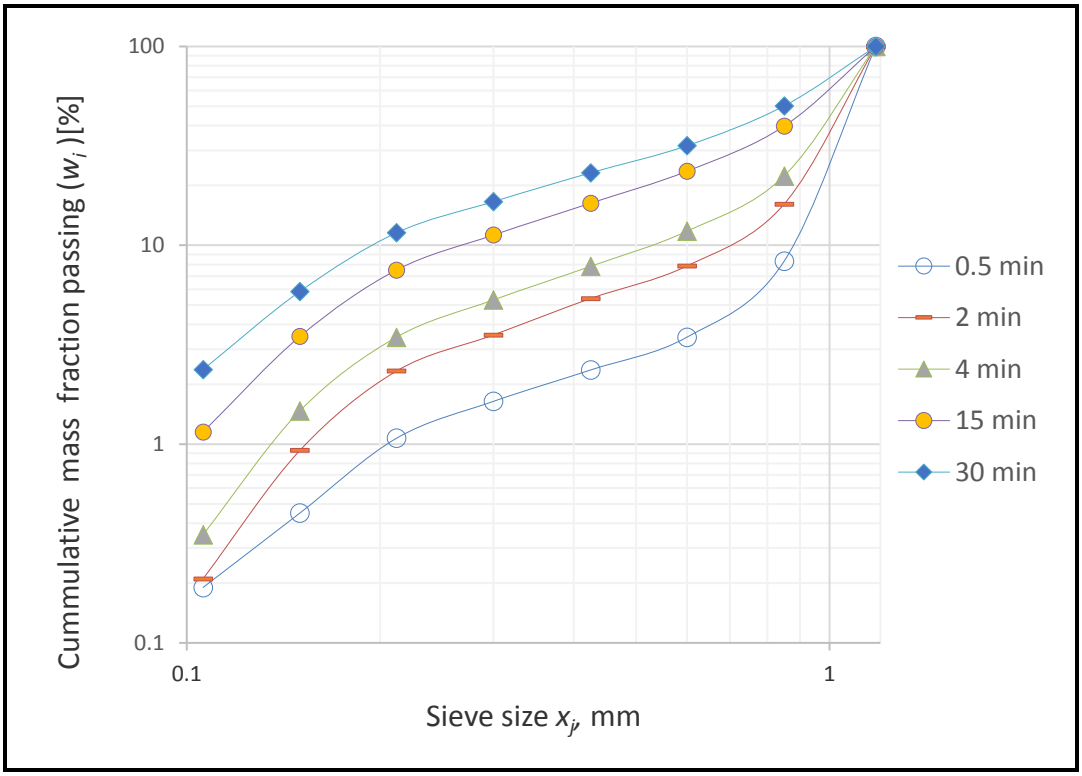

Figure 4.1 Particle size distributions produced from milling the platinum ore of feed size -1.180+0.850 mm under the following experimental conditions: ϕ_c = 20% of critical, U = 40%, J = 30%, and d = 20 mm.

4.3 Batch milling kinetics

Milling kinetics graph is plotted as mass fraction retained at the top sieve size class as a function of grinding time. Many researchers found the relationship as linear. Non-linear or non-first-order breakage was observed in some cases (Tangsathitkulchai, 2002; Chimwani et al., 2013; Austin and Bagga, 1981). Austin et al. (2007) also observed non-first-order breakage in one of his test works. It was reported that it was because there were large particles that could not be nipped by the employed ball size.

In the current study, non-first order breakage was also observed and it was observed for all runs, irrespective of the operating conditions (see Figures 4.2 and 4.3 as well as

Appendix C). It was realised that the material consisted of fast and slow breaking material, thus Equation (2.10) can be used to fit the experimental results.

Nonlinear regression technique was utilised to determine the equation parameters. This technique works by finding the best fitting parameters of a model by minimising the square of the error between the experimental values and the predicted ones. The function is defined as:

$$\mathrm{SSE} = \sum_{r=1}^{R} [P_{expt}(t) - P_{model}(t)\ ]^2 \qquad \textbf{(4.1)}$$

Where R is the number of runs considered to carry out a full batch test on given particle size X_i. Since each full test was done for 0, 0.5, 2, 4, 15, and 30 min successively, R = 6. $P_{expt}(t)$ is retained experimental mass fraction on the top size screen X_j at grinding time t. $P_{model}(t)$ is predicted mass fraction retained on size screen X_j after grinding of single-sized feed material of initial size X_0 for a total grinding time t.

Considering Table 4.4 for illustration, experimental data was predicted using Equation (2.10) to obtain model data. The equation was typed using initial estimated unknown variables ($S_{j,slow}$, $M_j(0)$ and $S_{j,fast}$) and then model data was predicted. The error between the experimental and model data was summed and squared as Equation (4.1). The unknown values of the model variables were then corrected using the Excel Tool Solver by finding the minimum optimum values for the equation used. In this case, the equation was:

$$M_j(t) = 79.44e^{[0.02(t)]} + [100 - 79.44]e^{[-0.59(t)]} \qquad \textbf{(4.2)}$$

A similar approach was followed with all the other batch grinding data so that Figures 4.2 and 4.3 were produced for illustration.

Table 4.4 Illustrative application of nonlinear regression to determine unknown parameters of Equation (2.10). Experimental conditions: feed size -1.180+0.850 mm, ϕ_c = 20% of critical, U = 40%, J = 20%, and d = 20 mm

Time (min)	Experimental	Predicted (Equation 2.10)	Squared Errors
0	100.00	100.00	0.00
1	91.57	94.10	6.40
2	83.57	83.21	0.13
4	77.14	76.37	0.60
15	59.57	62.23	7.09
30	48.86	48.75	0.01
		Sum of Squared Errors	14.23

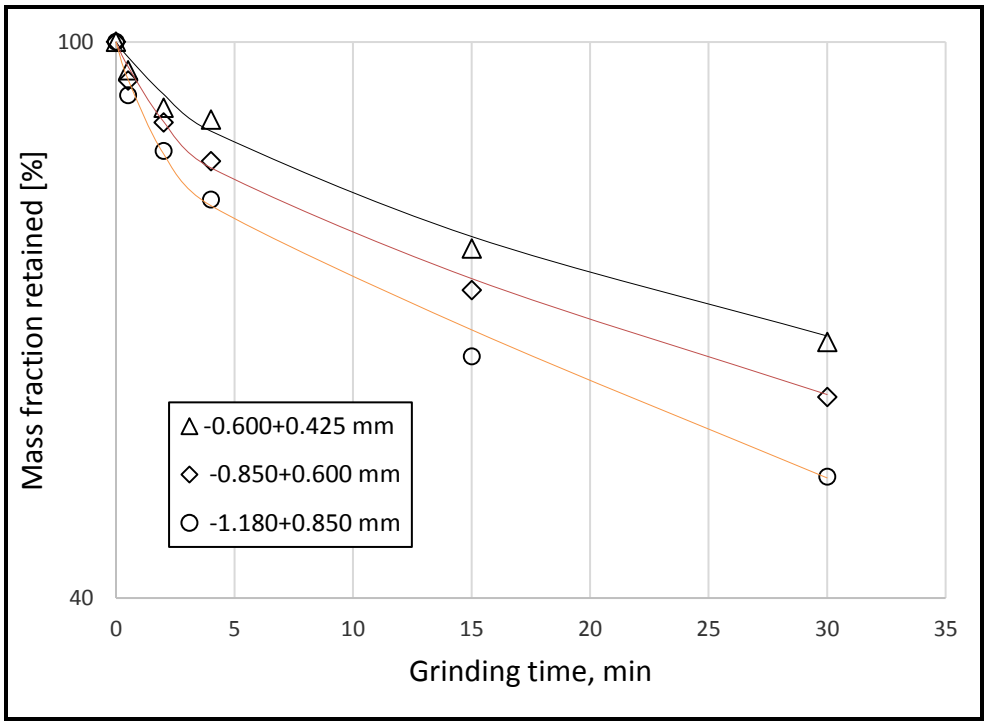

Figure 4.2 Milling kinetics of the UG2 platinum ore at ϕ_c = 20% of critical speed for various feed sizes. Milling conditions: U = 40%, J = 20%, and d = 20 mm

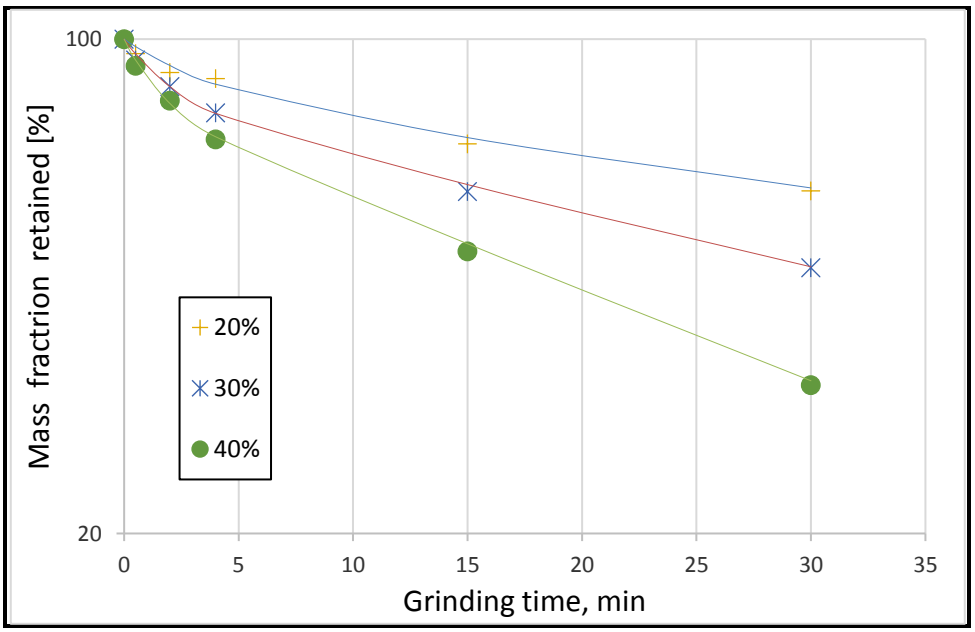

Figure 4.3 Milling kinetics of the UG2 platinum ore for feed size -0.600+0.425 mm milled at various fraction of critical speed ϕ_c. Milling conditions: U = 40%, J = 20%, and d = 20 mm

The predicted model line is shown through the experimental points in Figure 4.2. As can be seen, the graphs in Figure 4.2 show that there is non-first order breakage of the material, constituting of fast breakage and slow breakage. The average size decreases sharply during the first four minutes of grinding and then moves slowly as grinding proceeds. This is named as non-first order breakage (Austin et al., 1977).

As mentioned earlier that the non-first-order breakage was observed in every grinding test performed in this study. Figure 4.3 also shows this behaviour. The experimental data fit well with the model which can be used to predict what happens when the grinding time is further increased. Figure 4.3 also shows the effect of speed on the breakage rate. As can be seen, the increase of speed pulls the graph down, increasing the slope. Thus, it can be said that the speed increases the rate of breakage.

4.4 Determination of the selection function parameters

Austin et al. (1984) proposed that when a non-linear breakage is observed, the effective mean rate of breakage (selection function) can be determined. This is defined using the grinding time to 95% breakage and was adopted in this study. As a result, the time required to remain with 5% of feed size material on top sieve class was determined and substituted on first-order law Equation (2.6) to determine the effective mean value of the specific rate of breakage (S).

Using Equation (4.2) as model equation from Table 4.4 dataset, 169.9 min was determined as time required retaining 5% of the material in top sieve size class, i.e. $M_j(169.9) = 5$. The determined time (169.9 min) was substituted in first-order Equation (2.6) which looked as Equation (4.3) and effective mean specific rate of breakage (S_j) was solved.

$$5 = 100e^{[-S_j(169.9)]} \quad \textbf{(4.3)}$$

That is, $S_j = -\frac{\log 0.05}{169.9}$ = 0.0176

For all milling conditions effective mean selection function was calculated the same way and presented in Table 4.5.

Table 4.5 Effective selection function values for various feed sizes and for various fractional speeds

Feed size (mm)	20%	30%	40%
-1.180+0.850	0,0176	0,0161	0,0375
-0.850+0.600	0,0136	0,0187	0,0347
-0.600+0.425	0,0113	0,0192	0,0321
-0.452+0.300		0,0109	
-0.300+0.212		0,0096	

It can be seen from Table 4.5 that for feed size -0.850+0.600 mm and -0.600+0.425 mm the selection function is directly proportional to the mill speed. As for the coarsest size -1.180+0.850 mm, the selection function decreased from 20% to 30% of critical speed and increases again at 40% speed.

The selection functions values for each speed were plotted as a function of upper size (see Figure 4.4). The data points were fitted with the model Equation (2.8) using non-linear regression technique to determine the selection function parameters (a_0, α, μ, Λ) as illustrated by Table 4.6 and Figure 4.6.

Table 4.6 Use of Non-linear regression technique for determination of selection function parameters at 30% critical speed

Upper size (mm)	Experimental	Predicted (Equation 2.8)	Error
1.180	0.016	0.016	0.000051
0.850	0.019	0.019	0.000530
0.600	0.019	0.018	0.002335
0.425	0.011	0.013	0.003923
0.300	0.010	0.008	0.001153
		Sum of squared errors	0.007991

The selection function values in Table 4.5 were predicted as shown in Table 4.6 at 30% of critical speed. The predicted values differ slightly with experimental values which makes the predicted data more reliable. This was plotted graphically in Figure 4.4 below.

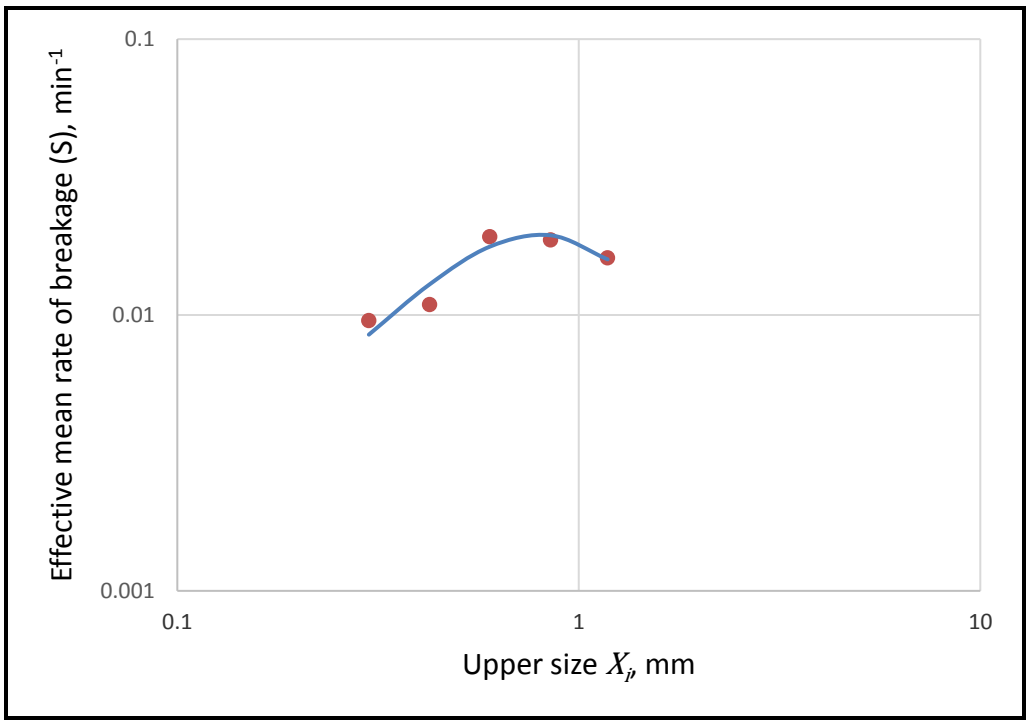

Figure 4.4 Selection function plotted as a function of feed size for the platinum ore under the following testing conditions: ϕ_c = 30% of critical speed, U = 40%, J = 30%, and d = 20 mm. Effective selection functions calculated at 95% of breakage (see Section 2.3.3 and Equation 4.3)

The fitted values in Figure 4.4 were a_0 = 0.04 min^{-1}, α = 1.36, μ = 0.9 mm, and Λ = 3.0. It can be seen that the breakage rate increases sharply up to 0.85 mm particle size and start decreasing as the feed size increases. The decrease of breakage rate was due to the large particles that cannot be nipped by the ball size used. It could also probably be due to the accumulation of the harder (stronger) material in the retained feed material.

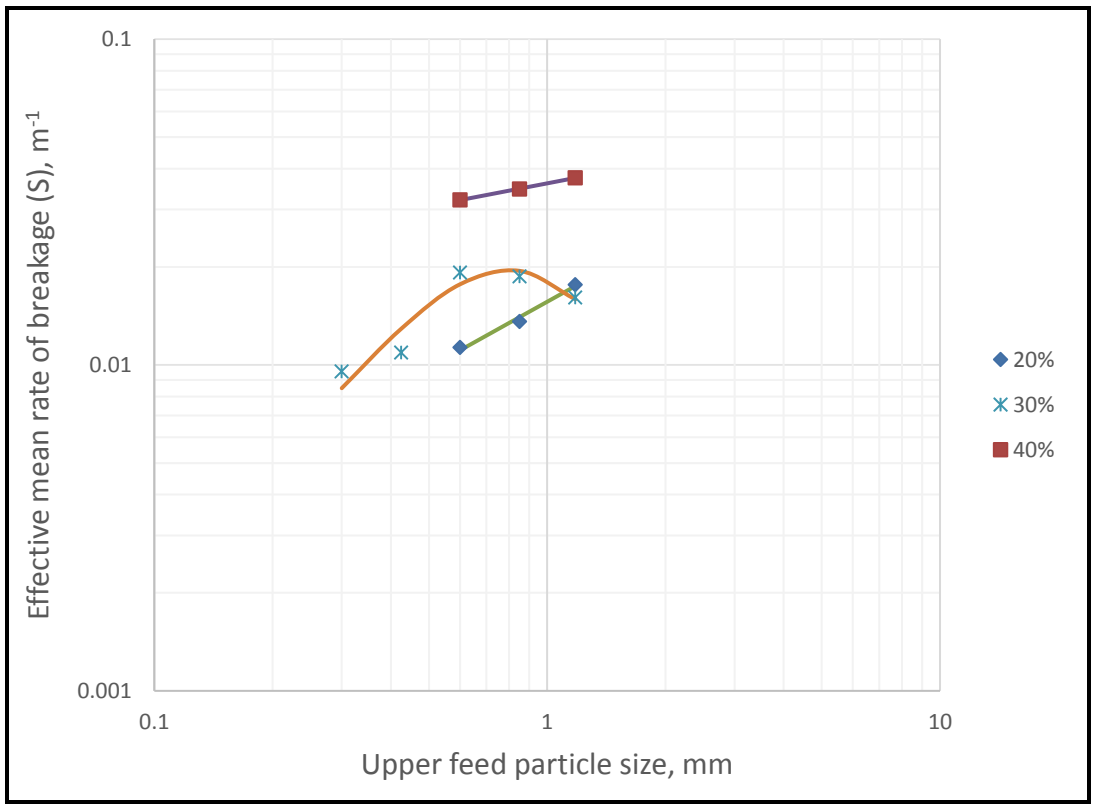

Figure 4.5 Comparison of Selection function plotted as a function of feed size for the platinum ore at 20%, 30% and 40% of critical speed respectively under the following conditions: U = 40%, J = 30%, and d = 20 mm balls

Figure 4.5 shows the effects of speed and feed size on the breakage rate. It can be seen that the rate of breakage increases with speed for all tested feed sizes and the maximum value of the rate of breakage was not reached except at 30 % of critical speed. At every mill speed, feed size affected the breakage rate differently. Again the rate of breakage at 40% of critical speed was higher than that at 20% speed. As for 30% of critical speed, different results were observed; the rate of breakage increased with size up to 0.850 mm and started to drop. Thus, it could be said that the optimum size at this speed is 0.850 mm.

Table 4.7 shows the fitted values of the selection function parameters for different feed fractions milled at 20% of the critical speed. The value of Λ and μ could not be

estimated because the maximum size was not reached; in other words, the breakage took place at the normal region only.

Table 4.7 Effect of feed size on the selection function parameters

Feed size (mm)	a_0 (min^{-1})	α (-)	μ (mm)	Λ (-)
+1.180-0.850	0.0003	1.48	-	-
+0.850-0.600	0.0002	1.56	-	-
+0.600-0.425	0.0004	1.36	-	-

Table 4.8 shows data to predict the effect of mill speed on the breakage rate of feed size -0.850+0.600 mm. The corresponding graph is shown in Figure 4.6.

Table 4.8 Effective mean rate of breakage feed size -0.850+0.600 mm

% critical speed	Experimental (S_i)	Predicted (Equation 2.8)	Error
20	0.014	0.011	0.004719
30	0.019	0.021	0.007697
40	0.035	0.034	0.001101
		Sum of squared errors	0.013520

It can be seen from Table 4.8 that the breakage rate increased with speed and maximum speed was not reached. Figure 4.6 below shows the graphical relationship. For all sizes presented, maximum speed was not reached and the rate of breakage increased with speed.

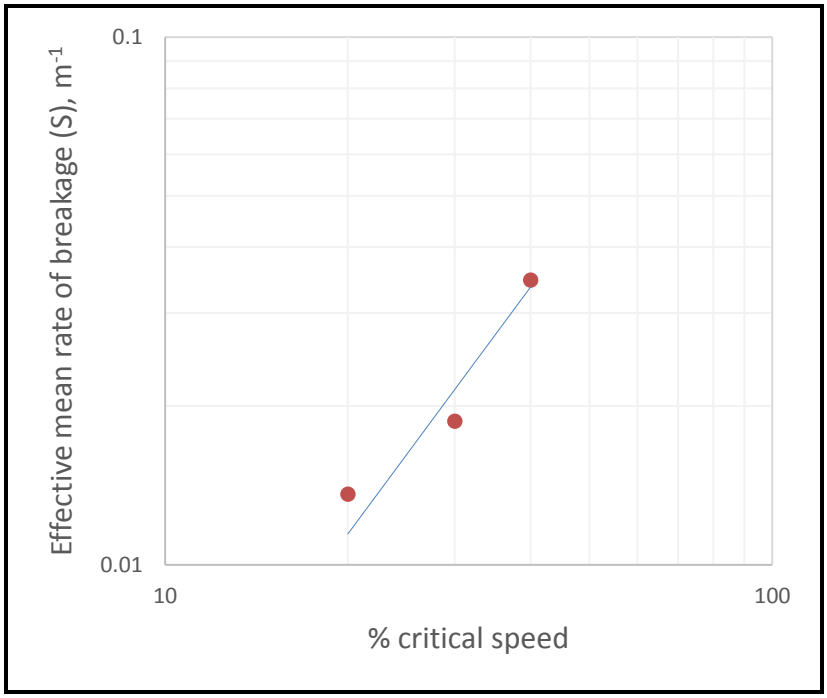

Figure 4.6 Selection function of the platinum ore of size -0.850+0.600 mm plotted as a function of mill speed. Experimental conditions: U = 40%, J = 30%, and d = 20 mm balls

Table 4.9 shows the effect of speed on selection function parameters. The values of a_0 increased with speed but the maximum value was not reached. As for α, the values increased with speed and dropped at 40% of the critical speed. It can be seen that the maximum speed was reached at 30% of the critical speed. Parameters μ and Λ were only identified at 30% of the critical speed.

Table 4.9 Effect of mill speed on the selection function parameters

Mill speed (% of critical)	a_0 (min^{-1})	α (-)	μ (mm)	Λ (-)
20%	0.03	0.68	-	-
30%	0.04	1.36	0.9	3.0
40%	0.07	0.24	-	-

4.5 Determination of cumulative breakage function parameters

The values of cumulative breakage function ($B_{i,j}$) were determined from the size distributions at short grinding times as proposed by Austin et al. (1984). This method is called B-II procedure and suggests the use of grinding time which results in not more than 30% broken material out of the top feed size to be considered in order to avoid re-breakage. Austin and Luckie (1971) showed that even 65% of broken material can still be used. Equation (2.26) was used for implementation. The shortest grinding time considered in this study was t = 0.5 min. Table 4.10 illustrates how the $B_{i,j}$ values were calculated.

Table 4.10 Illustration of the B-II method on the data corresponding to the following conditions: Feed size -1.180+0.850 mm, ϕ_c = 20% of critical, U = 40%, J = 30%, and d = 20 mm

Sieve size X_j (mm)	Cumulative % mass passing at 0 min	Cumulative % mass passing at 0.50 min	$B_{i,j}$ (Equation 2.26)
1.180	100	100	1.00
0.850	0.00	8.43	1.00
0.600	0.00	3.57	0.41
0.425	0.00	2.47	0.28
0.300	0.00	1.76	0.20
0.212	0.00	1.19	0.14
0.150	0.00	0.57	0.06
0.106	0.00	0.31	0.04

Table 4.10 shows cumulative mass fractions passing screen size before and after breakage with $B_{i,j}$ values for each fraction. The mass fractions were substituted in Equation (2.26) and $B_{i,j}$ values were calculated. For all the experimental conditions,

$B_{i,j}$ values were calculated the same way. Table 4.11 shows the $B_{i,j}$ values calculated at various speeds.

Table 4.11 Cumulative breakage functions obtained for feed size -1.180+0.850 mm milled at 20%, 30% and 40% of critical respectively, U = 40%, J = 20% and d = 20 mm

	Mill speed ϕ_c (% of critical)		
Sieve size X_j (mm)	20%	30%	40%
1.180	1.000	1.000	1.000
0.850	1.000	1.000	1.000
0.600	0.478	0.547	0.463
0.425	0.330	0.370	0.294
0.300	0.222	0.268	0.198
0.212	0.152	0.200	0.128
0.150	0.073	0.141	0.087
0.106	0.033	0.103	0.054

The cumulative breakage function values calculated were fitted by empirical Equation (2.27) using nonlinear regression technique, and the model parameters were then estimated.

Table 4.12 Use of non-linear regression for the determination of breakage function parameters. Experimental conditions: Feed size -1.180+0.850 mm, ϕ_c = 20% of critical, U = 40%, J = 30%, and d = 20 mm

Sieve size X_j (mm)	x_i/x_j	$B_{i,j}$ (Equation 2.26)	$B_{i,j}$ (Equation 2.27)	Error
1.180	1.000	1.000	1.000	0.000
0.850	0.720	1.000	1.000	0.000
0.600	0.508	0.412	0.515	0.011
0.425	0.360	0.284	0.322	0.001
0.300	0.254	0.201	0.212	0.000
0.212	0.180	0.136	0.141	0.000
0.150	0.127	0.065	0.094	0.001
0.106	0.090	0.035	0.063	0.001
			Sum of squared errors	0.014

The predicted cumulative breakage function values fitted the experimental as shown in Figure 4.7. All other data set were fitted the same way and breakage function parameters were estimated.

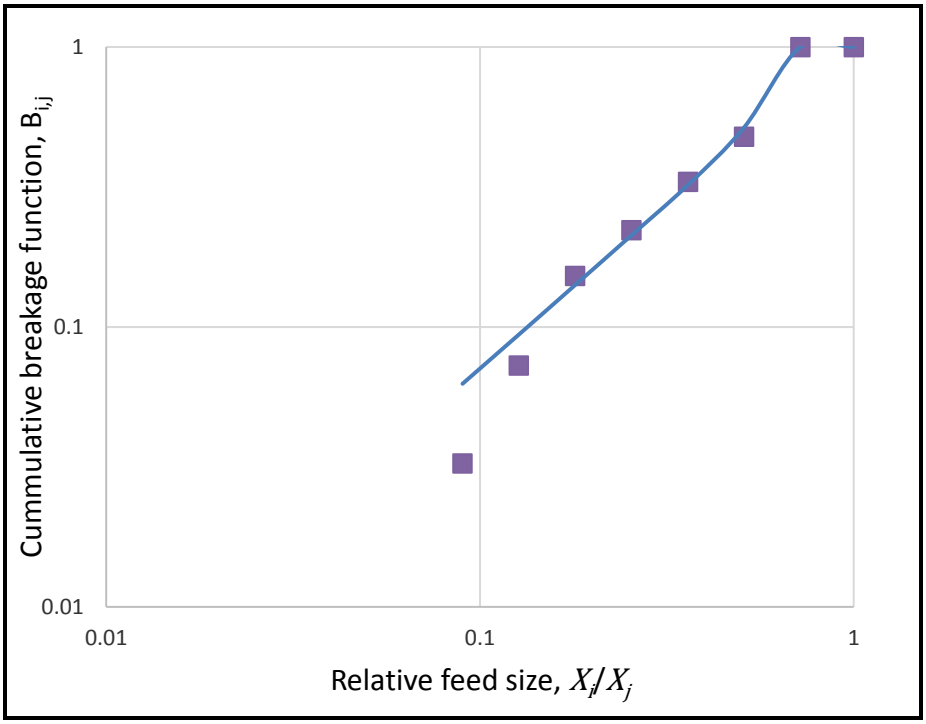

Figure 4.7 Cumulative breakage function plot for feed of size -1.180+0.850 mm milled at 30% of critical speed, U = 40%, J = 30%, and d = 20 mm balls

The breakage function parameters values obtained showed that β and γ were affected by neither size nor speed and the values were 6.3 and 1.17 respectively. The value of Φ was sensitive to the milling conditions and the values are shown in Table 4.13 for various mill speeds and feed sizes.

Table 4.13 Breakage function Φ for various mill speeds and feed sizes reported for average values β = 6.3 and γ = 1.17. Experimental conditions: U = 40%, J = 20% and d = 20 mm

	Mill speed (% of critical)		
Feed size (mm)	20%	30%	40%
-1.180+0.850	0.70	0.90	0.65
-0.850+0.600	0.50	0.55	0.60
-0.600+0.425	0.35	0.35	0.35
-0.425+0.300		0.25	
-0.300+0.212		0.35	

The results showed that Φ decreased with the decrease of feed size and started to increase again at the finest size. Change of Φ tells that the material is non-normalised. The higher value of Φ indicates that larger fractions of fine UG2 were produced in a single fracture event. Therefore, the feed size interval -1.180+0.850 mm broke faster than others at the short grinding time.

4.6 Summary

The breakage properties of UG2 platinum ore were determined using single-sized fraction method. Breakage function parameters (β, γ and Φ) and selection function parameters (a_0, α, μ, Λ) were determined for three mill speeds, i.e., 20%, 30% and 40% of the critical and compared. The milling kinetics of the ore showed that the material was breaking in a non-first-order manner. The rate of breakage (selection function) could not be determined by the slope of the breakage kinetics plot. As a result of this, the effective mean rate of breakage was determined by substituting the

time required to break 95% of feed material in Equation (2.6). Nonlinear regression techniques were utilised to determine the required time by fitting the experimental data with the model that described the experimental data. Basically, this technique works by finding the best fitting parameters of a model by minimising the square of the error between the experimental values and the predicted ones. The effective mean rate of breakage obtained was plotted as a function of feed size. It was observed that the rate of breakage increased with size, but at 30% of the critical speed, maximum size was reached and the breakage rate dropped. Again, the effective mean rate plot was fitted with selection function model and selection function parameters were determined. It was found at 20% and 40% of the critical that Λ and μ were not determined because the maximum size was not reached. As for the 30% of the critical speed, parameters a_0, α, μ, and Λ were determined as 0.04 min^{-1}, 1.36, 0.9 mm and 3.0 respectively.

Chapter 5 Assessment of the performance of a ball mill operated at low speed

5.1 Introduction

In this section, the performance of the ball mill was analysed by comparing the breakage parameters. It was also estimated in terms of energy expenditure and grind. Selection function parameter a_0 was scaled up in order to see if the population balance model can be used and extended to the application of ball mills operated at low speed. Equation 2.14 was used as a general function for scaling up breakage rate functions with changes in operating conditions.

5.2 Breakage characterisation

5.2.1 Non-normalisable breakage

Austin et al. (1984) mentioned that when the breakage function values are not constant, the material is said to be non-normalisable. It was observed in the previous chapter in Table 4.13 that the material (UG2 platinum ore) used in this study is non-normalisable, that is, Φ was changing with feed size and mill speed. The breakage function plot shown in Figure 5.1 also shows that the breakage function changed with feed size. The reason for this discrepancy is not known.

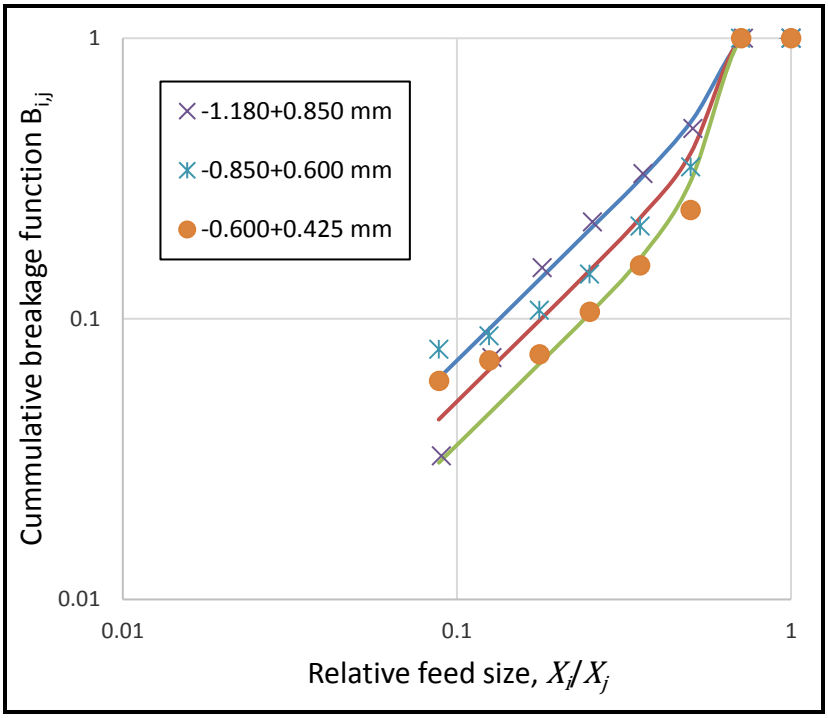

Figure 5.1 Cumulative breakage function plot for various feed sizes milled at 40% of the critical speed, U = 40%, J = 30%, and d = 20 mm balls

However, Chimwani et al. (2013) characterised the breakage function parameters of platinum ore and found that the ore was normalised.

5.2.2 Non-first order breakage

The grinding kinetics of the ore used in this study was reported in the previous chapter and it was observed that the ore followed a non-first order breakage. It was reported in literature that first order breakage of material is not always the case. Austin et al. (2007) observed a non-first-order breakage in one of their grinding tests. The researchers claimed that the milled fraction was too coarse to be broken by the ball size used since the finer fractions followed first-order under the same grinding conditions.

Gupta et al. (2007) suggested that the feed material should be pre-ground in order to stabilize the strength and shape distribution of the particle sizes so that weak particles can be removed to avoid fast and slow breakage. The pre-grinding was not done in this study since it's not a standard procedure. But it is believed that this could be one of the reasons leading to non-first-order breakage since the feed was not stabilised. Other possible factors contributing to non-first- order breakage may include sampling and sieving errors and the error due to abnormal motion of balls at the start and end of the mill rotation.

5.3 Scale-up of breakage parameters

Austin's scale-up procedure to batch grinding data was employed in the current study. The empirical model is shown as Equation (2.14), it takes into account the mill diameter (D), ball diameter (d), powder filling (Fc), ball filling (J) and mill speed (N). Chiwmwani et al. (2014) stated that since a_0 and μ depend on the conditions and the geometrical scale of the mill, their values have to be scaled up to the conditions of the mill to be simulated. Their scale-up procedures were shown in Equations (2.20) and (2.22) respectively.

The experimental "a_0" value obtained in this study was scaled up to conditions reported by Chimwani et al. (2013) because both studies used the same material, UG2 ore. Table 5.1 shows operating conditions of both studies. It can be seen that the scaled-up "a_0" value did not match the value by Chimwani et al. (2013). This could be due to errors via sample handling and the use of different equipment. Again, it could be that Chimwani's laboratory mill had lifters.

Table 5.1 Illustration of the scale-up of the value of parameter a_0 using conditions by Chimwani et al. (2013) as the baseline

	Chimwani et al. (2013)	Current study
Mill diameter (m)	0.302	0.175
Ball diameter (m)	0.01	0.02
Powder filling (U)	0.75	0.4
Ball filling (J)	0.2	0.2
Mill speed (ϕ_c)	0.75	0.20
a_0	0,32	0,04
Scaled up "a_0" value		0,03

The effect of speed on the model parameter a_0 is presented in Figure 5.2. The experimental data fitted with exponential function with R^2=0.9916. The obtained model was as follow:

$$a = 0.0134e^{4.1836Nc} \quad \textbf{(5.1)}$$

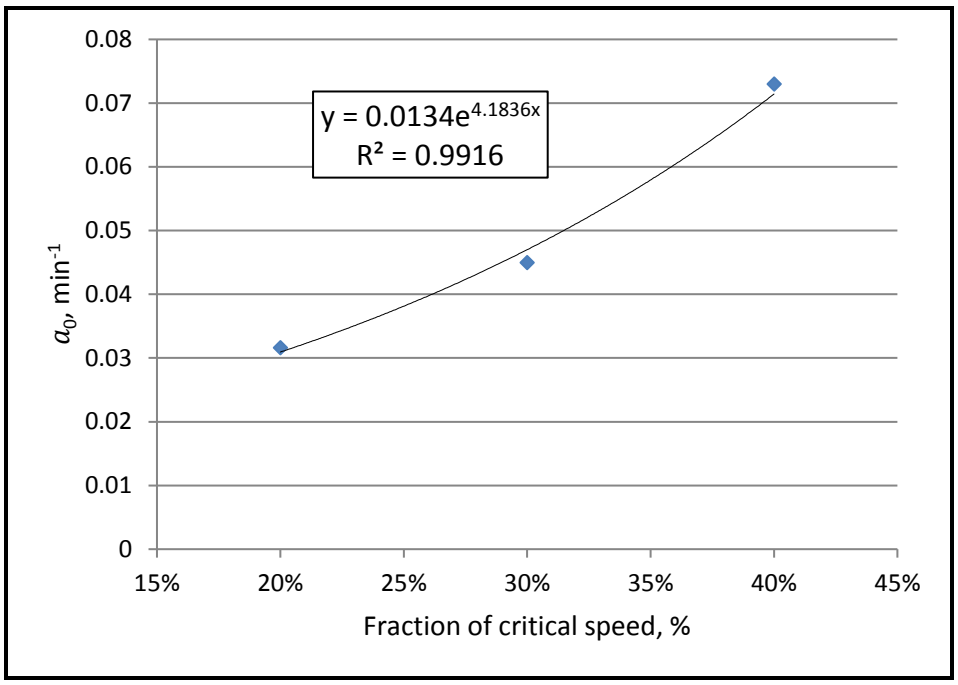

Figure 5.2 Variation of the value of a_0 with mill speed

The parameter a_0 describes how fast the feed size fraction breaks. Figure 5.2 shows how speed affects the breakage rate of the feed size class. It can be seen that the breakage rate increased with speed in an exponential form but the maximum speed was not reached. This suggests that higher speed can give good results in terms of breakage rate.

5.4 Mill performance: energy expenditure and grind

The mass fraction passing 75 µm is more preferable for measuring grind (Levin, 1992). In this study was found to be even more relevant as the UG2 ore needs finer grind for liberation of platinum group elements. Size specific energy is more effective regarding energy efficiency calculations because it is related to the generation of fines and not the reduction in the top size. In this section, effect of speed on grind and size specific energy was evaluated.

5.4.1 Effect of mill speed on grind

The results of the effect of speed on grind are shown in Figure 5.3. The results were fitted with a second-order polynomial function. It is clear that grinding for a longer period results in the higher grind, that is, more material passing 75 µm screen at all given mill speeds. Again it can be seen that the maximum grind is reached at different speeds depending on how long the milling takes place. The maximum grind was reached at approximately 30% of the critical speed when milling for 0.5 min, 2 min, 4 min, and 15 min. The longest grinding time of 30 min reached maximum grind at 40% of the critical speed. It does not help to increase the speed when grinding for short period i.e. less than 30 min since grind drops due to the agglomeration of particles as the mill speed increases.

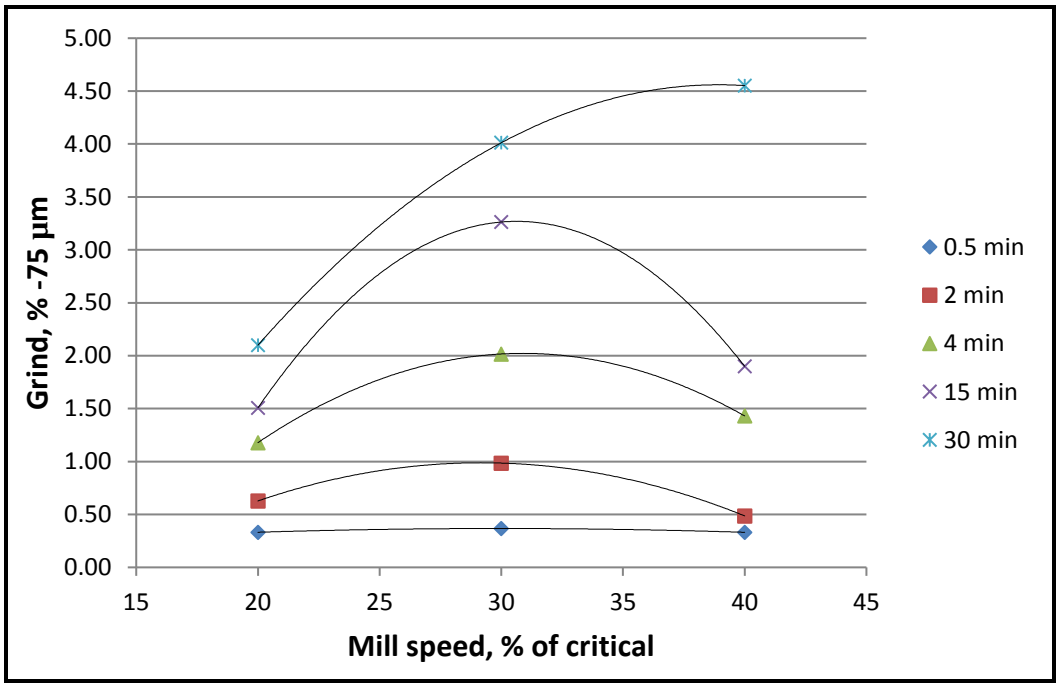

Figure 5.3 Effect of the rotational speed of the mill on the grind size

5.4.2 Size specific energy

The size-specific energy is a major input variable determining particle size reduction in a ball mill. It is calculated in three steps, i.e., mill power draw, mean specific energy and size-specific energy.

The power draw is modelled as the rate at which the potential and kinetic energy are imparted to the charge in the mill. Increasing the mill speed increases the imparted kinetic energy and also the potential energy (higher shoulder). Thus, higher power draws are expected with increased mill speed (Shi and Xie, 2015). Kelly and Spottiswood (1982) have shown in Figure 2.9 that power increase with speed is only up to point before power begins to drop. There is a point where the material starts to centrifuge as the speed increases leading to power drop. The maximum power draw was found around 90% of the critical speed and industries usually operate ball mills at 75%.

There are several methods for acquiring mill power draw. In this study, Equation (2.29) was used and the equation parameters are shown in Table 5.2.

Table 5.2 Calculations of mill power: the total load mass (i.e. mass of balls and sample) is M = 4.23+0.7 = 4.93kg; the rotating speeds are N= 0.36, 0.54, and 0.71 rps corresponding to 20%, 30% and 40% of the critical speed respectively; the mill diameter D = 0.18 m

N_c(rps)	M(kg)	D(m)	Power (W)
0.36	4.93	0.18	3.05
0.54	4.93	0.18	4.57
0.71	4.93	0.18	6.09

It is confirmed from Table 5.2 that power increases with mill speed. Figure 5.4 below shows this trend.

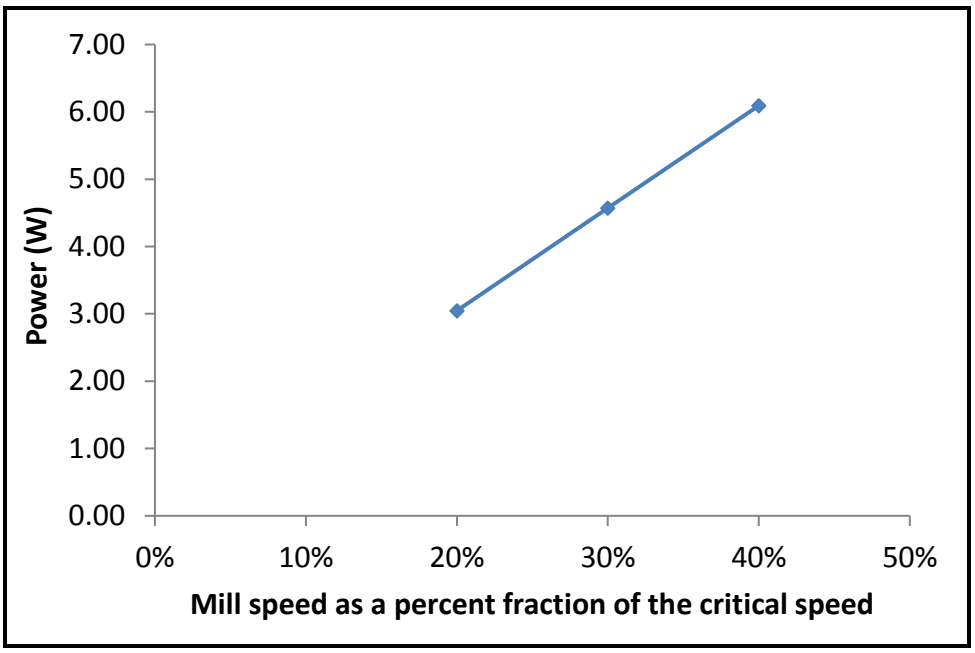

Figure 5.4 Effect of mill speed on the net power draw of the mill

It can be seen from Figure 5.4 that the power draw increases with increasing mill speed, but maximum speed was not reached as exemplified in Figure 2.9.

For the batch tests, the mill is loaded and rotated for a time t (sec) consuming energy $E = P\,t$ (Joules). This energy corresponds to a specific energy $e = E/m$ (Joules/ kg), where m is the mass (kg) of the sample. The energy that is consumed by the mill after each time interval and the corresponding estimated specific energy is shown in Table 5.3 and Table 5.4 respectively.

Table 5.3 Energy consumption as a function of mill speed and grinding time

	Energy Consumption (Joules)				
Power (W)	0.50 min	2.00 min	4.00 min	15.00 min	30.00 min
3.05	1.52	6.09	12.19	45.70	91.39
4.57	2.28	9.14	18.28	68.54	137.09
6.09	3.05	12.19	24.37	91.39	182.78

Table 5.4 Specific energy calculated from Table 5.3

	Specific energy (Joules/kg)				
Sample (kg)	0.50 min	2.00 min	4.00 min	15.00 min	30.00 min
0.70	2.18	8.70	17.41	65.28	130.56
0.70	3.26	13.06	26.11	97.92	195.84
0.70	4.35	17.41	34.82	130.56	261.12

According to Tables 5.3 and 5.4, it can be observed that more energy is consumed as the grinding time is prolonged.

There is a selection function governing the size-specific energy level: some particle sizes receiving more specific energy, while some other sizes receiving less. The available specific energy for each particle size, E_i (J /kg), is determined by a selection function S_i:

$$E_i = S_i * E \quad \textbf{(5.1)}$$

The results of the relationship between the size specific energy and the % grind passing 75 µm using data from Table 5.4 is given in Figure 5.5.

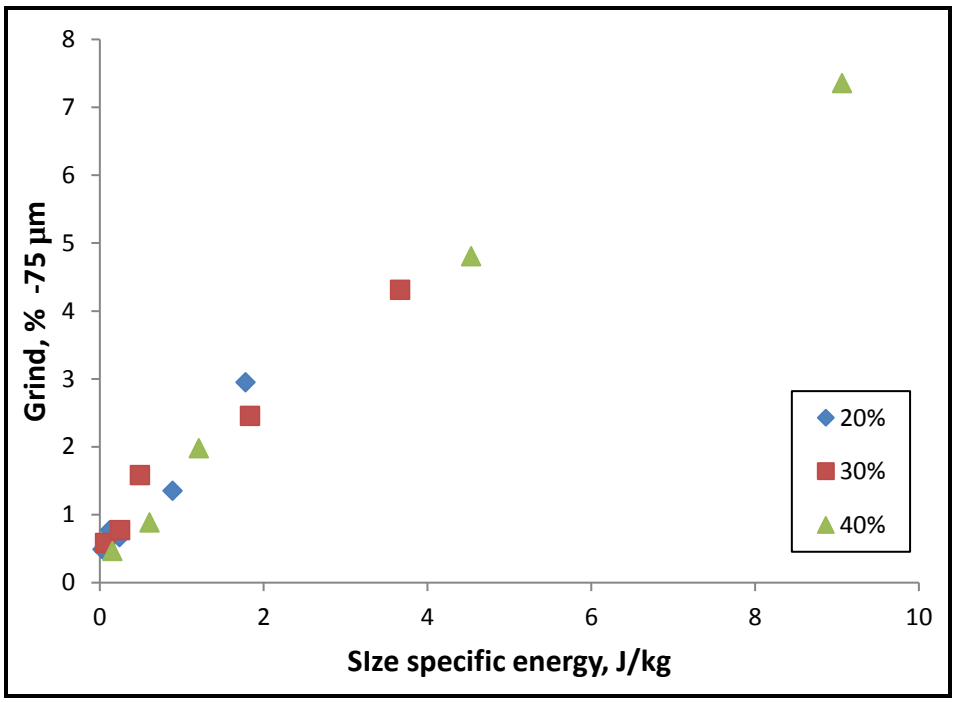

Figure 5.5 Size specific energy at various fractional speeds of the mill

According to Figure 5.5, the percentage grind increases as the size-specific energy increases at a specific operating speed. This was expected since more energy was needed to produce more grind or fines. However, a trend was seen at a very low size-specific energy closed to zero. At this point, as revealed by Figure 5.5, the data cluster together irrespective of the applied speed. This means that at this point the performance of the mill is approximately the same irrespective of the speed used. The behaviour at this point probably followed Bond's third law of communition which assigns the breakage of material only to the inherent physical property of the material (Bond., 1960). However, as the size-specific energy increased (e.g. close to 2 J/Kg), deviations in the performance in terms of % grind were observed for all tested speed. Moreover, the specific energy at 20% of the critical speed showed a deviation of positive slope compared to the negative slopes of the 30% and 40 % of the critical

speed. The reason for this deviation might be due to existence of lower energy due to lower speed.

5.5 Significance of the findings

In this study, it was found that the grinding kinetics of the UG2 ore followed a non-first-order breakage. The maximum grind was reached at approximately 30% of the critical speed when milling for 0.5 min, 2 min, 4 min, and 15 min while the longest grinding time of 30 min reached maximum grind at 40% of the critical speed. Also, it was observed that the breakage rate increased with speed in an exponential form while the power draw increased linearly with speed. This significantly means that when grinding for a short time (≤15 min), a speed of less than 40 % of the critical speed should be used, as greater speed will cause grind inefficiency due to higher power consumption and grind drop.

Chapter 6 Conclusions and recommendations

6.1 Introduction

The effects of mill rotational speed on the selection function and breakage function of a UG2 ore were investigated. Many researchers have investigated the matter (Gupta and Sharma, 2014; Austin et al., 1984; Deniz, 2013 & 2004; Ozkan et al., 2009; Fuerstenau, 1978) but not much literature can be found on low speed, that is, below 50% of critical speed. One size fraction method was employed in this study to determine breakage and selection function parameters. The parameters were then compared at different mill speed and feed size fraction. The milling kinetics of the ore was determined and it was found that the ore broke in a non-first-order manner. The deviation from the first-order was not large and the rate of breakage (selection function) was determined by the time required to break 95% of the ore. The population balance technique was successfully used to model the breakage behaviour of the UG2 ore at a low fraction of the critical speed.

The maximum grind was reached at approximately 30% of the critical speed when milling for 0.5, 2, 4, and 15 min while at 30 min maximum grind was reached at 40% of the critical speed. This means that speed of less than 40 % of the critical speed is required for a grind that requires less than or equal to 15 min to avoid poor grind performance and wasteful energy consumption. In terms of the speed, power draw and breakage rate, it was observed that the breakage rate increased with speed in an exponential form while the power draw increased linearly with speed. This altogether means, more energy is required to obtain more grinds.

6.2 Effect of mill speed on the breakage properties of the UG2 ore

Breakage and Selection function parameters are used to determine breakage properties of the material. Breakage function parameters are β, γ and Φ, and selection function parameters are a_0, α, μ and Λ.

6.2.1. Selection function parameters

The selection function values obtained showed that the breakage rate of size fractions used in this study increased with speed but maximum speed was not reached. Therefore, μ and Λ values were not defined. The values of α and a_0 were averaged to 0.76 and 0.04 min^{-1} respectively. It is recommended that more experiments be done at higher speeds to obtain optimum speed to be able to estimate accurately and precisely the values of μ and Λ .

6.2.2. Breakage function parameters

The breakage function parameters are known to be constant irrespective of the milling conditions (Austin et al., 1984). In this study, it was found that Φ changes with speed and feed size. This makes the material to be non-normalisable. The other parameters were found to be reasonably constant at β = 1.63, and γ = 1.17.

6.3 Size-specific energy

In terms of the size-specific energy, at lower specific energy, the % grind was approximately the same irrespective of the speed. This probably followed the bond's third theory of communition. Energy is expended the same way for useful grinding irrespective of mill speed or that the input energy determines the grind regardless of mill speed.

6.4 Recommendations for future work

As a result of the findings in this study, the following are recommended for future works:

- A pre-grind should be incorporated into the procedure to stabilize feed and thus, evaluate the possibility of obtaining a linear first-order breakage
- The mill speed greater than 40 % of the critical speed should be evaluated for the possibility of obtaining a maximum grind
- Ball mill with lifters same as Chimwani's should be used to see what difference could make on scaled-up value parameter a_0.

References

Acar, C., Hosten, C., 2013. Grinding kinetics of steady-state feeds in locked-cycle dry ball milling. Powder Technology, vol. 249, pp. 274–281

Arbiter, N., Harris, C.C., 1982. Scale-up and dynamics of large grinding mills-A case study. In Design and Installation of Comminution Circuits, Mular A.L and Jergensen G.V (Eds). Society of Mining Engineers of the American Institute of Mining, Metallurgical and Petroleum Engineers, pp. 491–505

Austin, L.G., 1971. A review introduction to the description of grinding as a rate process. Powder Technology, vol. 5, no. 1, pp. 1–17

Austin, L.G., Bagga, P., 1981. An analysis of fine dry grinding in ball mills. Powder Technology, vol. 28, no. 1, pp. 83– 90

Austin, L.G., Kesley J., de Souza A.S., Schneider C.L., 2007. Simulation of wet ball milling of iron ore at Carajas, Brazil. International Journal of Mineral Processing, vol. 84, no. 1-4, pp. 157–71

Austin, L.G., Klimpel, R.R., 1984. Modeling for scale-up of tumbling ball mills: Control '84. J.A. Herbst (eds), Society of Mining Engineers of the American Institute of Mining, Metallurgical and Petroleum Engineers, New York, pp. 167–184.

Austin L.G, Klimpel R.R, Luckie P.T., 1984, Process engineering of size reduction: ball milling. Society of Mining Engineers of the American Institute of Mining, Metallurgical and Petroleum Engineers, New York, USA.

Austin, L.G., Menacho, J.M., Pearcy, F.A., 1987. A general model for semi-autogenous and autogenous milling. Proceedings of the 20th International Symposium on the

Application of Computers and Mathematics in the Mineral Industries, Metallurgy, vol. 2, pp. 107–126

Austin, L.G., Trimarchi, T., Weymont, N.P., 1977. An analysis of some cases of non-first-order breakage rates. Powder Technology, vol. 17, no. 1, pp. 109–113

Ballantyne, G.R., Powell, M.S., 2014. Benchmarking comminution energy consumption for the processing of copper and gold ores. Minerals Engineering, vol. 65, pp. 109–114

Ballantyne, G.R., Peukert, W., Powell, M.S., 2015. Size specific energy (SSE) – energy required to generate minus 75 micron material. International Journal of Mineral Processing, vol. 136, pp. 2–6

Bhattacharyya, A., Tuzcu, E. T., Rajamani, R., 2016. Experimental study on non-linear behavior of breakage rates due to fines generation in wet batch milling. Minerals Engineering, vol. 99, pp. 19–29

Bilgili E., Scarlett B., 2005. Numerical simulation of open-circuit continuous mills using a non-linear population balance framework. Chemical Engineering Technololy, vol. 28, pp. 153–159

Bilgili, E., Hamey, R., Scarlett, B., 2004. Nano-milling of pigment agglomerates using a wet stirred media mill. Proceedings of the Second International Conference on Population Balance Modeling, Paper no. 20, Valencia, Spain

Bond F.C., 1960. Confirmation of the third theory. Transactions of the Society of Mining Engineers of the American Institute of Mining, Metallurgical and Petroleum Engineers, vol. 217, pp. 139–153

Bond F.C., 1961. Crushing and grinding calculations, Part I. British Chemical Engineering, vol. 6, pp. 378–385

Bond F.C., 1961. Crushing and grinding calculations, Part II. British Chemical Engineering, vol. 6, pp. 543–548

Bouchard, J., LeBlanc, G., Levesque, M., Radziszewski, P., Georges-Filteau, D., 2017. Breaking down energy consumption in industrial grinding mills, 49th annual Canadian mineral processors conference, Canadian Institute of Mining, Metallurgy and Petroleum, Ottawa, pp. 25 – 35

Cawthorn, R.G., 1999. The platinum and palladium resources of the Bushveld Complex, South African Journal of Science, vol. 95, pp. 481 – 489

Charkhi, A., Kazemian, H. and Kazemeini, M., 2010. Optimized experimental design for natural clinoptilolite zeolite ball milling to produce nano powders. Powder Technology, vol. 2, no. 2, pp. 389–396

Chierigati, A.C., 2001. Novo método de caracterização tecnológica para cominuição de minérios (in Portuguese), Universidade de São Paulo, Brazil

Chimwani, N., Glasser, D., Hildebrandt, D., Metzger, M.J., Mulenga F.K., 2013. Determination of the milling parameters of a platinum group minerals ore to optimize product size distribution for flotation purposes, minerals engineering, vol. 43–44, pp. 67–78

Chimwani N., Mulenga F.K., Hildebrandt, D., Glasser, D., Bwalya M.M., 2014. Scale-up of batch grinding data for simulation of industrial milling of platinum group minerals ore. Minerals Engineering, vol 63, pp. 100–109

Cho, H., Kwon, J., Kim, K., Mun, M., 2013. Optimum choice of the make-up ball sizes for maximum throughput in tumbling ball mills. Powder Technology, vol. 246, pp. 625–634

Cundall, P.A., Strack, O.D.L., 1979. A discrete numerical model for granular assemblies. Geotechnique, vol. 29, no. 1 pp. 47–65

Danha, G., Bhondayi C., Hlabangana N., Hildebrandt D., 2017. Determining the PGM bearing mineral phase in the UG2 ore. Powder Technology.vol. 315, pp. 236–242

Deniz, V., 2004. The effect of mill speed on kinetic breakage parameters of clinker and limestone. Cement and Concrete Research, vol. 34, no. 8, pp. 1365–71

Deniz, V., 2011. Influence of interstitial filling on breakage kinetics of gypsum in ball mill. Advanced Powder Technology, vol. 22, no. 4, pp. 512–517

Deniz, V., 2012. The effects of ball filling and ball diameter on kinetic breakage parameters of barite powder. Advanced Powder Technology, vol. 23, pp. 640–646

Deniz, V., 2013. Effects of mill speed on kinetic breakage parameters of four different particulate pumices. Particulate Science and Technology, vol. 31, pp. 101–108

Deniz, V., 2016. An investigation on the effects of the ball filling on the breakage parameters of natural amorphous silica. Advanced Powder Technology, vol. 27, no. 4 pp. 1272–1279

Deniz, V., Onur, T., 2002. Investigation of the breakage kinetics of pumice samples as dependent on powder filling in a ball mill. International Journal of Mineral Processing, vol. 67, pp. 71–78

Erdem, A. S., Ergun, S. L., 2009. The effect of ball size on breakage rate parameter in a pilot scale ball mill. Minerals Engineering, vol. 22, no. 7-8, pp. 660–664

Fogler, H.S., 1992. Elements of chemical reaction engineering, 2nd edition. Prentice-Hall, Englewood Cliffs, New York, USA.

Frances, C., Laguerie, C., Mazzarotta B., Veccia T., 1996. On the analysis of fine wet grinding in a batch ball mill. Chemical Engineering Journal and the Biochemical Engineering Journal, vol. 63, no. 3, pp. 141–147

Fuerstenau, D.W., 1978. Research on comminution process and simulation. Report no. BuMines OFR 39-79, National Technical Information Service, U.S. Department of Commerce, Springfield, VA. 22161

Gupta, V. K., 2016. Determination of the specific breakage rate parameters using the top-size-fraction method: Preparation of the feed charge and design of experiments, Advanced Powder Technology, vol. 27, no. 4, pp. 1710–1718

Gupta, V. K., 2018. Understanding production of fines in batch ball milling for mill scale-up design using the population balance model. Advanced Powder Technology, vol. 29, no. 4, pp. 2035–2047

Gupta, A., Yan, D.S., 2006. Mineral processing design and operation: An introduction, 1st Edition. Elsevier Science, ISBN: 978-0-4444-51636-7

Gupta, V. K., Sharma, S., 2014. Analysis of ball mill grinding operation using mill power specific kinetic parameters. Advanced Powder Technology, vol. 25, no. 2, pp. 265–634

Haeri, S., Wang, Y., Ghita, O., Sun, J., 2016. Discrete element simulation and experimental study of powder spreading process in additive manufacturing. Powder Technology, vol. 306, pp. 45–54

Han, Q., Setchi, R. and Evans, S.L. 2016. Synthesis and characterisation of advanced ball-milled Al-Al2O3 nanocomposites for selective laser melting. Powder Technology, vol. 297, pp. 183–192

Herbst, J.A., Fuerstenau, D.W., 1980. Scale-up procedure for continuous grinding mill design using population balance models. International Journal of Mineral Processing, vol. 7, no. 1, pp. 1–31

Herbst, J.A., Fuerstenau, D.W., 1973. Mathematical simulation of dry ball milling using specific power information. Transactions of the Society of Mining Engineers of the

American Institute of Mining, Metallurgical and Petroleum Engineers, vol. 254, pp. 343–348

Hilden, M., Suthers, S., 2010. Comparing energy efficiency of multi-pass high pressure grinding roll (HPGR) circuits. International Mineral Processing Congress, 2010 Proceedings, The Australasian Institute of Mining and Metallurgy, Brisbane, pp. 801–811

Hogg, R., Fuerstenau, D.W., 1972. Power relationships for tumbling mills. Transactions of the Society for Mining, Metallurgy and Exploration meeting, pp. 418–423

Hukki, R.T., 1979. Fundamentals of the closed grinding circuit. Engineering Mining Journal, vol. 180, pp. 102–109

Ipek, H., Ucbas, Y., 2005. Dry grinding kinetics of binary mixtures of ceramic raw materials by Bond milling. Ceramics International, vol. 31, no. 8, pp. 1065–1071

Jones, RT., 2005. An overview of Southern African PGM smelting, 44th Annual Conference of Metallurgists, Calgary, Alberta, Canada, pp. 147–178

Katubilwa, F.M., Moys, M.H., 2009. Effect of ball size distribution on milling rate. Minerals Engineering, vol. 22, no. 15, pp. 1283–1288

Kelly, E.G., Spottiswood, D.J., 1982. Introduction to mineral processing. Wiley, New York, United States of America

Kelsall, D.F., Reid, K.J., Restarick, C.J., 1968. Continuous grinding in a small wet ball mill – Part I. A study of the influence of ball diameter. Powder Technology, vol. 1, no. 5, pp. 291–300

Kime, M.B., Moys, M.H., 2017. Binary modelling the milling of UG2 ore using a matrix approach. Journal of Materials Research and Technology, vol. 6, no. 2, pp. 184–193

King, R.P., 2001. Modeling and simulation of mineral processing systems. Butterworth-Heinemann, Oxford, United Kingdom

Kotake, N., Mitsuyuki, K., Shinichi, K., Yoshiteru, K., 2011. Influence of dry and wet grinding conditions on fineness and shape of particle size distribution of product in a ball mill. Advanced Powder Technology, vol. 22, no. 1, pp. 86–92

Kwon, J., Heechan, C., Daeyang L., Rina, K., 2014. Investigation of breakage characteristics of low rank coals in a laboratory swing hammer mill. Powder Technology, vol. 256, pp. 377–384

Levin, J. 1992. Indicators of grindability and grinding efficiency. Journal of the South African Institute of Mining and Metallurgy, vol. 92, no. 10, pp. 283–290

Matijasis, G., Kurajica, S., 2010. Grinding kinetics of amorphous powder obtained by sol-gel process. Powder Technology, vol. 197, no. 3, pp. 165–169

Metzger, M.J., Desai, S.P., Glasser, D., Hildebrandt, D. and Glasser, B.J., 2011. Using the attainable region analysis to determine the effect of process parameters on breakage in a ball mill. American Institute of Chemical Engineers Journal, vol. 58, no. 9, pp. 2665–2673

Morrell, S., 1996. Power draw of wet tumbling mills and its relationship to charge dynamics. Part 1: A continuum approach to mathematical modelling of mill power draw. Transactions of the Institute of Mining and Metallurgy, vol. C105, pp. 43–53

Mulenga, F.K., 2017. Sensitivity analysis of Austin's scale-up model for tumbling ball mills — Part 2. Effects of full-scale milling parameters. Powder Technology, vol. 317, pp. 6–12

Mulenga, F.K., Mkonde, A.A., Bwalya, M.M., 2016. Effects of load filling, slurry concentration and feed flowrate on the attainable region path of an open milling circuit. Minerals Engineering, vol. 89., pp. 30–41

Mulenga, F.K., Moys, M.H., 2014a. Effects of slurry filling and mill speed on the net power draw of a tumbling ball mill. Minerals Engineering, vol. 56, pp. 45–56

Mulenga, F.K., Moys, M.H. 2014b. Effects of slurry pool volume on milling efficiency. Powder Technology, vol. 256, pp. 428–435

Musa, F., Morrison, R., 2009. A more sustainable approach to assessing comminution efficiency. Minerals Engineering, vol. 22, no. 7-8, pp. 593–601

Mwansa, S., Powell, M.S., 2005. AngloGold Ashanti Kopanang SAG mills Report 1 – Site report, raw data, and observations. Report delivered to AngloGold Ashanti

Napier-Munn, T.J.,Morrison, R.D., Kojovic, T., 1999. Minerals Comminution Circuits: Their operation and optimization. Julius Kruttschnitt Mineral Research Centre, University of Queensland, Australia

Oliveira, A.L.R., Tavares, L.M., 2018. Modeling and simulation of continuous open circuit dry grinding in a pilot-scale ball mill using Austin's and Nomura's models. Powder Technology, vol. 340, pp.77–87

Ozkan, A., Yekeler, M. Calkaya, M. 2009. Kinetics of fine wet grinding of zeolite in a steel ball mill in comparison to dry grinding. International Journal of Mineral Processing, vol. 90, no. 1-4, pp. 67–73

Petrakis, E., Stamboliadis, E., Komnitsas, K., 2017. Identification of optimal mill operating parameters during grinding of quartz with the use of population balance modeling. KONA Powder and Particle Journal, vol. 34, pp. 213–223

Reid, K.J., 1965. A solution to the batch grinding equation. Chemical Engineering Sciences, vol. 20, no. 11, pp. 953–963

Rosa, A.C., De Oliveira P.S., Donda J.D. 2014. Comparing ball and vertical mills performance: An industrial case study. International Mineral Processing Congress, 01.01.2014, pp. 1–9

Simba, K.P., Moys, M.H., 2014. Effects of mixtures of grinding media of different shapes on milling kinetics. Minerals Engineering, vol. 61, pp. 40–46

Stambodiadis, E., Emmanaoilidis S., Petrakis E.A., 2011. New approach to the calculation of work index and the potential energy of a particulate material. Geomaterisld, vol. 1, pp. 20–32

Tangsathitkulchai, C., 2002. Acceleration of particle breakage rates in wet batch ball milling. Powder Technology, vol. 124, no. 1-4, pp. 67–75

Tangsathitkulchai, C., 2003. Effects of slurry concentration and powder filling on the net mill power of a laboratory ball mill. Powder Technology, vol. 69, no. 3, pp. 29–47

Tangsathitkulchai, C., Austin, L.G., 1985. The effect of slurry density on breakage parameters of quartz, coal and copper ore in a laboratory ball mill. Powder Technology, vol. 42, no. 3, pp. 287–296

Tavares, L.M., 2007. Breakage of single particles: Quasi-static. Handbook of Powder Technology, pp. 3–68

Tavares, L.M., King, R.P., 1998. Single-particle fracture under impact loading. International Journal of Mineral Processing, vol. 54, no. 1, pp. 1–28

Teke, E., Yekeler, M., Ulusoy, U., Canbazoglu, M., 2002. Kinetics of dry grinding of industrial minerals: calcite and barite. International Journal of Mineral Processing, vol. 67, no. 1-4, pp. 29–42

Wills, B.A., Napier-Munn, T.J., 2005. Wills' mineral processing technology: An introduction to the practical aspects of ore treatment and mineral recovery, Seventh Edition, Elsevier, London, ISBN: 9780750644501

Wills, B.A., Finch, J.A., 2015. Wills' mineral processing technology: An introduction to the practical aspects of ore treatment and mineral recovery, Eighth Edition, Elsevier, London, ISBN: 9780080970530

Yildirim, K., Cho, H., Austin, L.G., 1999. The modelling of dry grinding of quartz in tumbling media mills. Powder Technology, vol. 105, no. 1-3, pp. 210–221

Zafar, U., Hare, C., Hassanpour, A., Ghadiri, M., 2014. Drop test: a new method to measure the particle adhesion force. Powder Technology, vol. 264, pp. 236–241

Zhao, R., Yuexin, H., Mingzhao, H., Yanjun, L., 2017. Grinding kinetics of quartz and chlorite in wet ball milling. Powder Technology, vol. 305, pp. 418–425

Appendices

A. Particle size distribution analysis

Table A.1 Cumulative mass fractions passing sieve for various batch milling times and mill speed ϕ_c = 20% of critical. Experimental conditions: feed size - 0.1180+0.850 mm, powder filling U = 40%, ball filling J = 20%, and ball size d = 20 mm

	Grinding time (min)				
Sieve size X_j (mm)	**0.5 min**	**2 min**	**4 min**	**15 min**	**30 min**
1.180	100.00	100.00	100.00	100.00	100.00
0.850	8.43	16.43	22.86	40.43	51.14
0.600	3.57	8.22	12.37	24.44	32.91
0.425	2.47	5.75	8.47	17.24	24.53
0.300	1.76	3.90	5.95	12.26	18.07
0.212	1.19	2.70	4.11	8.56	13.15
0.150	0.57	1.30	2.14	4.57	7.55
0.106	0.31	0.58	1.02	2.27	4.12

Table A.2 Cumulative mass fractions passing sieve for various batch milling times and mill speed ϕ_c = 30% of critical. Experimental conditions: feed size - 0.1180+0.850 mm, powder filling U = 40%, ball filling J = 20%, and ball size d = 20 mm

	Grinding time (min)				
Sieve size X_j (mm)	**0.5 min**	**2 min**	**4 min**	**15 min**	**30 min**

1.180	100.00	100.00	100.00	100,00	100.00
0.850	9.57	21.29	29.00	50.43	58.29
0.600	5.35	12.52	18.17	33.96	41.99
0.425	3.65	8.50	12.17	24.49	31.72
0.300	2.66	5.72	8.45	17.99	23.69
0.212	1.99	4.03	5.82	13.18	18.18
0.150	1.41	2.05	2.94	7.07	10.94
0.106	1.03	1.35	1.73	3.68	5.19

Table A.3 Cumulative mass fractions passing sieve for various batch milling times and mill speed ϕ_c = 40% of critical. Experimental conditions: feed size -0.1180+0.850 mm, powder filling U = 40%, ball filling J = 20%, and ball size d = 20 mm

	Grinding time (min)				
Sieve size X_j (mm)	**0.5 min**	**2 min**	**4 min**	**15 min**	**30 min**
1.180	100.00	100.00	100.00	100.00	100.00
0.850	12.43	27.86	39.29	61.00	74.57
0.600	5.96	14.61	22.21	40.03	53.89
0.425	3.83	9.52	15.11	29.88	43.04
0.300	2.59	6.35	10.21	21.70	33.40
0.212	1.68	3.97	6.58	15.13	24.01
0.150	1.15	2.67	4.28	10.00	17.52
0.106	0.71	1.37	2.43	4.64	9.34

Table A.4 Cumulative mass fractions passing sieve for various batch milling times and mill speed ϕ_c = 20% of critical. Experimental conditions: feed size - 0.850+0.600 mm, powder filling U = 40%, ball filling J = 20%, and ball size d = 20 mm

	Grinding time (min)				
Sieve size X_j (mm)	**0.5 min**	**2 min**	**4 min**	**15 min**	**30 min**
0.850	100.00	100.00	100.00	100.00	100.00
0.600	6.14	12.43	17.86	33.57	44.29
0.425	2.19	5.40	8.58	18.53	25.95
0.300	1.35	3.16	5.10	11.68	17.11
0.212	0.91	1.96	3.00	7.25	11.31
0.150	0.68	1.25	1.65	4.27	6.83
0.106	0.55	0.78	0.76	1.90	3.31
0.075	0.49	0.78	0.67	1.36	2.95

Table A.5 Cumulative mass fractions passing sieve for various batch milling times and mill speed ϕ_c = 30% of critical. Experimental conditions: feed size - 0.850+0.600 mm, powder filling U = 40%, ball filling J = 20%, and ball size d = 20 mm

	Grinding time (min)				
Sieve size X_j (mm)	**0.5 min**	**2 min**	**4 min**	**15 min**	**30 min**
0.850	100.00	100.00	100.00	100.00	100.00
0.600	7.71	16.43	24.71	43.43	55.29
0.425	2.85	7.71	11.82	24.92	33.99

0.300	1.75	4.27	7.05	15.69	22.84
0.212	1.17	2.69	4.42	10.16	15.39
0.150	0.82	1.68	2.81	6.23	9.67
0.106	0.60	0.97	1.61	3.26	5.38
0.075	0.59	0.78	1.58	2.46	4.31

Table A.6 Cumulative mass fractions passing sieve for various batch milling times and mill speed ϕ_c = 40% of critical. Experimental conditions: feed size -0.850+0.600 mm, powder filling U = 40%, ball filling J = 20%, and ball size d = 20 mm

	Grinding time (min)				
Sieve size X_j (mm)	**0.5 min**	**2 min**	**4 min**	**15 min**	**30 min**
0.850	100.00	100.00	100.00	100.00	100.00
0.600	9.14	21.86	31.43	56.57	69.71
0.425	4.30	10.90	16.66	35.39	48.76
0.300	2.51	6.23	9.84	23.01	34.15
0.212	1.60	3.80	6.17	15.13	23.54
0.150	1.06	2.46	4.01	10.20	16.89
0.106	0.62	1.25	2.72	6.63	9.88
0.075	0.47	0.89	1.98	4.81	7.36

Table A.7 Cumulative mass fractions passing sieve for various batch milling times and mill speed ϕ_c = 20% of critical. Experimental conditions: feed size - 0.600+0.425 mm, powder filling U = 40%, ball filling J = 20%, and ball size d = 20 mm

	Grinding time (min)				
Sieve size X_j (mm)	**0.5 min**	**2 min**	**4 min**	**15 min**	**30 min**
0.600	100.00	100.00	100.00	100.00	100.00
0.425	4.57	10.29	12.00	28.86	39.00
0.300	1.14	3.46	5.11	12.44	18.65
0.212	0.72	2.12	3.02	7.47	11.65
0.150	0.49	1.37	1.84	4.25	6.81
0.106	0.35	0.90	1.62	1.78	2.80
0.075	0.33	0.63	1.18	1.51	2.10
0.053	0.28	0.60	0.70	0.94	1.60

Table A.8 Cumulative mass fractions passing sieve for various batch milling times and mill speed ϕ_c = 30% of critical. Experimental conditions: feed size - 0.600+0.425 mm, powder filling U = 40%, ball filling J = 20%, and ball size d = 20 mm

	Grinding time (min)				
Sieve size X_j (mm)	**0.5 min**	**2 min**	**4 min**	**15 min**	**30 min**
0.600	100.00	100.00	100.00	100.00	100.00
0.425	6.51	14.26	21.29	39.12	52.47
0.300	1.83	5.21	8.66	19.47	28.74

0.212	1.09	2.95	5.12	11.33	18.13
0.150	0.69	1.69	3.08	6.87	11.52
0.106	0.44	1.01	2.09	3.34	6.73
0.075	0.37	0.99	2.02	3.26	4.01
0.053	0.27	0.57	1.30	1.53	1.94

Table A.9 Cumulative mass fractions passing sieve for various batch milling times and mill speed ϕ_c = 40% of critical. Experimental conditions: feed size -0.600+0.425 mm, powder filling U = 40%, ball filling J = 20%, and ball size d = 20 mm

	Grinding time (min)				
Sieve size X_j (mm)	**0.5 min**	**2 min**	**4 min**	**15 min**	**30 min**
0.600	100.00	100.00	100.00	100.00	100.00
0.425	8.29	18.14	27.86	49.86	67.57
0.300	2.40	6.80	11.60	25.70	41.74
0.212	1.40	3.74	6.74	15.49	27.48
0.150	0.83	1.95	3.85	8.61	17.01
0.106	0.45	0.77	2.01	3.55	10.12
0.075	0.33	0.49	1.43	1.90	4.55
0.053	0.28	0.35	1.13	1.30	3.33

Table A.10 Cumulative mass fractions passing sieve for various batch milling times and mill speed ϕ_c = 30% of critical. Experimental conditions: feed size -0.425+0.300 mm, powder filling U = 40%, ball filling J = 20%, and ball size d = 20 mm

	Grinding time (min)				
Sieve size X_j (mm)	**0.5 min**	**2 min**	**4 min**	**15 min**	**30 min**
0.425	100.00	100.00	100.00	100.00	100.00
0.300	4.29	8.00	10.71	22.57	32.14
0.212	0.85	2.38	4.12	9.52	14.79
0.150	0.51	1.39	2.42	5.22	7.97
0.106	0.29	0.96	1.66	3.13	4.48
0.075	0.22	0.76	1.65	2.25	2.97
0.053	0.20	0.72	1.22	1.95	2.20
0.038	0.17	0.69	0.96	1.48	1.36

Table A.11 Cumulative mass fractions passing sieve for various batch milling times and mill speed ϕ_c = 30% of critical. Experimental conditions: feed size -0.300+212 mm, powder filling U = 40%, ball filling J = 20%, and ball size d = 20 mm

	Grinding time (min)				
Sieve size X_j (mm)	**0.5 min**	**2 min**	**4 min**	**15 min**	**30 min**
0.300	100.00	100.00	100.00	100.00	100.00
0.212	5.66	6.91	7.05	16.22	29.50
0.150	0.66	1.43	2.16	6.02	10.88

0.106	0.41	0.78	1.11	2.87	5.63
0.075	0.37	0.73	1.07	1.94	5.50
0.053	0.23	0.35	0.43	1.07	2.37
0.038	0.11	0.10	0.17	0.43	1.14
0.025	0.00	0.08	0.15	0.38	1.00

B. Retained mass on feed size fraction

Table B.1 Retained mass percentages on top feed size. Experimental conditions: feed size -1.180+0.850 mm, U = 40%, J = 20%, and d = 20 mm

Time (min)	20% critical speed	30% critical speed	40% critical speed
0.00	100.00	100.00	100.00
0.50	91.57	90.43	87.57
2.00	83.57	78.71	72.14
4.00	77.14	71.00	60.71
15.00	59.57	49.57	39.00
30.00	48.86	41.71	25.43

Table B.2 Retained mass percentages on top feed size. Experimental conditions: feed size -0.850+0.600 mm, U = 40%, J = 20%, and d = 20 mm

Time (min)	20% Critical speed	30% critical speed	40% critical speed
0.00	100.00	100.00	100.00
0.50	93.86	92.29	90.86
2.00	87.57	83.57	78.14
4.00	82.14	75.29	68.57
15.00	66.43	56.57	43.43
30.00	55.71	44.71	30.29

Table B.3 Retained mass percentages on top feed size. Experimental conditions: feed size -0.600+0.425 mm, U = 40%, J = 20%, and d = 20 mm

Time (min)	20% critical speed	30% critical speed	40% critical speed
0.00	100.00	100.00	100.00

0.50	95.43	93.49	91.71
2.00	89.71	85.74	81.86
4.00	88.00	78.71	72.14
15.00	71.14	60.88	50.14
30.00	61.00	47.53	32.43

Table B.4 Retained mass percentages on top feed size. Experimental conditions: feed size -0.425+0.300 mm, U = 40%, J = 20%, and d = 20 mm

Time (min)	30% Critical speed
0.00	100.00
0.50	95.71
2.00	92.00
4.00	89.29
15.00	77.43
30.00	67.86

Table B.5 Retained mass percentages on top feed size. Experimental conditions: feed size -0.300+0.212 mm, U = 40%, J = 20%, and d = 20 mm

Time (min)	30% Critical speed
0.00	100.00
0.50	94.34
2.00	93.09
4.00	92.95
15.00	83.78
30.00	70.50

C. Milling kinetics

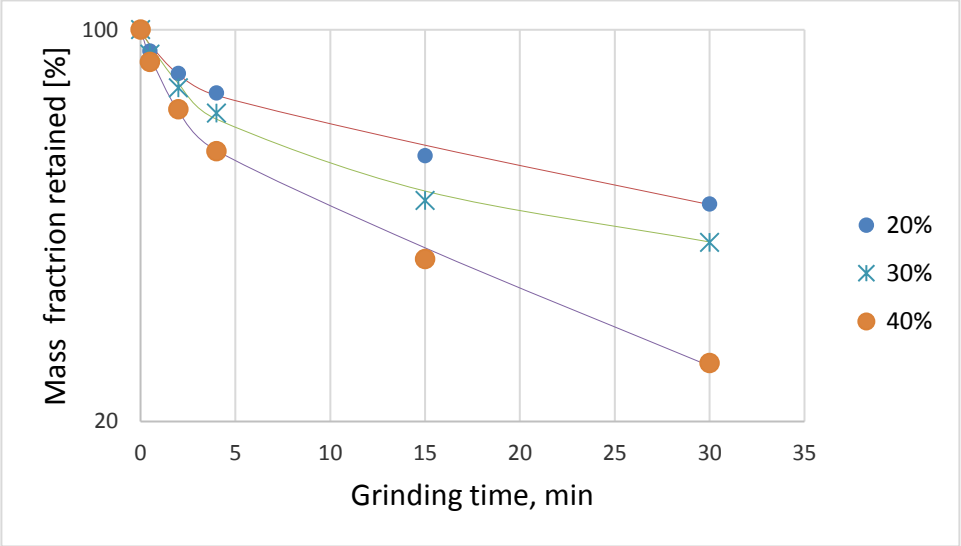

Figure C.1 Milling kinetics of the UG2 platinum ore for feed size -0.1.180+0.850 mm milled at various fraction of critical speed ϕ_c. Milling conditions: U = 40%, J = 20%, and d = 20 mm

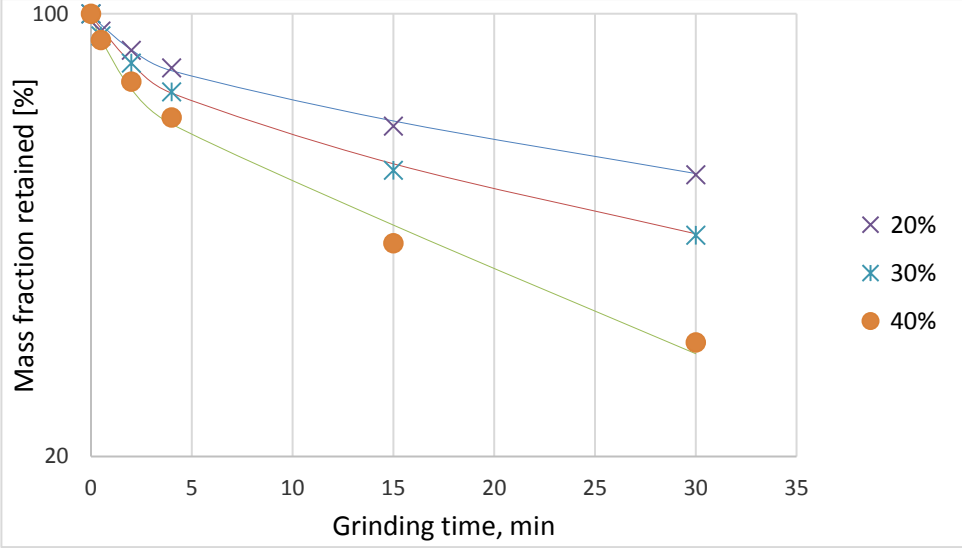

Figure C.2 Milling kinetics of the UG2 platinum ore for feed size -0.850+0.600 mm milled at various fraction of critical speed ϕ_c. Milling conditions: U = 40%, J = 20%, and d = 20 mm

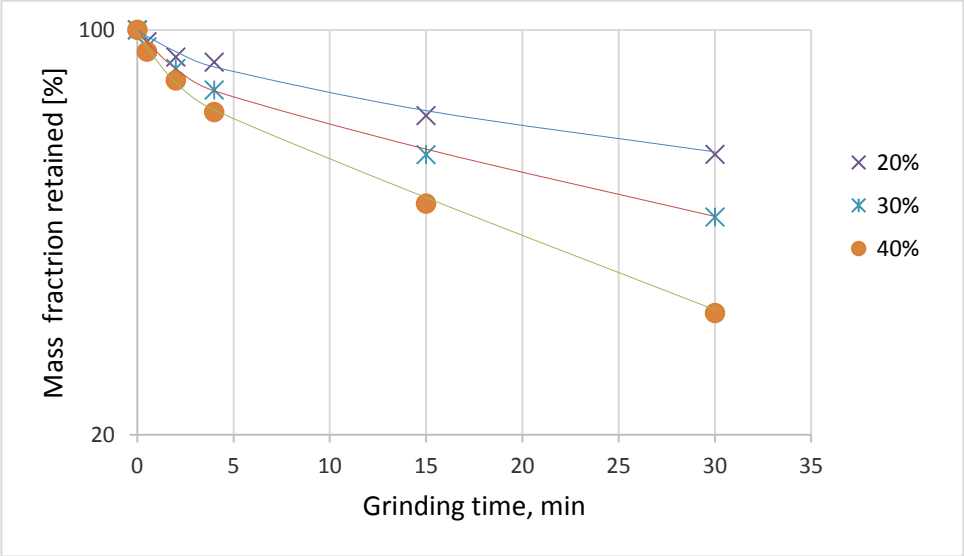

Figure C.3 Milling kinetics of the UG2 platinum ore for feed size -0.600+425 mm milled at various fraction of critical speed ϕ_c. Milling conditions: U = 40%, J = 20%, and d = 20 mm

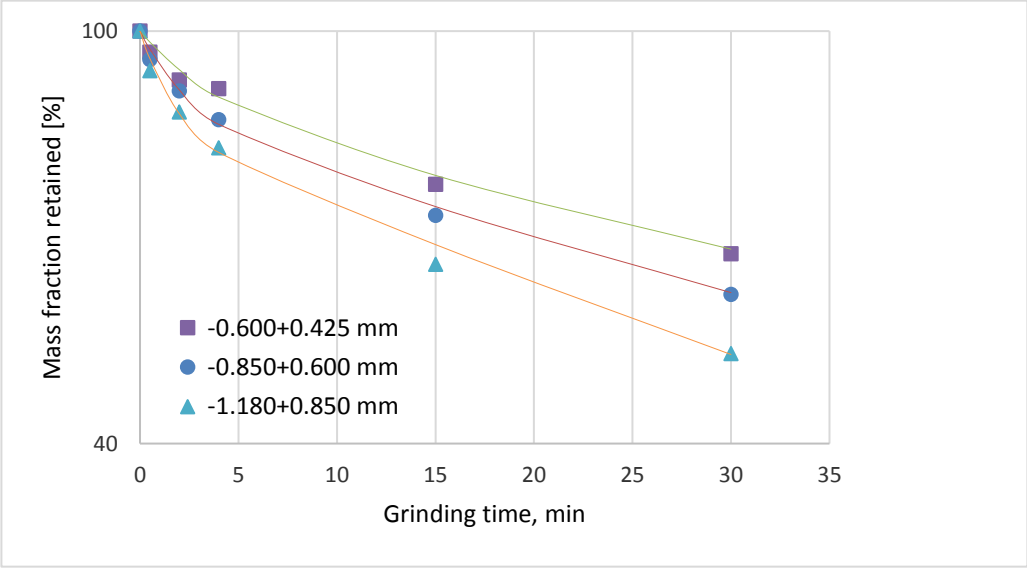

Figure C.4 Milling kinetics of the UG2 platinum ore at ϕ_c = 20% of critical speed for various feed sizes. Milling conditions: U = 40%, J = 20%, and d = 20 mm

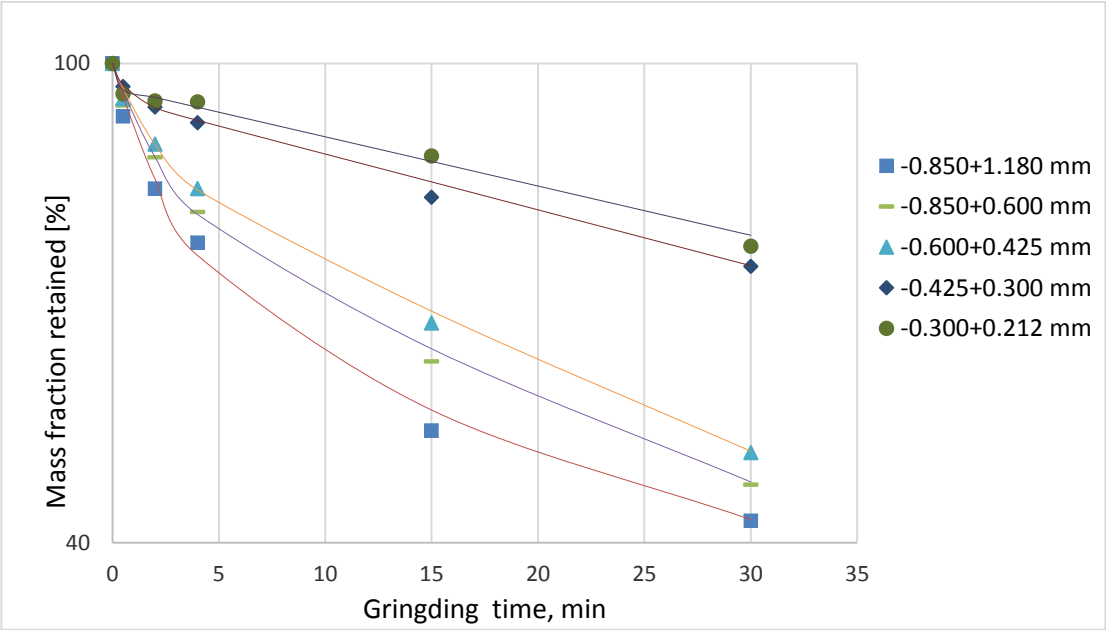

Figure C.5 Milling kinetics of the UG2 platinum ore at ϕ_c = 30% of critical speed for various feed sizes. Milling conditions: U = 40%, J = 20%, and d = 20 mm

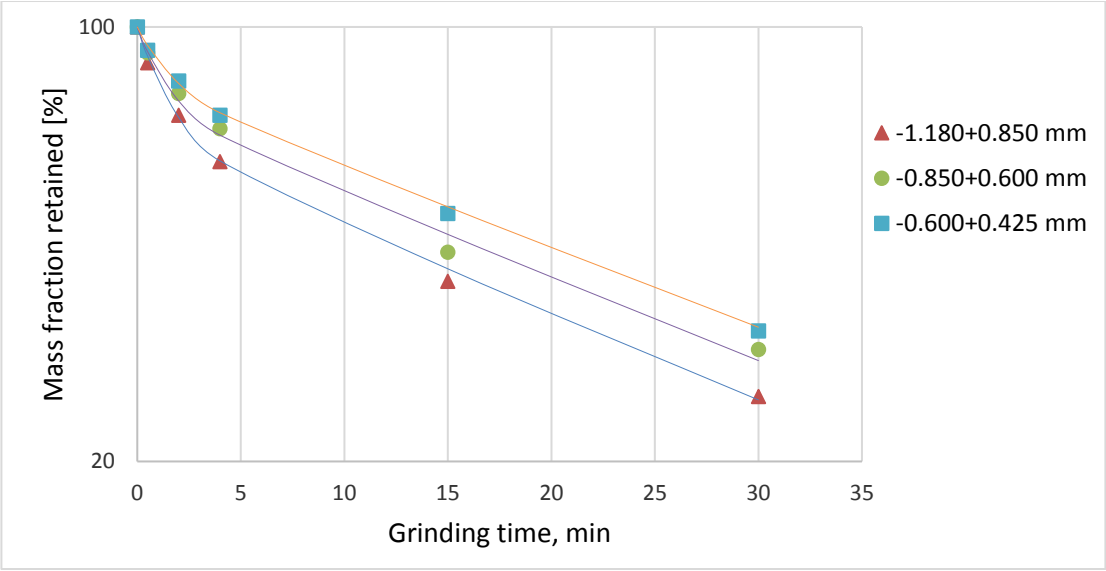

Figure C.6 Milling kinetics of the UG2 platinum ore at ϕ_c = 40% of critical speed for various feed sizes. Milling conditions: U = 40%, J = 20%, and d = 20 mm

D. Cumulative breakage functions

Table D.1 Cumulative breakage functions obtained for feed size -1.180+0.850 mm milled at 20%, 30% and 40% of critical respectively, U = 40%, J = 20% and d = 20 mm

		20% critical speed	30% critical speed	40% critical speed
Upper size	x_i/x_j	$B_{i,j}$	$B_{i,j}$	$B_{i,j}$
1.180	1.000	1.000	1.000	1.000
0.850	0.720	1.000	1.000	1.000
0.600	0.508	0.478	0.547	0.463
0.425	0.360	0.330	0.370	0.294
0.300	0.254	0.222	0.268	0.198
0.212	0.180	0.152	0.200	0.128
0.150	0.127	0.073	0.141	0.087
0.106	0.090	0.033	0.103	0.054

Table D.2 Cumulative breakage functions obtained for feed size -0.850+0.600 mm milled at 20%, 30% and 40% of critical respectively, U = 40%, J = 20% and d = 20 mm

		20% critical speed	30% critical speed	40% critical speed
Upper size	x_i/x_j	$B_{i,j}$	$B_{i,j}$	$B_{i,j}$
0.850	1.000	1.000	1.000	1.000
0.600	0.706	1.000	1.000	1.000
0.425	0.500	0.349	0.361	0.458
0.300	0.353	0.215	0.220	0.265
0.212	0.249	0.144	0.147	0.169

0.150	0.176	0.107	0.102	0.111
0.106	0.125	0.087	0.075	0.065
0.075	0.088	0.078	0.074	0.049

Table D.3 Cumulative breakage functions obtained for feed size -0.600+0.425 mm milled at 20%, 30% and 40% of critical respectively, U = 40%, J = 20% and d = 20 mm

		20% critical speed	**30% critical speed**	**40% critical speed**
Upper size	x_i/x_j	$B_{i,j}$	$B_{i,j}$	$B_{i,j}$
0.600	1.000	1.000	1.000	1.000
0.425	0.708	1.000	1.000	1.000
0.300	0.500	0.244	0.275	0.281
0.212	0.353	0.155	0.163	0.163
0.150	0.250	0.106	0.103	0.096
0.106	0.177	0.075	0.065	0.052
0.075	0.125	0.071	0.055	0.038
0.053	0.088	0.060	0.040	0.032

Table D.4 Cumulative breakage functions obtained for feed size -0.425+0.300 mm milled at ϕ_c = 30% of critical, U = 40%, J = 20% and d = 20 mm

		30% critical speed
Upper size	x_i/x_j	$B_{i,j}$
0.425	1.000	1.000
0.300	0.706	1.000

0.212	0.499	0.194
0.150	0.353	0.115
0.106	0.249	0.067
0.750	0.176	0.051
0.053	0.125	0.045
0.038	0.089	0.038

Table D.5 Cumulative breakage functions obtained for feed size -0.300+0.212 mm milled at ϕ_c = 40% of critical, U = 40%, J = 20% and d = 20 mm

		30% critical speed
Upper size	x_i/x_j	$B_{i,j}$
0.300	1.000	1.000
0.212	0.707	1.000
0.150	0.500	0.351
0.106	0.353	0.165
0.075	0.250	0.111
0.053	0.177	0.061
0.038	0.127	0.025
0.025	0.083	0.021

E. Cumulative breakage function plots

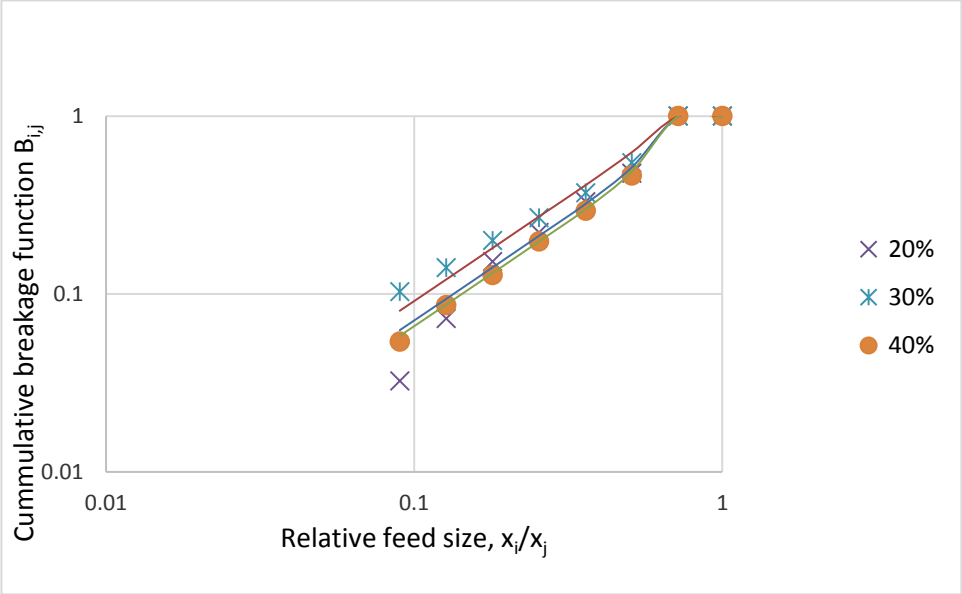

Figure E.1 Cumulative breakage function plot for feed of size -1.180+0.850 mm milled at various % critical speed, U = 40%, J = 30%, and d = 20 mm balls

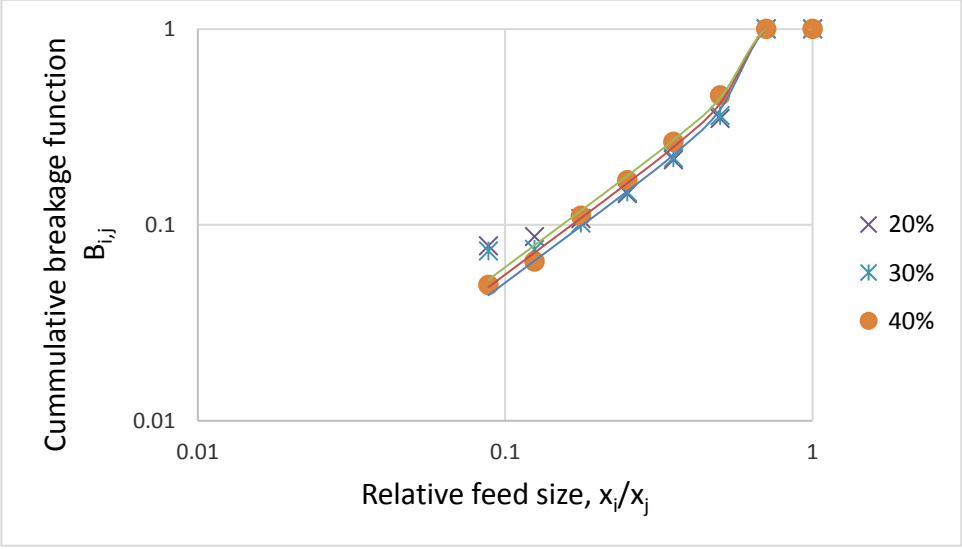

Figure E.2 Cumulative breakage function plot for feed of size -0.850+0.600 mm milled at various % critical speed, U = 40%, J = 30%, and d = 20 mm balls

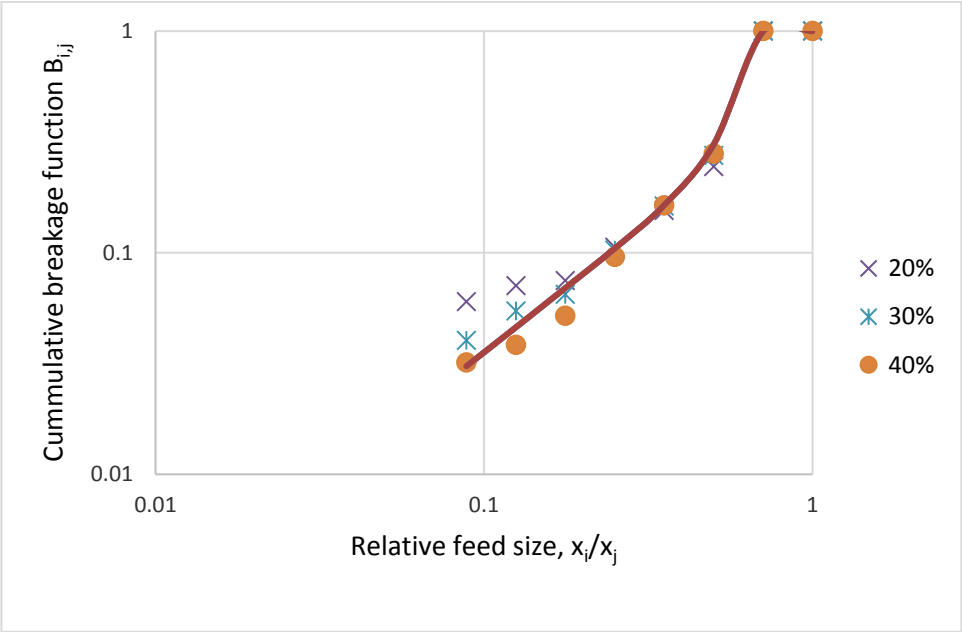

Figure E.3 Cumulative breakage function plot for feed of size -0.600+425 mm milled at various % critical speed, U = 40%, J = 30%, and d = 20 mm balls

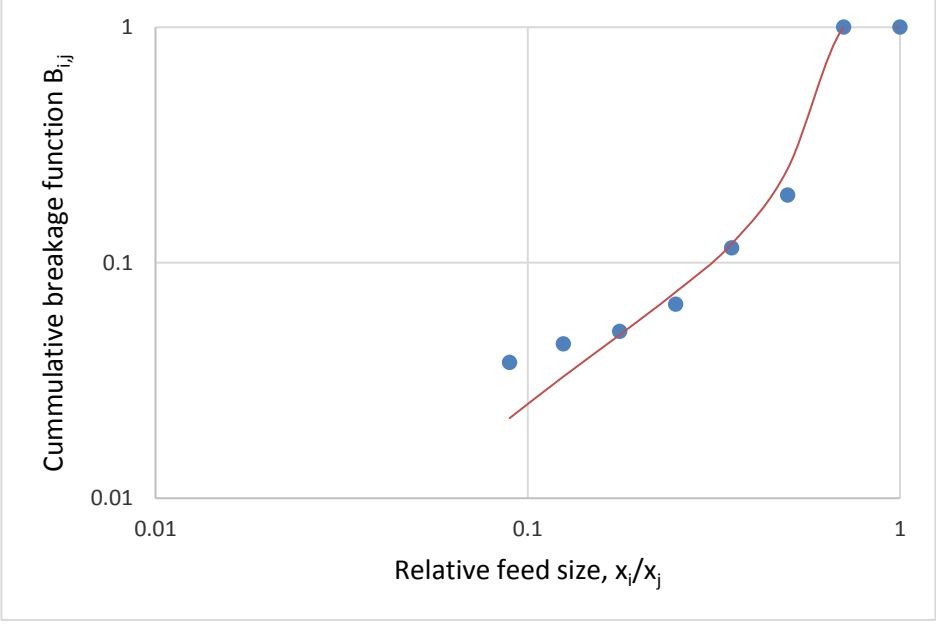

Figure E.4 Cumulative breakage function plot for feed of size -0.425+0.300 mm milled at at ϕ_c = 30% of critical, U = 40%, J = 30%, and d = 20 mm balls

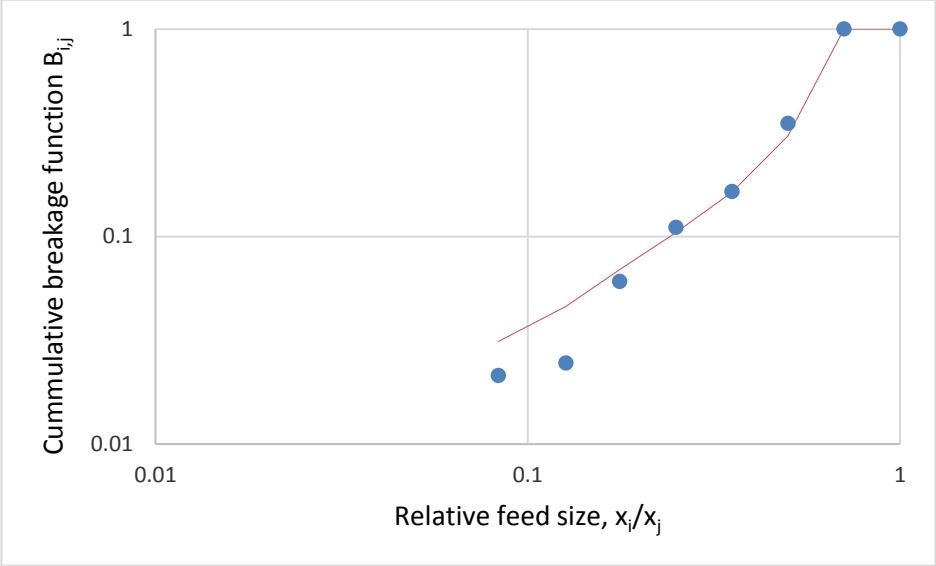

Figure E.5 Cumulative breakage function plot for feed of size -0.425+0.300 mm milled at at ϕ_c = 40% of critical, U = 40%, J = 30%, and d = 20 mm balls

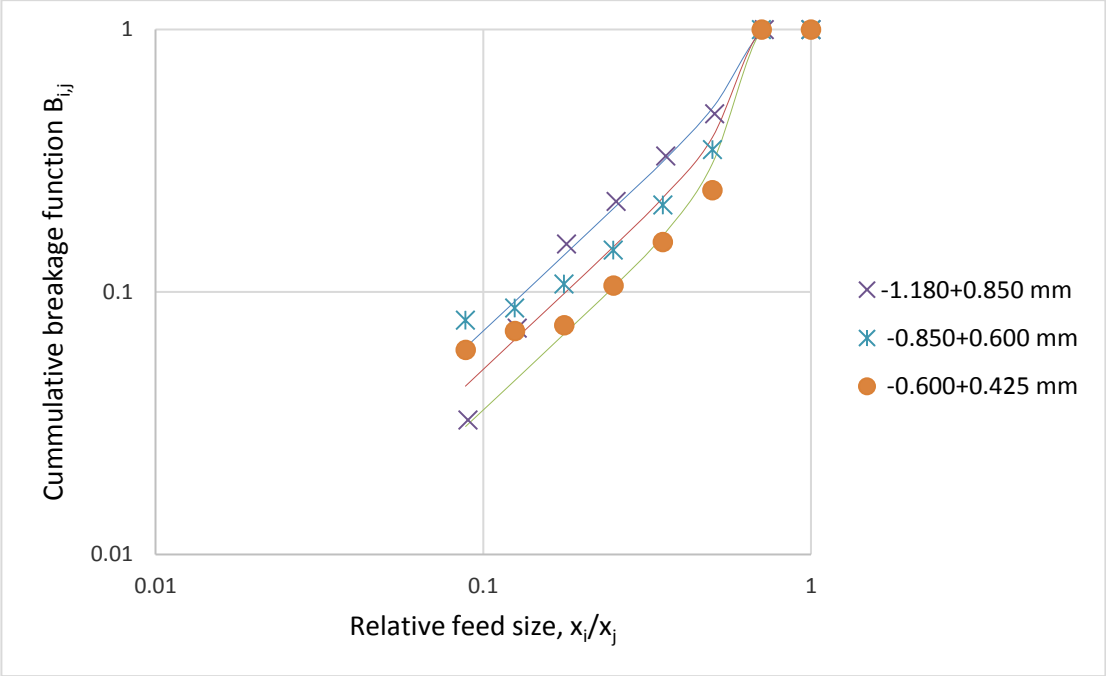

Figure E.6 Cumulative breakage function plot for feed for various feed sizes milled at ϕ_c = 20% of critical, U = 40%, J = 30%, and d = 20 mm balls

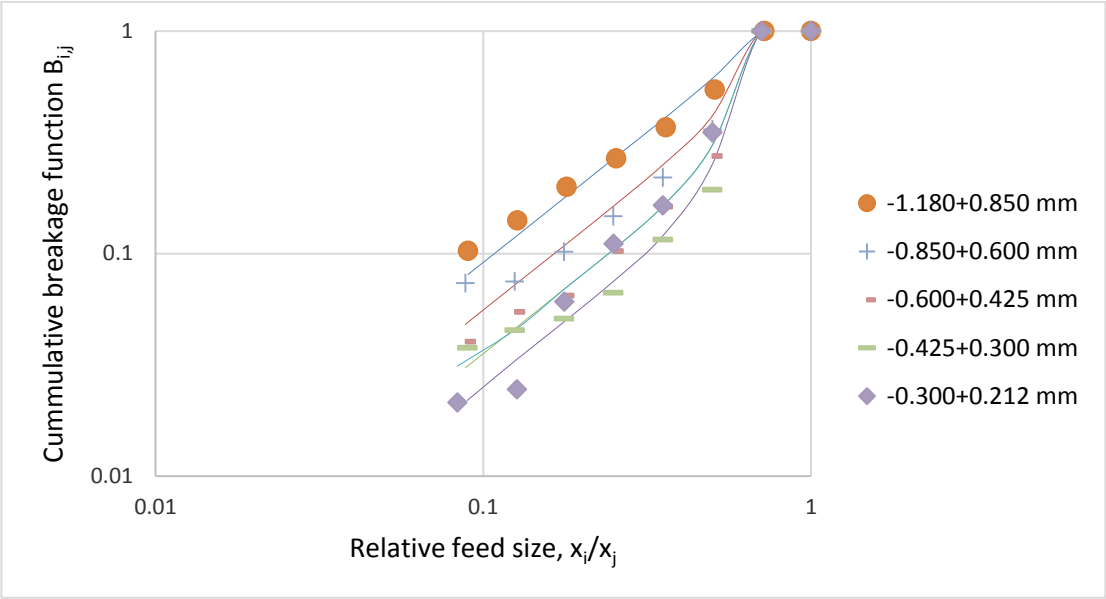

Figure E.7 Cumulative breakage function plot for feed for various feed sizes milled at ϕ_c = 30% of critical, U = 40%, J = 30%, and d = 20 mm ball

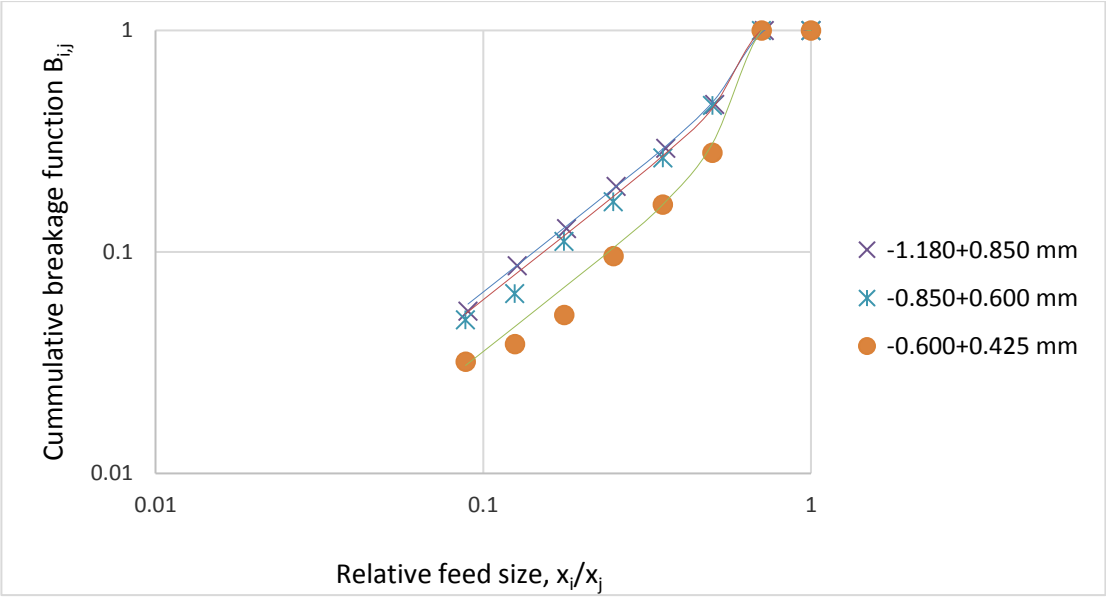

Figure E.8 Cumulative breakage function plot for feed for various feed sizes milled at ϕ_c = 40% of critical, U = 40%, J = 30%, and d = 20 mm ball